Journal of Medicinal Chemistry

pubs.acs.org/jmc

Article

Rational Design and Optimization of a Potent IDO1 Proteolysis Targeting Chimera (PROTAC)

Paige J. Monsen,[†] Prashant V. Bommi,[†] Arabela A. Grigorescu, Kristen L. Lauing, Yingyu Mao, Payton Berardi, Lijie Zhai, Oluwatomilayo Ojo, Manon Penco-Campillo, Taylor Koch, Michael Egozi, Sonam Jha, Sara F. Dunne, Hong Jiang, Guiqin Song, Fang Zhang, Steven Kregel, Ali Vaziri-Gohar, Sean W. Fanning, Pilar Sanchez-Gomez, Jacob M. Allen, Bakhtiar Yamini, Rimas V. Lukas, Derek A. Wainwright,* and Gary E. Schiltz*

Cite This: https://doi.org/10.1021/acs.jmedchem.5c00026

Read Online

ACCESS | Metrics & More | Article Recommendations | Supporting Information

ABSTRACT: Indoleamine 2,3-dioxygenase 1 (IDO1) is an immunosuppressive protein that inhibits antitumor immunity through both tryptophan metabolism and nonenzymatic functions. Drugs targeting IDO1 enzyme activity have failed to improve the overall survival of patients with cancer. Developing new therapeutics that neutralize both enzyme- and nonenzyme-derived immunosuppressive IDO1 effects is therefore of high interest. We previously described a novel proteolysis targeting chimera (PROTAC), NU223612, that degrades IDO1 in cultured human glioblastoma (GBM) cells, as well as in well-established brain tumors, *in vivo*. In this study, we rationally optimized the structure of our lead series to create NU227326, which degrades IDO1 with a DC_{50} of 5 nM in human GBM cells. Mechanistic studies showed that IDO1 degradation occurred through the ubiquitin−proteasome system and was sustained for at least 2 days, supporting NU227326 as a highly potent IDO1 PROTAC suitable for further studies in GBM and other human cancers.

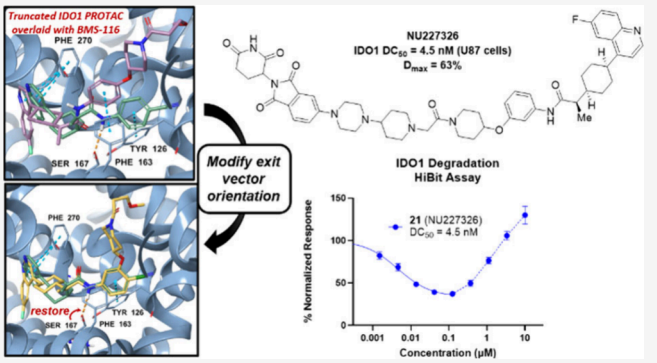

INTRODUCTION

Glioblastoma (GBM; IDHwt) is the most commonly malignant primary central nervous system cancer in adults and accounts for ≥50% of all malignant glioma.[1] Standard of care treatment for patients with GBM involves surgical resection of the tumor followed by adjuvant radiation and Temozolomide chemotherapy.[2] Despite this aggressive treatment regimen, the survival rate for GBM patients remains low with a median overall survival (mOS) rate of less than 20 months and a 5-year survival rate of less than 10%.[3] The use of cancer immunotherapy to reinvigorate the antitumor immune response is an active area of research and has been a breakthrough for many types of cancers.[4] Over the last 15 years, the development of immune checkpoint inhibitors (ICIs) targeting PD-1, PD-L1, and CTLA-4 have provided notable survival benefits to patients with a variety of different cancer types.[5−7] However, treatment with ICIs has failed to improve the mOS of GBM patients across broad patient populations studied in phase 3 clinical trials to-date.[8−10]

The kynurenine (Kyn) pathway of tryptophan (Trp) metabolism has been studied for its role in tumor-induced immunosuppression.[11−13] Indoleamine 2,3-dioxygenase 1 (IDO1) is a rate-limiting enzyme that converts the essential amino acid, Trp, into downstream Kyn metabolites. Low Trp or high Kyn levels suppress T cell function(s) and/or induce cell death when evaluated *in vitro*.[14,15] Expression of IDO1 is prevalent in a number of cancers including GBM[16,17] and high expression is associated with poor survival outcomes.[17−25] Several IDO1 enzyme inhibitors including epacadostat (**1**),[26,27] navoximod (**2**),[28,29] PF-0684003 (**3**),[30] and BMS-986205 (**4**)[31,32] have been widely studied over the past decade (Figure 1). To-date, small molecule IDO1 enzyme inhibitor treatment has generally failed to provide a survival benefit to patients with cancer. This has resulted in questioning whether IDO1 is a valid target for cancer immunotherapy.[27,33] Beyond IDO1 enzyme-dependent effects, we and others have demonstrated that IDO1 also possesses nonenzymatic functions that mediate immunosuppression.[23−25,34] The data collectively support the hypothesis that one of the reasons IDO1 enzyme inhibitors have failed

Received: January 4, 2025
Revised: February 6, 2025
Accepted: February 10, 2025

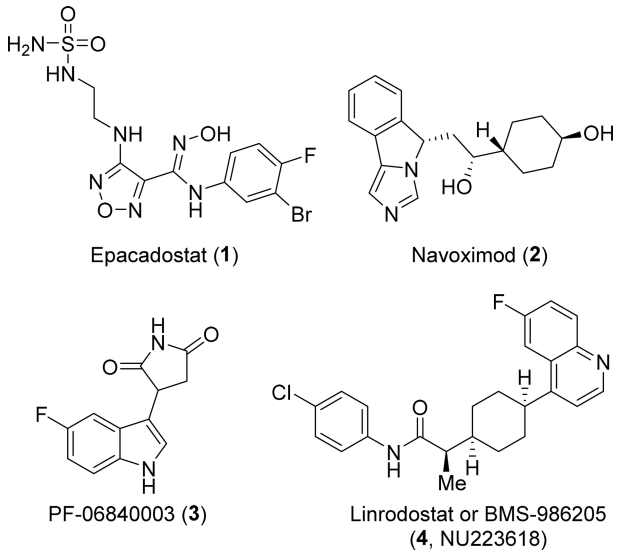

Figure 1. Representative IDO1 inhibitors.

to improve cancer patient survival among clinical trials to-date is due to IDO1 nonenzyme-mediated mechanisms. Therefore, the simultaneous targeting of both IDO1 enzyme and nonenzyme activities are required to effectively inhibit immunosuppression and achieve immunotherapeutic efficacy for glioblastoma.

Targeted protein degradation (TPD) is a powerful approach to therapeutically regulate proteins that are termed "undruggable", embody undesirable nonenzymatic functions, or have the potential to develop mechanisms of resistance when treated with small molecule targeted enzyme inhibitors.[35,36] Proteolysis targeting chimeras (PROTACs) are heterobifunctional small molecules that exploit the ubiquitin-proteasome system for targeted protein degradation.[37] Structurally, a PROTAC consists of three components: a targeting ligand that is specific for recruiting and binding to the protein of interest (POI), a warhead ligand to recruit and bind to an E3 ligase, and a linker to tether the two binding ligands (Figure 2A). Over the past 20 years, the development and optimization of PROTACs to become drug candidates has validated this approach in medicinal chemistry and drug discovery.[35] In addition to PROTACs providing a unique drug discovery approach, they can be utilized as a chemical knockdown tool to further study the biology and noncatalytic roles of proteins. Therefore, the investigation into developing PROTACs to degrade IDO1 protein and inhibit IDO1 enzyme and nonenzyme activities represents a promising strategy to fully inhibit IDO1-mediated immunosuppression as well as further study the role of IDO1 in cancer.

To date, the characterization of two potent IDO1 PROTACs have been reported (Figure 2B). In 2020, Hu et al. developed the first IDO1 degrader, **5**, consisting of epacadostat (**1**) as the IDO1 targeting ligand and the cereblon (CRBN) ligand, pomalidomide, as the E3 ligase recruiting ligand.[38] The epacadostat-based degrader displayed a DC_{50} = 2.8 μM in cultured HeLa cells however no *in vivo* validation studies were performed. In 2022, our group reported the development of an IDO1 PROTAC, **6** (**NU223612**), incorporating the BMS-986205 (**4**) enzyme inhibitor as the IDO1 targeting ligand into a CRBN-based PROTAC for subjects with an intracranial primary brain tumor.[39] Our work focused on using BMS-986205 as the IDO1-targeting ligand because this compound had fewer hydrogen-bond donors than epacadostat, making it more likely to have better cell permeability and brain penetration. BMS-986205 also possesses high selectivity for IDO1 over related enzymes IDO2 and TDO, it advanced into Phase 3 clinical trials suggesting it possesses a favorable off-target and toxicity profile, and importantly, X-ray crystal structures of it bound to IDO1 suggested clear opportunities to attach a solvent-exposed linker.[32] Degrader **6** possessed a DC_{50} = 0.33 μM in cultured U87 human GBM cells, reached a concentration of 2 μM in brain tissue (IP), and was able to degrade IDO1 in established brain tumors that yielded a survival benefit in mice with intracranial GBM.[39]

Our previous work described the first report of a PROTAC possessing sufficient brain exposure to produce *in vivo* efficacy in a GBM model and established the therapeutic potential of developing IDO1 PROTACs for the treatment of GBM.[39] Although encouraged by these results, we recognized an opportunity to further optimize our lead series of degraders to (i) enhance the IDO1 degradation potency and efficacy and (ii) improve the brain exposure and pharmacokinetic (PK) characteristics of the IDO1 degrader. Recently, there has been increasing reports of structural factors and physicochemical properties of PROTACs, such as molecular weight (MW), rigidity or number of rotatable bonds (RB), and the number of hydrogen bond donors (HBDs) and acceptors (HBAs), playing influential roles in potency, permeability and ADME (absorption, distribution, metabolism and excretion) properties.[40−42] Herein, we report the optimization of lead IDO1 PROTAC, **6** (**NU223612**), in which structural modifications to the CRBN ligand, linker, and IDO1 ligand were performed in a modular fashion to study the influence on potency, efficacy, and bioavailability.

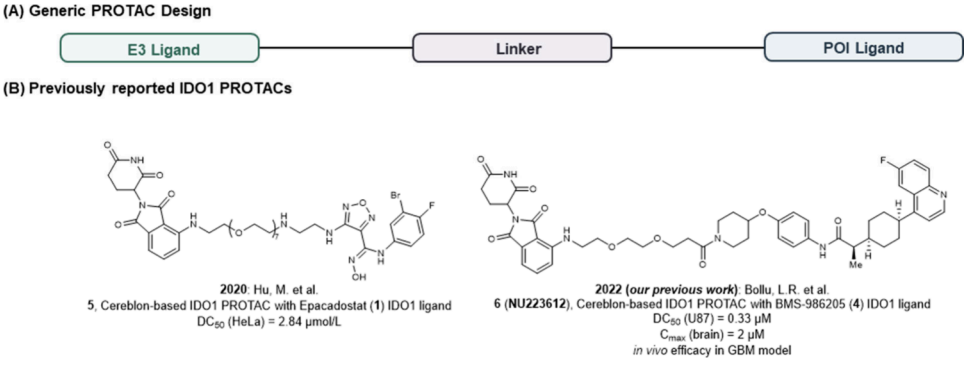

Figure 2. (A) General PROTAC design. (B) Structures of reported IDO1 PROTACs to-date.

https://doi.org/10.1021/acs.jmedchem.5c00026
J. Med. Chem. XXXX, XXX, XXX−XXX

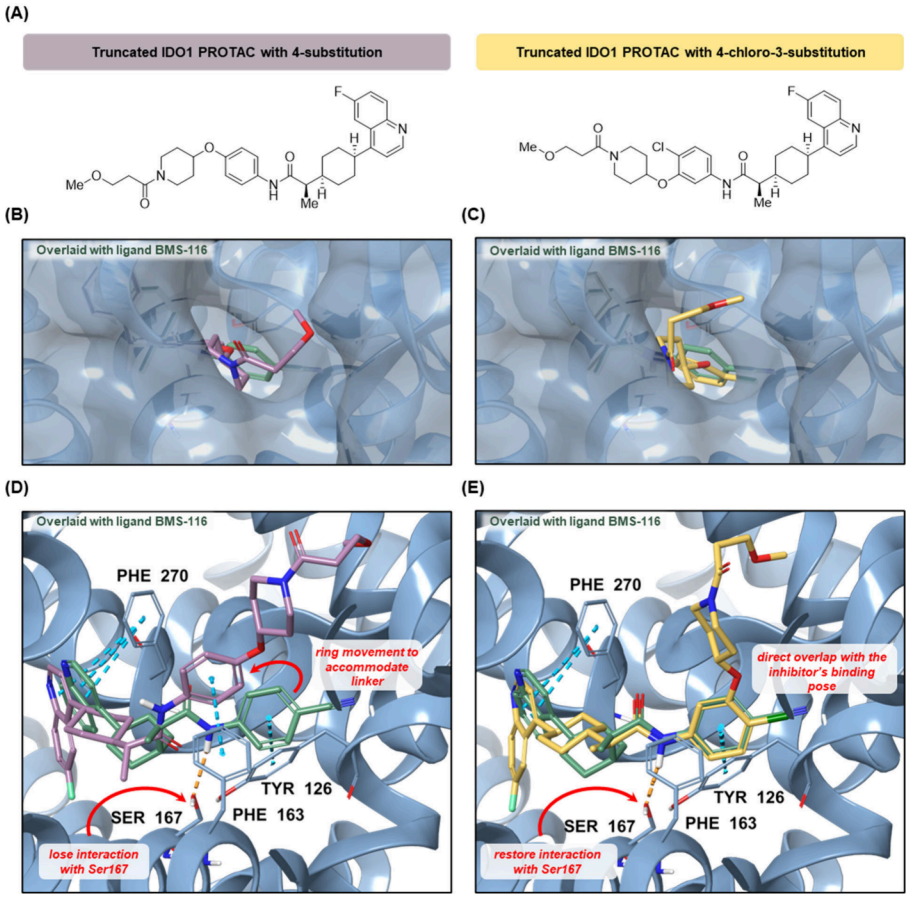

Figure 3. (A) Structures of truncated 4-substituted and 4-chloro-3-substituted type IDO1 PROTACs used in docking studies. (B, C) Surface representations of the cocrystal structure of IDO1 (blue, PDB 6AZW) with the ligand BMS-116 (green) overlaid with either the 4-substituted type analog (purple) or the 4-chloro-3-substituted type analog (gold) demonstrating the orientation of the exit vector and linker. (D, E) Binding pose of BMS-116 (green) modeled with either the 4-substituted type analog (purple) or the 4-chloro-3-substituted type analog (gold) in the IDO1 active site with representative interactions displayed to demonstrate the influence in altering the substitution position of the linker.

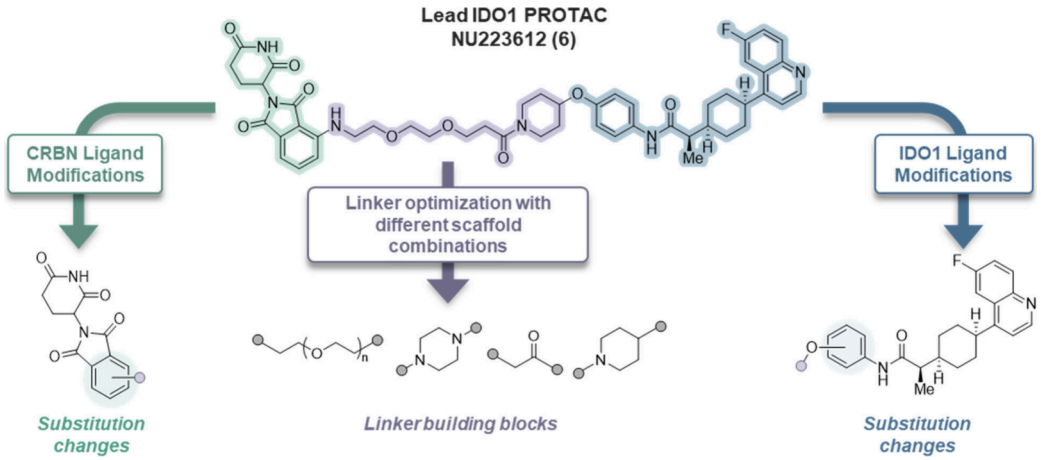

Figure 4. Design of novel IDO1 PROTACs based on modular structural optimizations of lead IDO1 PROTAC **6** (**NU223612**).

RESULTS

Design of Potent Second Generation IDO1 PROTACs.

Previously, we reported the development of a first generation series of degraders to establish IDO1 PROTAC proof of concept and obtain structure−activity relationship (SAR) data.[39] Molecular docking studies revealed the phenyl ring of the parental IDO1 inhibitor, **4** (**NU223618**, BMS-986205), is solvent exposed and provided a suitable anchor for the attachment of linkers. Therefore, IDO1 degraders were designed with an ether connection of the linker to the phenyl ring at either the 3-position to retain the chlorine atom native to the inhibitor or at the 4-position, thereby replacing the chlorine atom. Docking studies were performed with truncated analogs of both substitution options to allow for further investigation into the influence the linker substitution to the warhead has on binding

https://doi.org/10.1021/acs.jmedchem.5c00026
J. Med. Chem. XXXX, XXX, XXX−XXX

Table 1. Initial Optimization of IDO1 PROTACs

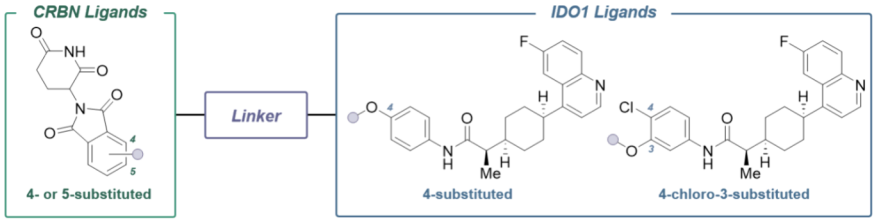

Compound	CRBN ligand	IDO1 ligand	IDO1 Degradation[a]		Linker
			DC_{50} (μM)	D_{max} (%)	
6	4	4-substituted	0.43 ± 0.14	79	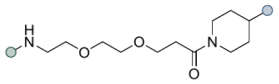
7	5	4-substituted	>10	<10	
8	4	4-chloro-3-substituted	>10	<10	
9	5	4-chloro-3-substituted	>10	<10	
10	4	4-substituted	>10	<10	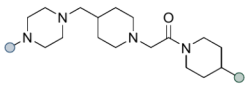
11	5	4-substituted	0.34 ± 0.16	26	
12	4	4-chloro-3-substituted	>10	<10	
13	5	4-chloro-3-substituted	0.008 ± 0.004	48	
14	4	4-substituted	>10	<10	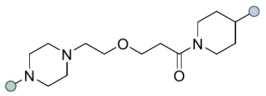
15	5	4-substituted	>10	<10	
16	4	4-chloro-3-substituted	>10	<10	
17	5	4-chloro-3-substituted	>10	<10	
18	5	4-substituted	0.034 ± 0.16	21	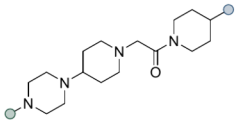
19	5	4-chloro-3-substituted	0.007 ± 0.002	51	

[a]IDO1 degradation activity was tested using HiBiT assay with 24 h treatment time. DC_{50} = dose that reduces IDO1 protein by 50%. D_{max} = maximum reduction of IDO1 protein achieved by the compound. DC_{50} results are the mean of triplicate data, and standard deviations are reported.

to the IDO1 protein (Figure 3A). When overlaid with the bound IDO1 inhibitor (BMS-116), the analog with the ether-piperidine group at the 4-position results in movement of the targeting ligand to accommodate the exiting of the linker into the solvent (Figure 3B and Figure 3D). This movement leads to a loss in interaction between the amide NH of the ligand and Serine 167 (Figure 3D). Conversely, attachment of the ether-piperidine group at the 3-position allows for a direct overlap with the parental inhibitor and appears to restore the key interaction between the amide *N*–*H* and Serine 167 (Figure 3C and Figure 3E). In addition to restoring this interaction, the orientation of the exit vector out of the binding site is slightly modified when the linker is attached to the 4-chloro-3-position versus the 4-position and therefore may allow for the PROTAC to facilitate a unique ternary complex upon binding to the IDO1 and E3 ligase proteins. These observations suggest the 4-chloro-3-substituted position may be a preferred connection site for linkers in comparison to the 4-substituted position and was therefore explored further during the initial optimizations of lead degrader, **6** (**NU223612**) (Figure 4).

As previously reported, a variety of E3 ligase ligands were investigated in the initial screening and SAR analysis revealed both CRBN and Von Hippel-Lindau (VHL)-type ligands can be used as recruiting warheads in the PROTAC design to induce degradation of IDO1. To improve the PK profiles and blood brain barrier (BBB) penetration of the IDO1 degraders, CRBN-based PROTACs were of more interest as they have both decreased MW and fewer RBs compared to VHL-based PROTACs. Consequentially, optimization of degrader **6** (**NU223612**) involves simple modifications to the CRBN ligand, specifically through altering the substitution position to the linker scaffold (Figure 4). Numerous reports provide increasing evidence that linker length and composition play a major role in the bioactivity of a PROTAC.[35,43] Since SAR data from the original degrader library suggested amine-connected linkers to the CRBN ligand are preferred in comparison to ether or oxyacetamide type functional groups, we further investigated the amine-type connectivity to the E3 warhead. Utilizing various linker building blocks, the flexible polyethylene glycol (PEG) linker could be replaced entirely or in part with short, rigid heterocycles, which would allow us to evaluate the degradation of IDO1 with less-flexible linkers. Therefore, taking into consideration the SAR data established in our initial report, we developed a new series of IDO1 degraders.

Optimization of IDO1 Degraders. Altering the substitution positions of the linker to both the CRBN and IDO1 ligands was undertaken to investigate the effect on IDO1 degradation. To quantitatively determine the degradation potency (DC_{50}) and efficiency (D_{max}) of the designed IDO1 degraders, a HiBiT degradation assay for IDO1 protein in the U87 glioblastoma cell line was developed and employed. HiBiT was inserted by CRISPR/Cas9 to the N-terminus of IDO1 protein and degradation was obtained through measuring the loss of luminescence following a 24 h treatment with the synthesized PROTACs.[44]

The initial IDO1 degraders contained 4-substituted thalidomide-type CRBN ligands, therefore altering the linker substitution to the 5-position was explored. Furthermore, investigation into the IDO1-ligand substitution preference was performed through analyzing both the 4-substituted and 4-

https://doi.org/10.1021/acs.jmedchem.5c00026
J. Med. Chem. XXXX, XXX, XXX−XXX

Table 2. Optimization of *meta*-Substituted IDO1 PROTACs

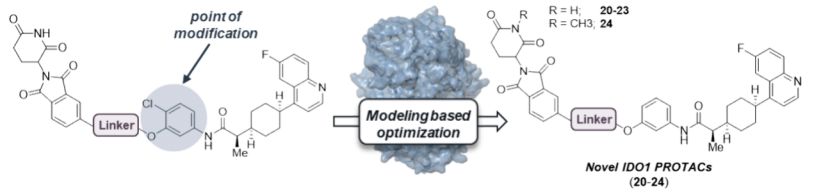

Compound	Linker	IDO1 Degradation[a]	
		DC_{50} (μM)	D_{max} (%)
20	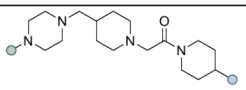	0.020 ± 0.004	67
21	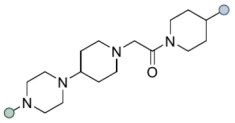	0.005 ± 0.001	63
22	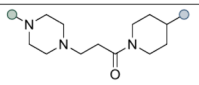	>10	<10
23	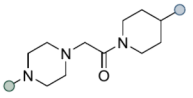	>10	<10
24	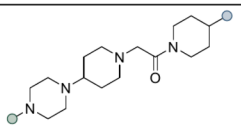	>10	<10

[a]IDO1 degradation activity was tested using HiBiT assay with 24 h treatment time. DC_{50} = dose that reduces IDO1 protein by 50%. D_{max} = maximum reduction of IDO1 protein achieved by the compound. DC_{50} results are the mean of triplicate data, and standard deviations are reported.

chloro-3-substituted phenyl rings. Therefore, while keeping the amino-PEG2-amide-piperidine linker consistent, novel analogs **7**−**9** were synthesized to embody differential substitution patterns to both the CRBN and IDO1 ligands and were evaluated for IDO1 degradation (Table 1). Changing the substitution position to the CRBN ligand from the 4- to the 5-postion resulted in inactive degrader, **7**. Similarly, modifying the substitution of the IDO1 ligand from the 4-substitution to the 4-chloro-3-substitution position yielded inactive analog, **8**. Altering both the substitution to the CRBN and IDO1 ligands provided PROTAC, **9**, with decreased potency (DC_{50} > 10 μM degradation).

The observed loss in potency resulting from small changes of the connectivity to the CRBN and IDO1 ligands lead us to focus our efforts on optimization of the linker moiety of the IDO1 degrader series. Therefore, we replaced the entire flexible amino-PEG2 with a rigidified linker scaffold to provide PROTACs **10** - **13**. To retain some flexibility, a methylene unit was utilized as a connecting scaffold between the piperazine and piperidine ring systems. Replacement of both the hydrogen bond donating amine and the entire PEG linker resulted in inactive analog **10**. Modifying the substitution to the CRBN ligand from the 4- to 5-position resulted in degrader **11** with slightly enhanced potency (DC_{50} = 340 nM) but decreased efficacy (D_{max} = 26%). Keeping the 4-subsituted CRBN ligand intact while altering the IDO1 ligand substitution from the 4- to the 4-chloro-3-subsituted to provide analog **12**, lead to a complete loss in potency. Interestingly, changing both the CRBN and IDO1 substitutions yielded a highly potent degrader **13**, with a DC_{50} of 7.6 nM and a D_{max} of 48%, suggesting that the rigidification of the linker may be more tolerated when connected at the CRBN 5-position and the IDO1 4-chloro-3-position. The enhanced IDO1 degradation resulting from replacement of the flexible linker in analogs **7** and **9** with a more rigid linker in degraders **11** and **13** suggests the linker composition is highly responsible for degradation activity.

To investigate the optimized linker rigidity, we replaced the central piperidine ring with a flexible PEG_1 unit to yield analogs **14**−**17**. Derigidifying the central unit of the PROTAC linker, while retaining rigid ring systems to both the E3 and IDO1 ligands led to a complete loss in IDO1 degradation potency, implying the entire flexible PEG linker should be replaced with a rigid linker.

To further increase the rigidity of the more potent analogs, **11** and **13**, the methylene unit was removed, providing degraders **18** and **19**, which both possessed the 5-subsitution to the CRBN ligand though different substitutions to the IDO1 ligand, 4-subsituted and 4-chloro-3-substituted, respectively. Shortening the length of the linker by only one carbon increased the potency by 10-fold for the 4-substituted degrader (**18**, DC_{50} = 34 nM), though the D_{max} remained at just 21%. The 4-chloro-3substituted analog, **19**, displayed both enhanced potency with a DC_{50} value of 6.6 nM and enhanced efficiency with a D_{max} of 51%.

Taken all together, the above data demonstrates that the combination of the linker composition and the substitution patterns to the E3 ligase and IDO1 ligands collectively play an important role in the ability of the PROTACs to reduce levels of IDO1 in U87 cells. Additionally, we were able to establish the optimal structural combination to include the 5-subsituted

https://doi.org/10.1021/acs.jmedchem.5c00026
J. Med. Chem. XXXX, XXX, XXX−XXX

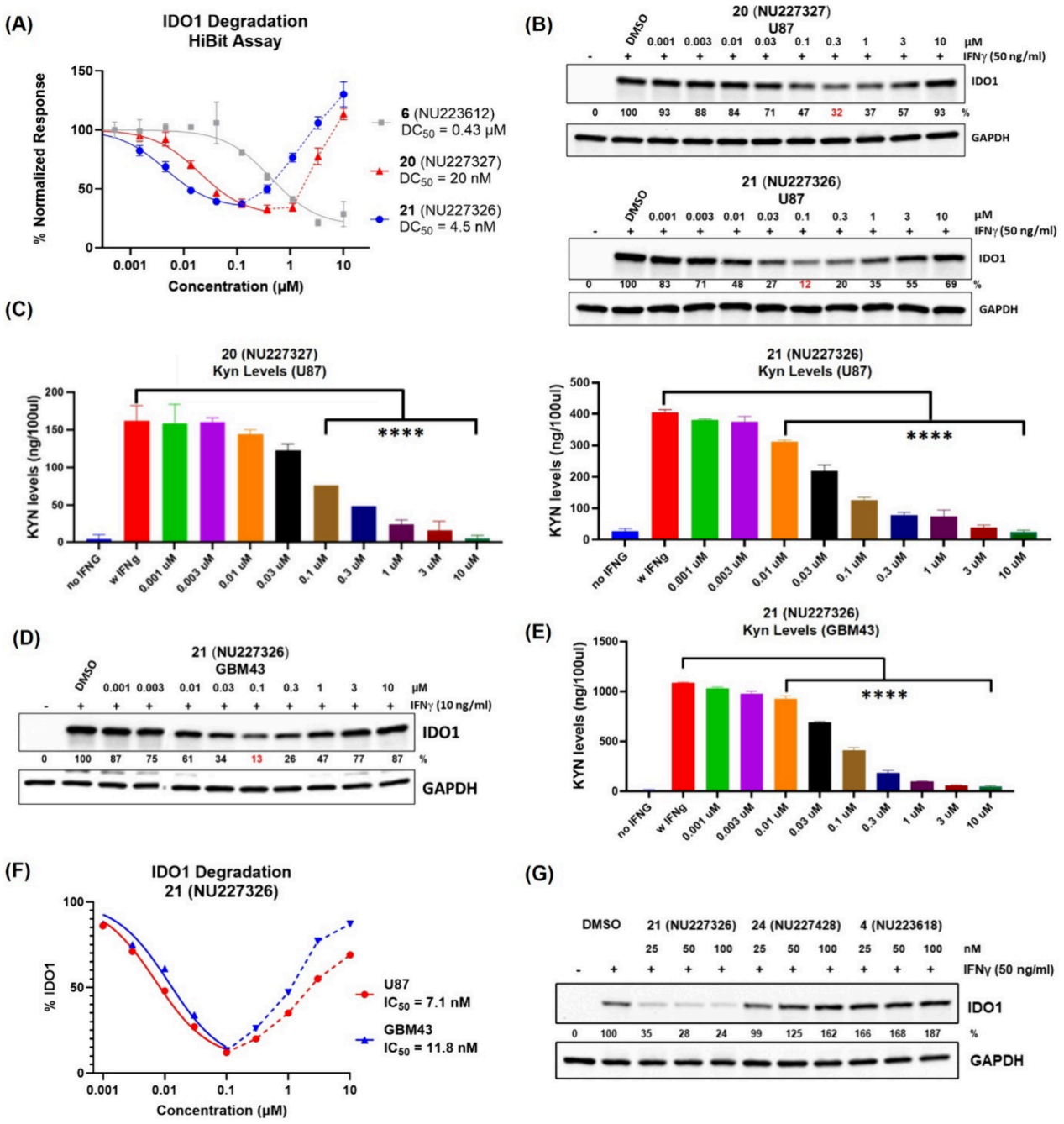

Figure 5. Characterization of IDO1 degradation by PROTACs **20** and **21**. (A) Degradation of IDO1 by **20**, **21**, and **NU223612** in the HiBiT assay. DC_{50} was calculated from the lowest concentration down to where maximum degradation was observed and excluded data points within the Hook effect range. $R^2 = 0.94$ for **20**; $R^2 = 0.93$ for **21**. (B) Dose-dependent degradation by compounds **20** and **21** on IDO1 in U87 cells treated with an extended dose range of **20** or **21** for 24 h and protein samples were analyzed by Western blotting. (C) Effects of **20** and **21** on kynurenine production in U87 human GBM cells. Cells were treated with **20** or **21** in the presence of 50 ng/mL IFNγ beginning at 24 h after plating the cells and for a total of 24 h, followed by the collection of cell culture supernatants to measure IFNγ-induced kynurenine levels using Ehrlich's reagent. Cells cultured in the absence of IFNγ served as the control group. (D) GBM43 cells were treated with an extended dose range of **21** for 24 h, and protein samples were analyzed by Western blotting. (E) Effect of **21** on kynurenine production in GBM43 cells. Cells were treated with **21** in the presence of 10 ng/mL IFNγ for 24 h, and cell culture supernatants were collected to measure IFNγ-induced kynurenine levels using Ehrlich's reagent. Cells cultured in the absence of IFNγ served as the control group. (F) Representative curves of percent IFNγ-induced IDO1 levels that were normalized to untreated samples as calculated in U87 and GBM43 cells to determine DC_{50} that produces 50% of IDO1 degradation (n = 3 independent experiments). Data are presented as mean ± SEM. Statistical significance was determined using Tukey's multiple comparison test for comparisons between more than two groups. Significance levels are indicated as follows: $P < 0.05$ (*), $P < 0.01$ (**), $P < 0.001$ (***), and $P < 0.0001$ (****). (G) Western blotting analysis of IDO1 protein in U87 cells. IDO1 was induced in U87 cells with 50 ng/mL human IFNγ for 24 h followed by a 25, 50, or 100 nM treatment with IDO1 PROTAC (**21**, **NU227326**), inactive PROTAC (**24**, **NU227428**) or IDO1 enzyme inhibitor (**4**, **NU223618**) for 24 h before protein samples were prepared for Western blotting analysis. Percent of normalized IDO1 protein levels were derived from densitometric analysis of band intensities. Western blotting results are representative of outcomes from 3 separate experimental replicates.

https://doi.org/10.1021/acs.jmedchem.5c00026
J. Med. Chem. XXXX, XXX, XXX−XXX

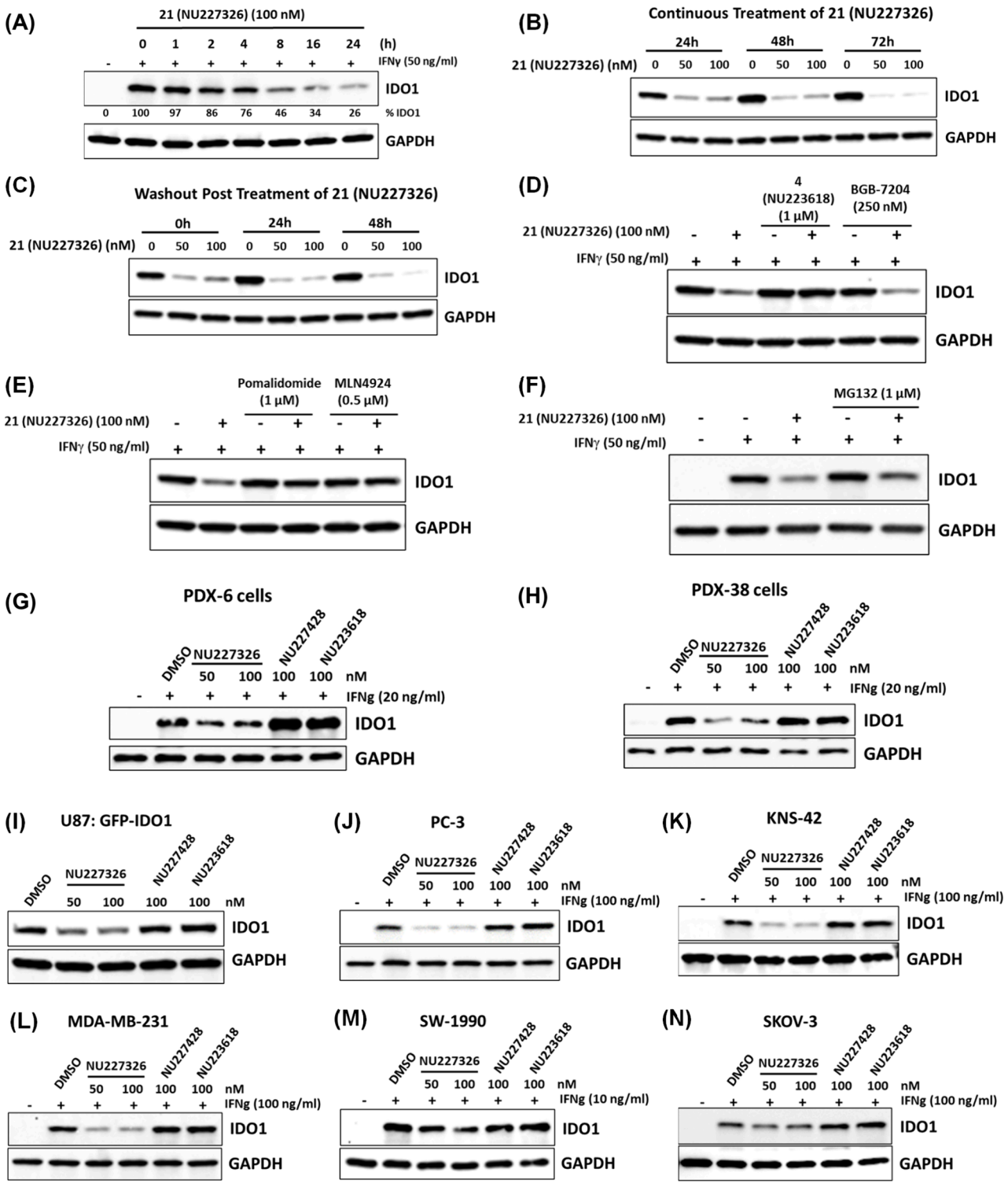

Figure 6. Characterization of **21** (**NU227326**) as a potent IDO1 PROTAC. (A) Western blot analysis of IDO1 and GAPDH to determine the kinetics of **21** (**NU227326**)-induced IDO1 protein degradation in U87 cells. (B) Western blot analysis of IDO1 to determine the effect of a single continuous treatment of **21** (**NU227326**) on IDO1 protein levels at multiple time points in U87 cells. (C) Similar to (B), U87 cells were treated with **21** (**NU227326**) for 24 h, and cells were cultured without **21** (**NU227326**) for up to 48 h. Protein samples were tested in Western blot analysis to determine IDO1 levels upon withdrawal of the IDO1 PROTAC. (D) Western blotting analysis of IDO1 and GAPDH to determine the effect of parental competitive IDO1-inhibitor (**4**, **NU223618**) and noncompetitive IDO1-inhibitor (BGB-7204); (E) E3 ligase ligand (pomalidomide) and E1 ligase neddylation inhibitor (MLN4924); and (F) proteasome inhibitor (MG132) on NU227326-induced IDO1 degradation. Western blotting analysis to determine the effect of **NU227326** on IFNγ-induced IDO1 levels in human adult PDX cells; PDX-6 (G) and PDX-38 (H), U87 cells exogenously overexpressing GFP-fused IDO1 (I), prostate cancer PC-3 cells (J), human pediatric KNS42 GBM cells (K), triple negative breast cancer MDA-MB-231 cells (L), pancreatic cancer SW-1990 cells (M), and ovarian SKOV-3 cells (N). Cells treated with either **21** (**NU227326**), **24** (**NU227428**), or **4** (**NU223618**) at indicated concentrations for 24 h and protein samples were analyzed for IDO1 and GAPDH using Western blotting analysis. Western blotting results are representative of outcomes from 3 separate experimental replicates.

https://doi.org/10.1021/acs.jmedchem.5c00026
J. Med. Chem. XXXX, XXX, XXX−XXX

CRBN ligand and the 4-chloro-3-substituted IDO1 ligand with a highly rigid nitrogen-heterocycle containing linker.

Optimization of Degraders 13 and 19. The initial linker and substitution optimizations led to the identification of degraders **13** and **19** which possessed improved potency for IDO1 degradation compared to the initial lead PROTAC **6**. Analysis of the structural modifications made to the degrader series suggests that replacement of the flexible PEG linker with a more rigid, nitrogen heterocycle-containing linker can be achieved with the optimal combination of substitution patterns to both the E3 ligase and IDO1 ligands. More specifically, a common trend was noted, in which 4-chloro-3-substitution to the IDO1 ligand was more preferential compared to the 4-substitution. Based on this observation, the previously described docking studies, and the increased potency correlating to the IDO1 substitution modification, we chose to focus our attentions on optimizing the exit vector of the IDO1 ligand. Since substitution at the 3-position provides an ideal orientation for the linker to exit (Figure 3E), we kept the substitution of the linker to the phenyl ring consistent and removed the chlorine atom (Table 2). We hypothesized that replacement of this larger substituent with a hydrogen atom would allow for more flexibility of the targeting ligand within the binding site to accommodate the attached ether-piperidine linker, while still allowing for the formation of key interactions. Therefore, we synthesized several 3-substituted IDO1 PROTACs with various linkers and analyzed them for IDO1 protein degradation using the HiBiT degradation assay (Table 2).

We began by investigating **13** and **19** derived analogs, in which the CRBN substitution and linkers were kept consistent, and the chlorine atom on the IDO1 ligand was removed to provide the corresponding IDO1 PROTACs, **20** and **21**. Upon removal of the chlorine group, an increase in IDO1 degradation potency and efficiency was observed. Degrader **20**, the analog of PROTAC **13**, exhibited a DC_{50} of 20 nM and a D_{max} of 67% and **21**, the direct analog of **19**, possessed a DC_{50} of 4.5 nM and a D_{max} of 63%. In an effort to decrease the MW of the degraders, the linker was shorted via the removal of the central piperidine ring to yield analogs **22** and **23**. Reducing the length of the linker resulted in a complete loss of potency, suggesting that shortening the length of the linker disrupted the ability of the degraders to form the ternary complex and induce IDO1 degradation.

***In Vitro* Analysis of Potent IDO1 PROTACs 20 and 21.** Analogs **20** and **21** were identified as novel lead IDO1 degraders possessing DC_{50} values of 20 nM and 4.5 nM, respectively, in the HiBit degradation assay (Figure 5A). Therefore, PROTACs **20** and **21** underwent additional and extensive *in vitro* analysis. Both **20** and **21** were subjected to Western blot analysis at an extended dose range to measure IDO1 degradation effect in cultured U87 cells (Figure 5B). The results indicated both analogs dose-dependently degrade IDO1 with **20** reaching maximum degradation at 300 nM (68% IDO1 degraded) and **21** reaching maximum degradation at 100 nM (88% IDO1 degraded). In addition to their IDO1 degradation potency, both **20** and **21** dose dependently inhibit the amount of Kyn levels present in treated U87 cells (Figure 5C). Since IDO1 PROTAC **21** displayed the highest percentage of IDO1 degradation at the lowest dose, **21** was further evaluated in human GBM43 cells. Degrader **21** was found to dose-dependently decrease protein levels in GBM43 cells as well as decrease the levels of Kyn, similarly to the response in U87 cells (Figure 5D and Figure 5E). We also compared the abilities of the most potent degrader, compound **21**, the inactive control compound **24**, and the parental IDO1 enzyme inhibitor **4** (**NU223618**, **BMS-986205**) to inhibit kynurenine production in GBM cells (Supplementary Figure 1). In U87 cells, compound **4** (**NU223618**, **BMS-986205**) was found to be the most potent inhibitor, with nearly all kynurenine production blocked at 25 nM. Inactive control compound **24**, which cannot bind to cereblon but has the same IDO1-binding moiety as **21**, was a much weaker inhibitor, while degrader **21** showed significantly greater potency than the inactive control. In GBM43 cells, the same trend was observed, with the most significant difference being a greater potency of the enzyme inhibitor.

Additionally, the DC_{50} was determined through evaluating the concentration of the drug at which 50% of the IDO1 protein is degraded. A DC_{50} of 7.1 nM and 11.8 nM in U87 and GBM43 cells, respectively, was determined (Figure 5F). It should be noted that a hook effect is observed for the potent degraders **20** and **21** in both the HiBit assay and Western blot analysis resulting in increased levels of IDO1 protein at increased PROTAC concentrations. Interestingly, even though IDO1 protein levels rise at higher PROTAC concentrations because of the hook effect, Kyn levels continue to decrease with increasing doses (Figure 5C and 5E), presumably due to increased enzymatic inhibition. Furthermore, analysis of the parental BMS IDO1 inhibitor (**4**) and the E3 ligase dead analog of **21** (**24**, **NU227428**) show no degradation of IDO1 (Figure 5G).

Mechanism and Validation of IDO1 Degrader 21 (NU227326). The kinetics of protein degradation by IDO1 PROTAC shows that **21** (**NU227326**) begins initial active degradation between 8 and 16 h (Figure 6A). In evaluating the sustained degradation potential of analog **21** (**NU227326**), we subjected cells to continuous treatments of 50 and 100 nM of **21** (**NU227326**) (Figure 6B). Remarkably, the impact endured for up to 72 h. Notably, even after a 24-h pulse treatment with subsequent withdrawal, the profound effect of **21** (**NU227326**) persisted significantly for at least 48 h post washout (Figure 6C). This observation suggests that the pharmacological effects of degrader **21** (**NU227326**) will exhibit enduring efficacy beyond the initial administration.

To study the basic principle of the PROTAC's mechanism for protein degradation, we sought to assess the protein degradation capability of compound **21** (**NU227326**). Treatment of U87 cells with a combination of **21** (**NU227326**) and the competitive IDO1 enzyme inhibitor **4** (**BMS-986205**, **NU223618**) markedly reduced IDO1 protein degradation as compared to the treatment of **21** (**NU227326**) alone (Figure 6D). This effect was conspicuously absent when U87 cells were treated with the combination of IDO1 PROTAC **21** (**NU227326**) and the noncompetitive IDO1 enzyme inhibitor, BGB-7204[34] (Figure 6D). This implies that the binding site occupied by the competitive inhibitor hinders the degradation ability of IDO1 PROTAC **21** (**NU227326**).

Analogously, the administration of an excess of the E3 ligase ligand, pomalidomide, hinders the binding of **21** (**NU227326**) to the E3-ligase CRBN and eliminates the degrader's ability to degrade the target protein (Figure 6E). Introducing disruption to the multimeric E3 ubiquitin ligase complex through the addition of the E1 (ubiquitin-activating enzyme) ligase inhibitor, MLN4924,[45] which renders the CRL complex ($CRL4^{CRBN}$) inactive and disrupts CRBN-cullin-RING ligase-mediated protein turnover, resulted in the accumulation of IDO1 protein compared to treatment with **21** (**NU227326**)

https://doi.org/10.1021/acs.jmedchem.5c00026
J. Med. Chem. XXXX, XXX, XXX−XXX

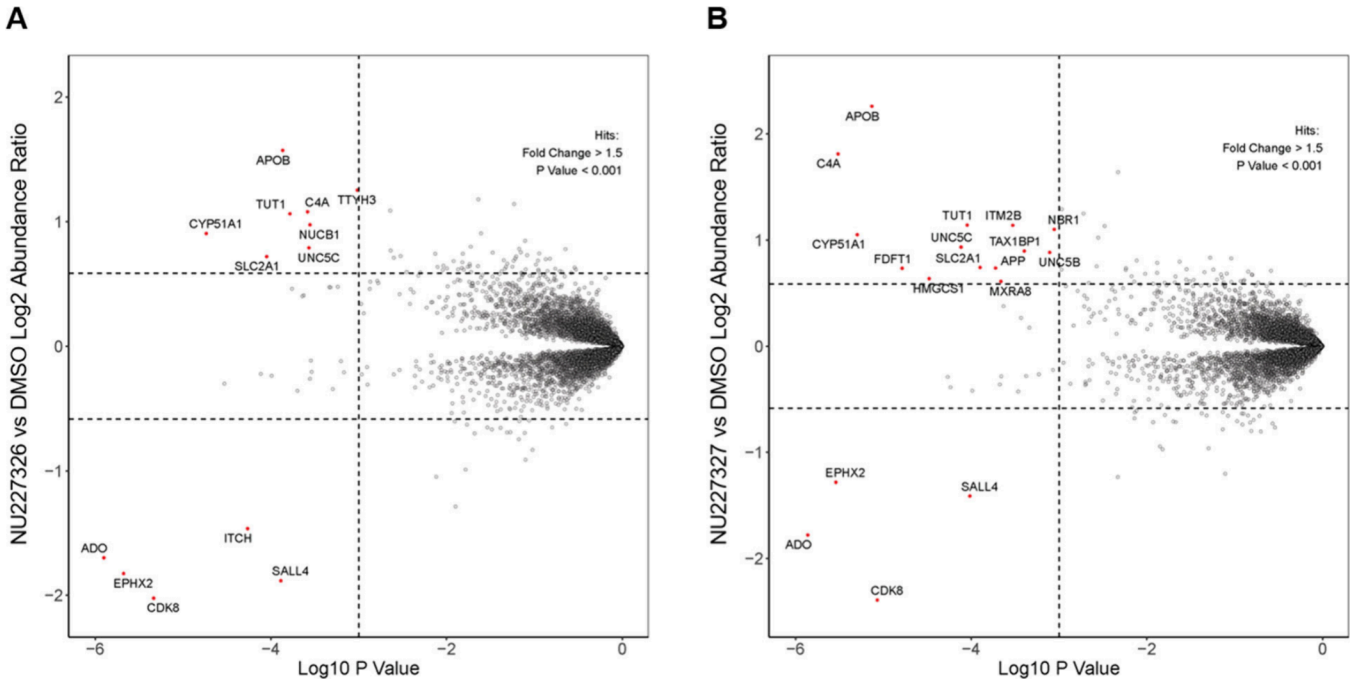

Figure 7. Scatter plot of protein expression changes based on global quantitative proteomics. Kelly cells were treated with 1 μM compound for 24 h and analyzed as described in the Experimental Section. (A) Treatment with **NU227326**. (B) Treatment with **NU227327**.

alone (Figure 6E). Furthermore, treatment with proteasome inhibitor MG132 in combination with degrader **21** (**NU227326**) results in no degradation of IDO1 protein (Figure 6F). Collectively, these findings support the necessity of the $CRL4^{CRBN}$-mediated E3 ubiquitin ligase complex for the effective degradation of targeted protein substrates by IDO1 PROTAC **21** (**NU227326**). To further investigate the broad degradation potential of compound **21** (**NU227326**), we extended our testing to additional glioblastoma (GBM) models including two patient-derived xenograft (PDX) lines, PDX-6 (Figure 6G) and PDX-38 (Figure 6H), the pediatric GBM cell line, KNS-42 (Figure 6K), as well as a genetically engineered U87 line expressing an IDO1 cDNA fused to GFP (Figure 6I). We also explored the efficacy of **21** (**NU227326**) across a wide range of human tumor types including pancreatic-, triple-negative breast-, ovarian-, and prostate-cancers (Figures 6J, 6L−6M). Compound **21** (**NU227326**) consistently demonstrated potent, dose-dependent degradation of IDO1, whereas neither the inactive PROTAC **24** (**NU227428**) nor the parental compound **4** (**NU223618**) elicited comparable effects. The selective activity of Compound **21** (**NU227326**) reinforces its specificity and generalizability for targeting IDO1 across multiple tumor types and confirms its reproducible efficacy in both GBM and other solid tumors (Figure 6G−6N). Strikingly, we observed a dose-dependent reduction in kynurenine levels across all tested cell lines after treatment with **NU227326**, indicating that Compound **21** is also able to influence IDO1 enzyme activity (Supplementary Figure 2). These findings highlight the broad and consistent activity of Compound **21** (**NU227326**) and supports its potential as a targeted therapeutic across a spectrum of IDO1-driven cancers.

Proteomics of NU227236 and NU227327. To define the selectivity of our lead degraders and identify any other proteins that they degrade, **NU227326** and **NU227327** were tested in global quantitative proteomics (Figure 7). Very few human cancer cell linesexpress high IDO1 levels under normal, non-IFN-stimulated conditions. The compounds were therefore tested for proteomics in Kelly cells, as these have been extensively studied in proteomic degradation experiments and provide broad coverage of the degradable proteome that include CRBN substrates.[46,47] Because they are a neuroblastoma cell line, they possess some neuronal characteristics which also provides relevance to GBM studies. Each compound was tested at 1 μM for 24 h. in Kelly cells without induction by IFN-γ to assess unperturbed cells. As these cells do not endogenously express IDO1, mass spectrometry did not detect IDO1. Treatment with either compound only resulted in a significant decrease of 4−5 proteins. With both compounds, proteins ADO, EPHX2, CDK8, and SALL4 were found to be decreased, while **NU227326** also degrades ITCH (Figure 7).

Characterization of IDO1 Binding. Intrigued by the *in vitro* degradation profiles, **20** (**NU227327**) and **21** (**NU227326**) were further assessed using biolayer interferometry (BLI) to measure their ability to form binary and ternary complexes with recombinant IDO1 and CRBN proteins in vitro. Biolayer interferometry is a label-free optical technique used to analyze bimolecular interactions in real time.[48] Both **20** and **21** were confirmed to directly bind to CRBN, possessing binding affinities (K_d) of 520 nM and 380 nM, respectively (Figure 8A). In comparison to initial lead analog **6** (K_d = 290 nM) degraders **20** and **21** exhibited weaker binding to CRBN. As expected, no measurable binding to CRBN was observed for IDO1 inhibitor **4** (**NU223618**) lacking an E3 ligaseligand or inactive PROTAC **24** (**NU227428**) (Supplementary Figure 3). Analysis of PROTAC binding to IDO1 revealed **20** and **21** possessed stronger interactions compared to **6** (K_d = 640 nM), with binding affinities of 370 nM and 140 nM, respectively (Figure 8B). This enhancement in binding affinity to IDO1 could be attributable to both optimized PROTACs (**20** and **21**) possessing the 3-substituted versus the 4-substituted IDO1 ligand. The previously described docking studies provide evidence that this substitution position offers a more favorable

https://doi.org/10.1021/acs.jmedchem.5c00026
J. Med. Chem. XXXX, XXX, XXX−XXX

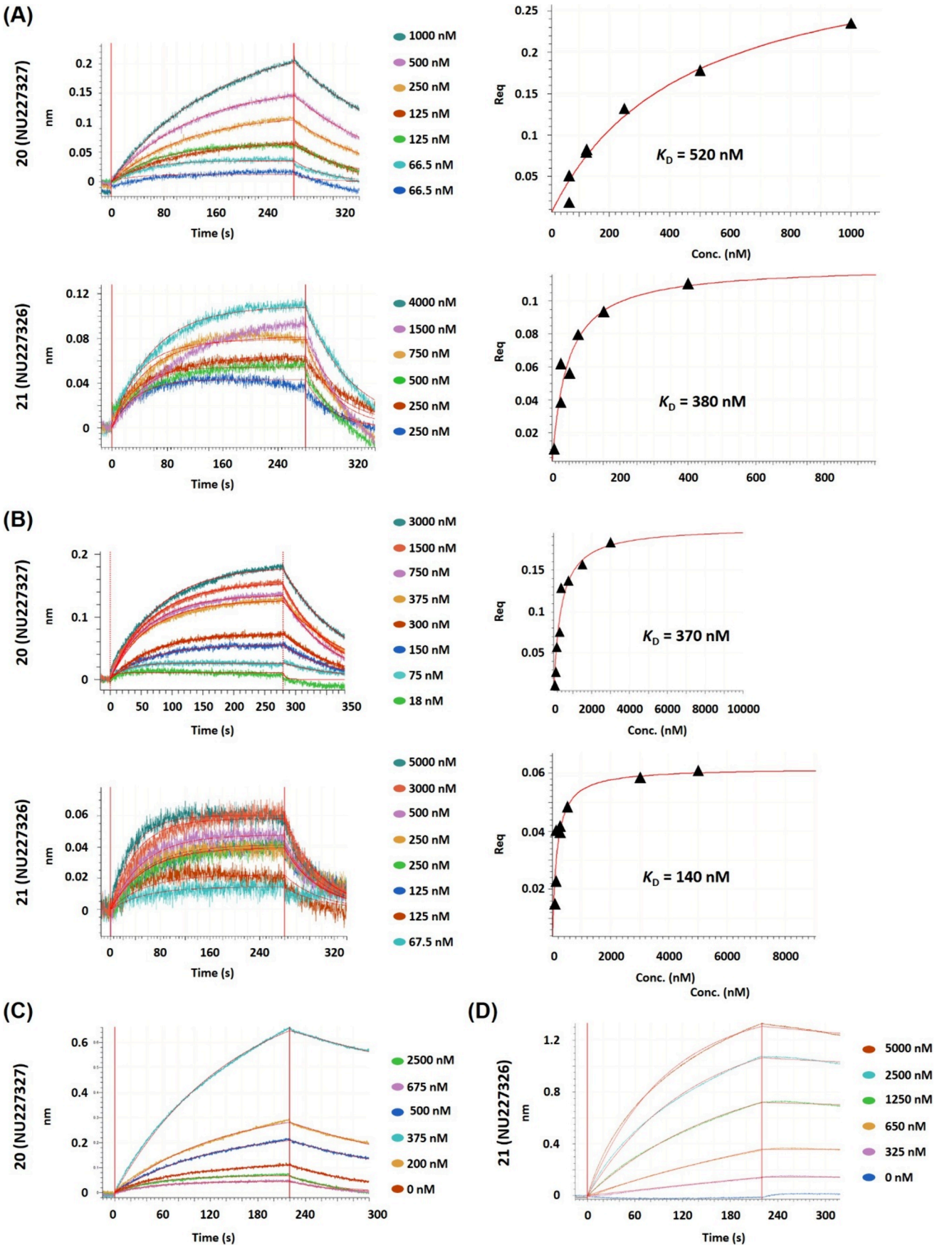

Figure 8. (A) Left: BLI sensorgrams showing association and dissociation of compounds **20** (**NU227327**) (upper) and **21** (**NU227326**) (lower) with CRBN (immobilized on AR2G sensors). Steady-state data fitted as described above yielded K_d values of 520 ± 106 nM and 380 ± 63 nM for the binary complexes formed by CRBN with **20** and **21**, respectively. (B) Left: BLI sensograms showing association and dissociation of compounds **20**

https://doi.org/10.1021/acs.jmedchem.5c00026
J. Med. Chem. XXXX, XXX, XXX−XXX

Figure 8. continued

(**NU227327**) (upper) and **21** (**NU227326**) (lower) to IDO1 protein (loaded on NI NTA sensors). Right: For each complex, the equilibrium dissociation constant (K_d) was obtained by fitting the steady state data (Req as a function of compound concentration) with a 1:1 binding model. The measured affinities for the binary complexes formed by IDO1 with compounds **20** and **21** were determined to be 370 ± 62 nM and 240 ± 49 nM, respectively. (C) BLI sensograms monitoring the association and dissociation kinetics of IDO1-**20**-CRBN (left) and IDO1-**21**-CRBN (right) ternary complexes. IDO1 protein was loaded on NiNTA biosensors. Double-referenced data sets fitted globally with a 1:1 kinetic model yielded K_d values of 321 ± 54 nM for IDO1-**21**-CRBN and 997 ± 143 nM for IDO1-**20**-CRBN. The k_{off} values obtained from the kinetic fits translate into the following lifetimes ($t_{1/2}$): IDO1-**20** binary = 53 s, IDO1-**20**-CRBN ternary = 256 s; IDO1-**21** binary = 38.6 s, IDO1-**21**-CRBN ternary = 1039 s.

exit vector orientation. Following similar procedures, the ternary IDO1-PROTAC-CRBN complex could be characterized. IDO1 degraders **20** and **21** were preincubated with an excess of CRBN to provide a PROTAC-CRBN binary complex. Binding of the resulting PROTAC-CRBN binary complex to IDO1 was detected and measured in real-time using BLI (Figure 8C). Interestingly, degrader **21** possessed a stronger ternary complex compared to degrader **20**, with binding affinities of 321 nM and 997 nM, respectively. Analog **21** also exhibited a more stable ternary interaction as evidenced by a longer half-life ($t_{1/2}$) of 1039 s compared to a 256 s half-life for analog **20**. This enhancement in ternary complex formation and stability for degrader **21** over degrader **20** may be attributable to the loss in flexibility of the linker moiety via loss of a methylene unit between the piperazine and piperidine ring systems. Furthermore, the more desirable ternary complex interaction of **21** is consistent with the slightly increased potency of **21** compared to **20**.

Pharmacokinetics of 21 (NU227326). To characterize its suitability for future use in *in vivo* experiments, we measured the mouse pharmacokinetics of degrader **21** (**NU227326**) in plasma and brain tissue. After identifying 50 mg/kg as the maximum dose that could be administered without producing clinical signs of toxicity, 50 mg/kg was dosed intraperitoneally (IP) in mice and the resulting plasma and brain homogenate drug concentrations were measured (Figure 9). Initial studies tested

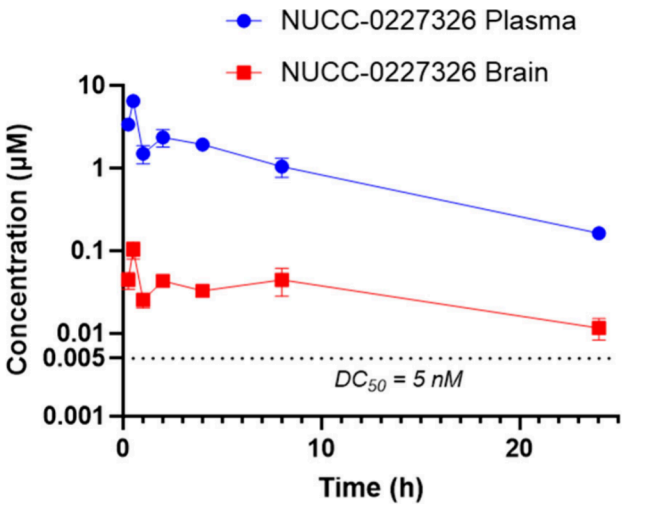

Compound	Dose (mg/kg)	$T_{1/2}$ (h)	T_{max} (h)	C_{max} (μM)	$AUC_{0-\infty}$ (μM·h)	MRT_{INF} (h)	CL/F_obs (mg/kg)/μM/h
NUCC-0227326 (plasma)	50	5.7	0.5	6.5	26.9	7.1	1.9
NUCC-0227326 (brain)	50	11.8	0.5	0.1	1.0	15.0	51.4

Figure 9. Pharmacokinetics of **NU227326** (**21**) in mice. Compound was dosed at 50 mg/kg by IP in mice.

NU227326 for oral bioavailability using oral gavage administration but found very little plasma exposure (data not shown). Degrader **NU227326** was found to have a favorable half-life (5.7 h) in plasma and was retained in brain tissue for approximately twice as long ($t_{1/2}$ = 11.8 h). Similar to virtually all other PROTACs described to date, **NU227326** has a limited ability to cross the blood-brain barrier (BBB). Total drug exposure in the brain was 1.0 μM·h, with a C_{max} of 0.1 μM, which indicated 4% of drug was able to cross the BBB. We also tested the PK of compound **NU227327** (**20**) and found it had lower plasma exposure, but a greater ability to cross the BBB, with total brain exposure being 10% of that in plasma (Supplementary Figure 4). Both compounds were >99% plasma protein bound as measured by a 6 h rapid equilibrium dialysis.

Chemistry. IDO1 PROTACs **6**–**23** were all designed to embody a piperidine ring unit as an attachment anchor for the linker to the IDO1 ligand. Therefore, to provide an efficient route toward diversification of the degrader structures, the synthesis of piperidine-containing IDO1 ligands to provide an amine building block for amide coupling was of interest. This strategy would allow for early stage functionalization of the E3 ligase ligand with various linker motifs, simplifying the syntheses of the new IDO1 degraders.

To synthesize both the 4-chloro-3-substituted and 3-susbtituted type IDO1 ligand building blocks, alkylation of phenol **25** or **26** with *tert*-butyl 4-((methylsulfonyl)oxy)-piperidine-1-carboxylate under basic conditions provided aryl nitro intermediates **27** and **28** in moderate to good yields, 90% and 60% respectively (Scheme 1). Selective reduction of the aryl nitro groups via catalytic hydrogenation using palladium on carbon afforded aryl amines **29** and **30**, which were taken forward without further purification. Both intermediates were reacted with previously described (*R*)-2-((1*S*,4*S*)-4-(6-fluoroquinolin-4-yl)cyclohexyl)propanoic acid[49] under amide coupling EDCI conditions followed by acid-mediated Boc-removal to provide 4-chloro-3-substituted (**31**) and 3-susbtituted (**32**) piperidine analogs.

With the IDO1 binder building blocks in hand, the bifunctionalized CRBN-linker components and subsequent final degraders were synthesized. Final targets, **7**–**9**, were synthesized by first performing a nucleophilic aromatic substitution between either 4-fluoro- or 5-fluororo-thalidomide, **33** and **34**, and amino-PEG_2-acid-*tert*-butyl ester in the presence of DIPEA (Scheme 2). Following an acid-mediated removal of the *tert*-butyl group to afford carboxylic acids **35** and **36**, the desired bifunctionalized derivatives were coupled with the previously synthesized 4-substituted amine or the 4-chloro-3-substituted amine (**31**) to provide the corresponding final PROTACs.

Introduction of the rigid linkers first involved implementing a piperazine ring connector to the E3 ligase ligand. Therefore, treatment of either **33** or **34** with *N*-Boc-piperazine under SnAr conditions followed by deprotection with TFA yielded 4-

https://doi.org/10.1021/acs.jmedchem.5c00026
J. Med. Chem. XXXX, XXX, XXX−XXX

Scheme 1. Synthesis of 4-Chloro-3-substituted and 3-Substitutied Piperidine IDO1 Binder Building Blocks 31 and 32[a]

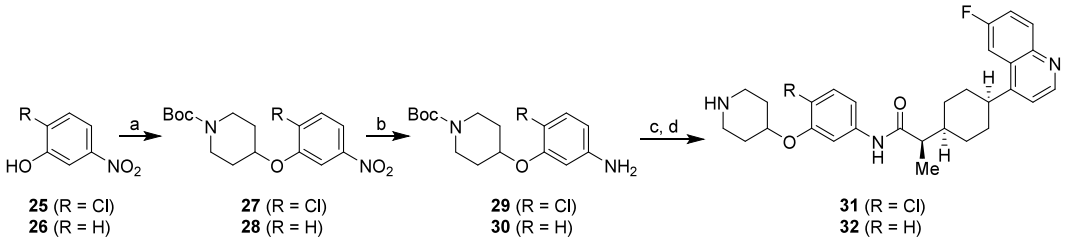

[a]Reagents and conditions: (a) *tert*-butyl 4-((methylsulfonyl)oxy)piperidine-1-carboxylate, K_2CO_3, DMF, 75 °C, 12 h; (b) Pd/C, H_2 (g), EtOH, 23 °C, 24−36 h; (c) (*R*)-2-((1*S*,4*S*)-4-(6-fluoroquinolin-4-yl)cyclohexyl)propanoic acid, EDCI, pyridine, 0 to 23 °C, 12 h; (d) 4 N HCl in dioxane, 23 °C, 12 h.

Scheme 2. Synthesis of IDO1 Degraders 7−9[a]

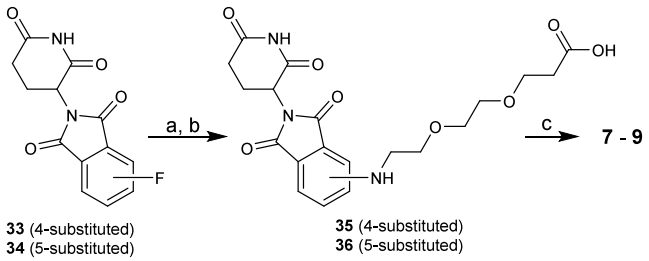

[a]Reagents and conditions: (a) *tert*-butyl 3-(2-(2-aminoethoxy)-ethoxy)propanoate, DIPEA, DMF, 75 °C, 12−48 h; (b) CF_3COOH, CH_2Cl_2, 0 to 23 °C, 1 h; (c) (R)-2-((1*S*,4*S*)-4-(6-fluoroquinolin-4-yl)cyclohexyl)-N-(4-(piperidin-4-yloxy)phenyl)propanamide or **31**, HATU, DIPEA, DMF, 0 to 23 °C, 6−12 h.

piperazine and 5-piperazine-thalidomide derivatives, **37** and **38**, in excellent yields (98% and 85%) (Scheme 3). Further functionalization of the piperazine intermediates via DIPEA promoted *N*-alkylation with *tert*-butyl 3-(2-iodoethoxy)-propanoate and subsequent Boc removal afforded the desired acid intermediates, **39** and **40**. Amidation with the corresponding piperidine functionalized IDO1 ligands resulted in the formation of final degraders **10**−**13**. Incorporation of an entire rigid linker was achieved with further derivatization of thalidomide-piperazine intermediates, **37** and **38**. Therefore, through *N*-alkylation with *tert*-butyl 4-(bromomethyl)-piperidine-1-carboxylate in the presence of DIPEA followed by acid mediated Boc removal, 4- and 5-thalidomide-piperazine-methylene-piperidine intermediates, **41** and **42**, respectively, were synthesized. Additionally, subjecting **38** to a reductive amination protocol with 1-Boc-4-piperidone and subsequent deprotection with TFA yielded 5-thalidomide-piperazine-piperidine intermediate, **43**. Piperidine analogs **41**−**43** were then treated with *tert*-butyl 2-bromoacetate and DIPEA to provide *N*-alkylated intermediates which upon acid-mediated removal of the *tert*-butyl group provided acids **44**−**46**. Amide coupling between the bifunctionalized acids with the previously described piperidine IDO1 intermediates provided the target IDO1 PROTACs **14**−**21**.

Truncated PROTACs, **22** and **23**, were synthesized according to Scheme 4. Utilizing the 5-piperazine-thalidomide derivative, **38**, *N*-alkylation with either *tert*-butyl 2-bromoacetate or *tert*-butyl 3-bromopropionate under basic conditions followed by deprotection to the acid yielded the corresponding intermediates, **47** and **48**. Subsequent amide coupling with the 3-substituted piperidine, **38**, resulted in the formation of target degraders **22** and **23**.

Synthesis of the inactive PROTAC, **24**, was achieved through methylation of the glutarimide nitrogen of the 5-fluoro-thalidomide starting material (**34**) with methyl iodide and potassium carbonate to provide **49** in 82% yield (Scheme 5). With *N*-Boc-piperazine, an SnAr reaction followed by acid-mediated deprotection yielded intermediate **50** in excellent yield. Reductive amination with 1-Boc-4-piperidone and sodium triacetoxyborohydride formed the desired piperazine-piperidine connectivity. Acid mediated Boc removal with TFA provided free amine **51**, which was alkylated with *tert*-butyl 2-bromoacetate under basic conditions. Subsequent cleavage of the *tert*-butyl group yielded carboxylic acid **52**. The final amide coupling with the previously synthesized 3-substituted piperidine intermediate (**32**) afforded the desired, inactive PROTAC **24**.

DISCUSSION

Indoleamine 2,3 dioxygenase 1 (IDO1) is highly expressed in many intractable cancers including prostate, pancreatic, ovarian, colorectal, and glioblastoma (GBM).[50] The relationship between IDO1 and its potent inhibition of the anticancer immune response is well-established.[12,51] The genetic knockdown of IDO1 in glioma cells leads to the spontaneous eradication of bulk tumor mass through a T cell-dependent mechanism.[18,52,18,52] In addition, IDO1-expressing nontumor cells also inhibit the antitumor immune response.[17] While IDO1 is not normally expressed at high levels throughout a majority of tissues including the brain, human GBM-infiltrating T cells induce significant IDO1 expression in the bulk tumor mass.[53] Furthermore, GBM cell IDO1 cDNA expression increases intratumoral Treg levels over that of GBM cells without forced IDO1 expression, and importantly, the IDO1-mediated recruitment of immunosuppressive Tregs is not reversed with the treatment of a potent IDO1 enzyme inhibitor.[34] Similarly, glioma cell expression of both wild-type IDO1 cDNA leading to enzymatically active IDO1 protein expression, as well as, mutant IDO1 cDNA leading to enzymatically inactive IDO1 protein expression, similarly increase intratumoral Treg levels compared to the effects of IDO1-deficient glioma cells that express an empty cDNA vector.[25] Notably, although the IDO1 enzyme inhibitor fails to improve survival in older wild-type (WT) mice, similarly treated age-matched older adult IDO1KO mice demonstrate a significantly improved overall survival,[24] suggesting that the genetic absence of IDO1 in nontumor cells synergizes with RT + PD-1 mAb during old age and that this beneficial effect is not recapitulated with an IDO1 enzyme inhibitor. Collectively, the data suggest that an IDO1 PROTAC targeting tumor cell-derived and nontumor cell-derived IDO1

https://doi.org/10.1021/acs.jmedchem.5c00026
J. Med. Chem. XXXX, XXX, XXX−XXX

Scheme 3. Synthesis of IDO1 Degraders 10−21[a]

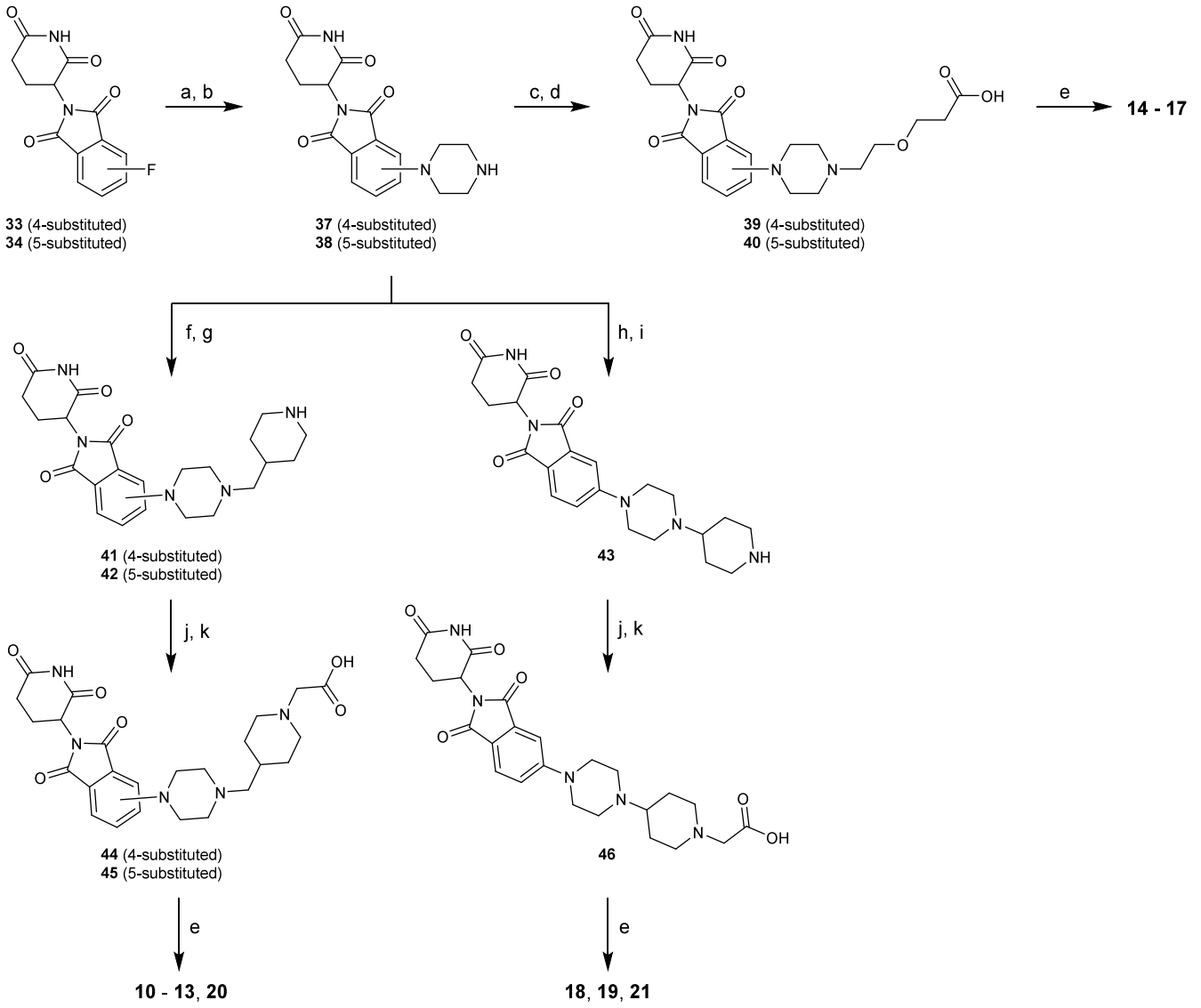

[a]Reagents and conditions: (a) *tert*-butyl piperazine-1-carboxylate, DIPEA, DMSO, 100 °C, 12 h; (b) CF_3COOH, CH_2Cl_2, 0 to 23 °C, 1 h; (c) *tert*-butyl 3-(2-iodoethoxy)propanoate, DIPEA, DMF, 75 °C, 24 h; (d) CF_3COOH, CH_2Cl_2, 0 to 23 °C, 1 h; (e) (c) (R)-2-((1*S*,4*S*)-4-(6-fluoroquinolin-4-yl)cyclohexyl)-N-(4-(piperidin-4-yloxy)phenyl)propanamide, **31** or **32**, HATU, DIPEA, DMF, 0 to 23 °C, 1.5−24 h; (f) *tert*-butyl 4-(bromomethyl)piperidine-1-carboxylate, DIPEA, DMF, 75 °C, 12 h; (g) CF_3COOH, CH_2Cl_2, 0 to 23 °C, 1−2.5 h; (h) *tert*-butyl 4-oxopiperidine-1-carboxylate, STAB, DMF, 23 °C, 2 h; (i) CF_3COOH, CH_2Cl_2, 0 to 23 °C, 1 h; (j) *tert*-butyl 2-bromoacetate, DIPEA, DMF, 23 °C, 2−3 h; (k) CF_3COOH, CH_2Cl_2, 0 to 23 °C, 2−4 h; (l) (c) (R)-2-((1*S*,4*S*)-4-(6-fluoroquinolin-4-yl)cyclohexyl)-N-(4-(piperidin-4-yloxy)phenyl)propanamide, **31** or **32**, HATU or T3P, DIPEA, DMF, 0 to 23 °C, 1−48 h.

will possess a maximum net survival benefit for older adults with GBM. Based on the increased immunosuppression mediated by both IDO1 enzymatic and nonenzymatic functions of, we sought to develop IDO1 PROTACs to abolish all of these functions. We previously reported a first generation IDO1 PROTAC that possesses *in vivo* efficacy in a mouse model with intracranial GBM.[39] That work motivated us to refine and optimize our IDO1 PROTAC into more potent and effective degraders.

Here, we describe our work in rationally designing and synthesizing a new series of potent IDO1 PROTACs. Using insights gained from molecular modeling studies, we designed new compounds that allowed more favorable binding to IDO1 and allowed more efficient access of the linker to the solvent. We also incorporated more rigid linkers to improve ternary complex formation and to increase pharmaceutical properties. Our improved compound described in this work, **NU227326** (**21**), has a 5 nM IDO1 DC_{50} in U87 cells and is similarly potent in PDX GBM43 cells. NU227326 further demonstrated generalizability for IDO1 protein degradation across many types of human cancers including additional human PDXs for GBM6 and GBM38, pediatric GBM KNS-42, prostate cancer line PC-3, breast cancer line MDA-MB-231, pancreatic cancer line SW-1990, as well as ovarian cancer line SKOV-3. The compound shows the expected reliance on CRBN and the ubiquitin-proteasome system for its degradation. We also found that in both U87 and GBM43 cells, the degrader **NU227326** blocks kynurenine production through a combination of IDO1 inhibition and IDO1 degradation, as the potency of this compound is significantly greater than the inactive control

https://doi.org/10.1021/acs.jmedchem.5c00026
J. Med. Chem. XXXX, XXX, XXX−XXX

Scheme 4. Synthesis of IDO1 Degraders 22 and 23[a]

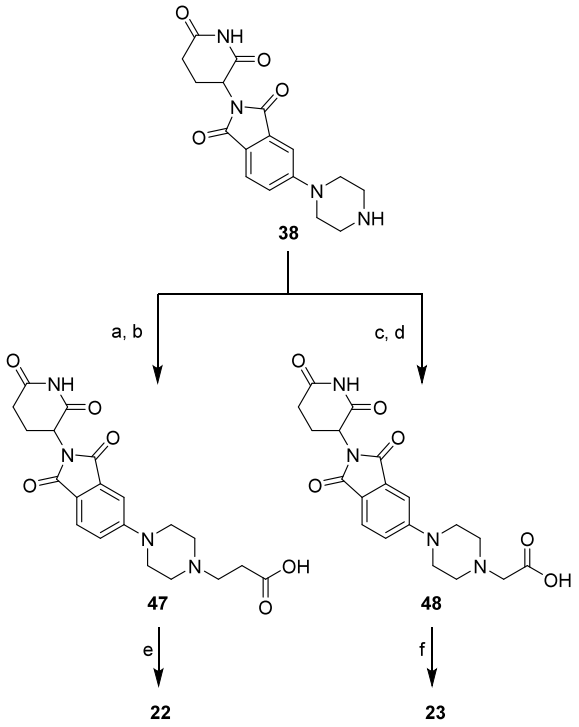

[a]Reagents and conditions: (a) *tert*-butyl 3-bromopropionate, DIPEA, DMF, 23 °C, 12 h; (b) CF_3COOH, CH_2Cl_2, 0 to 23 °C, 24 h; (c) *tert*-butyl 2- bromoacetate, DIPEA, DMF, 23 °C, 2 h; (d) CF_3COOH, CH_2Cl_2, 0 to 23 °C, 24 h; (e) **37**, HATU, DIPEA, DMF, 0 to 23 °C, 30 min.

compound **24** which cannot engage cereblon and degrade IDO1 protein. We also found that **NU227326** achieves profound IDO1 degradation for at least 48 h after washout from U87 cells and confirms a long-lasting effect. We also developed a HiBiT-based assay in U87 GBM cells to enable quantitative measurement of IDO1 degradation which provided orthogonal confirmation of **NU227326**'s potency. Compound **NU227326** was tested for mouse PK and we found it possessed favorable half-life and plasma exposure. It also crossed the BBB with 4% penetration. A closely related IDO1 degrader we describe here (**20**, **NU227327**) was found to achieve 10% brain penetration, suggesting this series of degraders has the ability for further structural optimization of brain exposure. Finally, to define the selectivity of our lead compounds and identify any off-targets that are degraded, global quantitative proteomics were performed. Proteomics showed that both **NU227326** and **NU227327** significantly degraded ≤5 non-IDO1 proteins, indicating a high degree of selectivity. Notably, SALL4, which is a common cereblon neosubstrate, was degraded by both compounds. Ongoing work by our group aims to characterize the *in vivo* effects of our new IDO1 degrader **NU227326** on the tumor- and nontumor immune response in immunocompetent GBM tumor models across the lifespan.

EXPERIMENTAL SECTION

General Chemical Methods. All chemical reagents were acquired from commercial suppliers and utilized without further purification. Reactions were completed without taking precautions to exclude air or moisture, unless otherwise noted. Normal-phase column chromatography was performed using silica gel columns and ACS grade solvents. ^{1}H NMR and ^{13}C NMR spectroscopy were recorded on Bruker 400 MHz or Bruker Avance III 500 MHz spectrometers. The chemical shifts for ^{1}H NMR are reported to the second decimal place in parts per million (ppm). Proton coupling constants are expressed in hertz (Hz). Standard abbreviations were used to denote spin multiplicity for ^{1}H NMR data. The chemical shifts for ^{13}C NMR are reported to the first decimal place in ppm. The representative residual solvent peaks ($CDCl_3$, ^{1}H δ = 7.27 ppm, ^{13}C δ = 77.16 ppm; CD3OD-d_4, ^{1}H δ = 3.31 ppm, ^{13}C δ = 49.00 ppm; DMSO-d_6, ^{1}H δ = 2.50 ppm, ^{13}C δ = 39.52 ppm) were used as an internal standard. High- resolution mass spectrometry (HRMS) values were measured and calculated with an Agilent 6545 QTOF mass spectrometer coupled with an Agilent 1200 series LC, with direct loop injection (no column). All compounds presented in the manuscript are >95% pure by HPLC analysis.

***tert*-Butyl 4-(2-Chloro-5-nitrophenoxy)piperidine-1-carboxylate (27).** To a solution of *tert*-butyl 4-((methylsulfonyl)oxy)-piperidine-1-carboxylate (3.0 g, 0.01 mol, 2.0 equiv) and **25** (1.0 g, 0.01 mol, 2.0 equiv) in DMF (15 mL) was added K_2CO_3 (2.0 g, 0.01 mol, 2.0 equiv). The resulting mixture was stirred at 75 °C for 12 h. The reaction mixture was allowed to cool to 23 °C and then diluted with DI water (20 mL). The resulting mixture was extracted with EtOAc (3 × 20 mL), and the organic layers were combined, washed with brine (2 × 30 mL), dried over anhydrous $MgSO_4$, filtered, and concentrated under reduced pressure. The crude product was purified by column chromatography (SiO_2, hexanes/EtOAc, 100:0 to 50:50) to give **27** (1.9 g, 90%) as an off white solid. ^{1}H NMR (500 MHz, $CDCl_3$) δ 7.83–7.76 (m, 2H), 7.53 (d, J = 8.5 Hz, 1H), 4.69 (tt, J = 6.6, 3.4 Hz, 1H), 3.64 (ddd, J = 12.7, 8.5, 3.7 Hz, 2H), 3.52 (dd, J = 12.6, 6.9 Hz, 2H), 1.96 (td, J = 9.1, 4.3 Hz, 2H), 1.87 (ddt, J = 10.8, 7.1, 3.9 Hz, 2H), 1.48 (s, 9H). Spectral data matched previously reported characterization data.[54]

Scheme 5. Synthesis of Inactive IDO1 PROTAC 24[a]

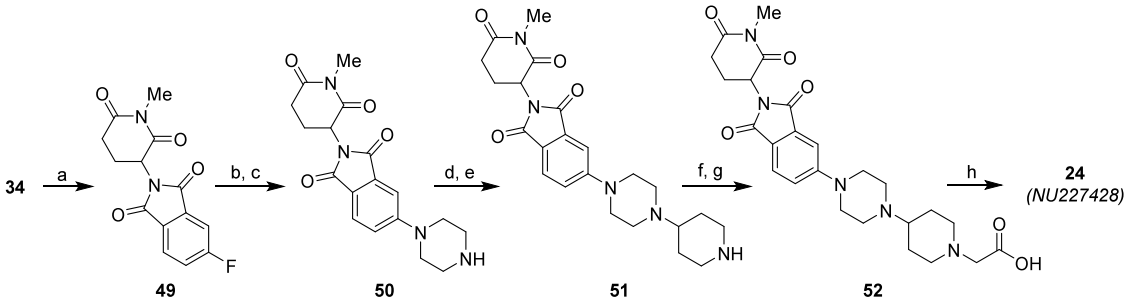

[a]Reagents and conditions: (a) MeI, K_2CO_3, DMF, 0 to 23 °C, 12 h, 82%; (b) *tert*-butyl piperazine-1-carboxylate, DIPEA, DMSO, 100 °C, 2.5 h, 90%; (c) CF_3COOH, CH_2Cl_2, 0 to 23 °C, 2 h, 90%; (d) *tert*-butyl 4-oxopiperidine-1-carboxylate, STAB, DMF, 23 °C, 1.5 h; (e) CF_3COOH, CH_2Cl_2, 0 to 23 °C, 12 h, 77% over 2 steps; (f) *tert*-butyl 2-bromoacetate, DIPEA, DMF, 23 °C, 12 h; (g) CF_3COOH, CH_2Cl_2, 0 to 23 °C, 4 h, 72% over 2 steps; (h) **32**, HATU, DIPEA, DMF, 0 to 23 °C, 30 min, 48%.

https://doi.org/10.1021/acs.jmedchem.5c00026
J. Med. Chem. XXXX, XXX, XXX−XXX

***tert*-Butyl 4-(3-Nitrophenoxy)piperidine-1-carboxylate (28).** To a solution of *tert*-butyl 4-((methylsulfonyl)oxy)piperidine-1-carboxylate (4.0 g, 0.01 mol, 2.0 equiv) and **26** (1.0 g, 7.0 mmol, 1.0 equiv) in DMF (20 mL) was added K_2CO_3 (2.0 g, 0.01 mol, 2.0 equiv). The resulting mixture was stirred at 75 °C for 12 h. Upon completion of the reaction, the mixture was allowed to cool to 23 °C, diluted with DI water, and extracted with EtOAc (3 × 15 mL). The organic layers were combined, washed with brine (1 × 30 mL), dried over anhydrous $MgSO_4$, and concentrated *in vacuo*. The crude residue was purified by column chromatography (SiO_2, hexanes/EtOAc, 100:0 to 50:50) to yield **28** (1.5 g, 60%) as a yellow oil. Spectral data matched previously reported characterization data.[55]

***tert*-Butyl 4-(5-Amino-2-chlorophenoxy)piperidine-1-carboxylate (29).** To a solution of **27** (850 mg, 2.38 mmol, 1.0 equiv) in EtOH (30 mL) was added Pd/C (12.7 mg, 10% Pd on charcoal, wet, containing 50% H_2O) (catalytic) at 23 °C. The reaction was fitted with a hydrogen balloon and allowed to stir at 23 °C for 36 h. The resulting mixture was filtered through a Celite pad with EtOH rinses and the filtrate was concentrated to yield **29** (720 mg, 92%) as a yellow oil. Spectral data matched previously reported characterization data.[54]

***tert*-Butyl 4-(3-Aminophenoxy)piperidine-1-carboxylate (30).** To a solution of **28** (1.5 g, 4.7 mmol, 1.0 equiv) in EtOH (4 mL) was added Pd/C (50 mg, 10% Pd on charcoal, wet, containing 50% H_2O) (catalytic) at 23 °C. The reaction mixture was fitted with a hydrogen gas balloon and allowed to stir at 23 °C for 24 h. The resulting mixture was filtered through a Celite pad with EtOH rinse, and the filtrate was concentrated under reduce pressure to provide **28** (1.0 g, 70%) as a yellow oil. Spectral data matched previously reported characterization data.[56] The product was taken forward without further purification.

(*R*)-*N*-(4-Chloro-3-(piperidin-4-yloxy)phenyl)-2-((1*S*,4*S*)-4-(6-fluoroquinolin-4-yl)cyclohexyl)propenamide (31). To a solution of **29** (4.0 g, 0.01 mol, 1.0 equiv) and (*R*)-2-((1*S*,4*S*)-4-(6-fluoroquinolin-4-yl)cyclohexyl)propanoic acid (3.0 g, 0.01 mmol, 1.0 equiv) in pyridine (20 mL) was added EDCI (3 g, 0.01 mmol, 1.5 equiv) at 0 °C. The resulting mixture was allowed to stir at 23 °C for 12 h. The reaction was poured into 1 N HCl (100 mL) and extracted with EtOAc (3 × 75 mL). The combined organic layers were washed with 1 N HCl (3 × 30 mL), Sat Na_2CO_3 solution (3 × 50 mL), dried over anhydrous $MgSO_4$, filtered and concentrated under reduced pressure to provide *tert*-butyl 4-(2-chloro-5-((*R*)-2-((1*S*,4*S*)-4-(6-fluoroquinolin-4-yl)cyclohexyl)propanamido)phenoxy)piperidine-1-carboxylate as an orange residue. The resulting product was taken forward without additional purification. To a solution of the crude *tert*-butyl 4-(2-chloro-5-((*R*)-2-((1*S*,4*S*)-4-(6-fluoroquinolin-4-yl)cyclohexyl)-propanamido)phenoxy)piperidine-1-carboxylate in 1,4-dioxane (5 mL) was added a solution HCl/Dioxane (10 mL, 4 molar). The resulting mixture was allowed to stir at 23 °C overnight. Upon reaction completion, the mixture was diluted with cold Et_2O and the solid precipitate was collected via vacuum filtration to yield **31** (4 g, 70% over two steps) as a dark yellow solid. ^{1}H NMR (DMSO, 500 MHz): δ = 10.77 (s, 1H), 9.22 (d, 1H, J = 4.4 Hz), 9.08 (s, 1H), 8.53−8.17 (m, 3H), 8.04 (dt, 1H, J = 26.6, 7.8 Hz), 7.85 (t, 1H, J = 1.4 Hz), 7.45−7.14 (m, 2H), 4.62 (tt, 1H, J = 6.9, 3.2 Hz), 3.68−3.57 (m, 1H), 3.23−3.17 (m, 2H), 3.11 (d, 3H, J = 11.8 Hz), 2.29−2.08 (m, 3H), 1.98−1.57 (m, 10H), 1.12 (d, 3H, J = 6.6 Hz) ppm. ^{13}C NMR (126 MHz, DMSO) δ 175.4, 162.0, 160.0, 151.8, 145.7, 142.4, 139.6, 130.0, 128.1, 128.0, 127.1, 122.8, 122.6, 120.0, 116.4, 113.2, 108.8, 108.6, 107.4, 70.7, 48.6, 38.6, 35.5, 28.4, 27.8, 27.1, 27.0, 26.9, 26.2, 16.3 ppm. HRMS (m/z): $[M + H]^+$ calcd. for $C_{29}H_{34}ClFN_3O_2$ 510.2324; found, 510.2337.

(*R*)-2-((1*S*,4*S*)-4-(6-Fluoroquinolin-4-yl)cyclohexyl)-*N*-(3-(piperidin-4-yloxy)phenyl)propenamide (32). To a solution of **30** (1.0 g, 4.0 mmol, 1.0 equiv) and (*R*)-2-((1*S*,4*S*)-4-(6-fluoroquinolin-4-yl)cyclohexyl)propanoic acid (1.0 g, 3.0 mmol, 1.0 equiv) in pyridine (15 mL) was EDCI (1.0 g, 5.0 mmol, 1.5 equiv) at 0 °C. The resulting mixture was allowed to stir at 23 °C overnight. The resulting mixture was poured into 1 N HCl (75 mL) and extracted with EtOAc (3 × 50 mL). The organic layers were combined, washed with 1 N HCl (3 × 30 mL), Sat Na_2CO_3 solution (3 × 50 mL), dried over anhydrous $MgSO_4$, filtered, and concentrated *in vacuo* to a provide a brown residue. The crude mixture was purified by column chromatography (SiO_2, hexanes/EtOAc, 100:0 to 50:50) to provide *tert*-butyl 4-(3-((*R*)-2-((1*S*,4*S*)-4-(6-fluoroquinolin-4-yl)cyclohexyl)propanamido)phenoxy)piperidine-1-carboxylate (700 mg, 40%) as a yellow solid. ^{1}H NMR (500 MHz, $CDCl_3$) δ 8.76 (d, J = 4.6 Hz, 1H), 8.10 (dd, J = 9.2, 5.6 Hz, 1H), 8.04 (s, 1H), 7.63 (dd, J = 10.5, 2.8 Hz, 1H), 7.51−7.40 (m, 2H), 7.28 (d, J = 4.6 Hz, 1H), 7.17 (t, J = 8.1 Hz, 1H), 7.01 (d, J = 8.0 Hz, 1H), 6.68−6.58 (m, 1H), 4.45 (dt, J = 7.0, 3.6 Hz, 1H), 3.64 (ddd, J = 13.4, 7.7, 3.7 Hz, 2H), 3.31 (ddt, J = 16.0, 8.0, 3.9 Hz, 3H), 2.63 (dd, J = 10.9, 6.7 Hz, 1H), 2.18−2.09 (m, 1H), 1.92−1.58 (m, 12H), 1.46 (s, 9H), 1.29−1.24 (m, 3H) ppm. To *tert*-butyl 4-(3-((*R*)-2-((1*S*,4*S*)-4-(6-fluoroquinolin-4-yl)cyclohexyl)propanamido)phenoxy)piperidine-1-carboxylate (700 mg, 1.22 mmol, 1.0 equiv) was added a solution of TFA:CH_2Cl_2 (1:1, 3 mL) at 0 °C. The resulting mixture was stirred at 23 °C for 2 h. The reaction mixture was concentrated under nitrogen atmosphere and the crude residue was triturated with cold Et_2O (2 × 15 mL) to provide pure **32** (650 mg, 90.8%) as an orange solid. ^{1}H NMR (500 MHz, DMSO-d_6) δ 10.07 (s, 1H), 9.00 (d, J = 4.9 Hz, 1H), 8.69 (d, J = 36.0 Hz, 2H), 8.16 (ddd, J = 32.8, 10.0, 4.3 Hz, 2H), 7.79 (ddd, J = 22.5, 11.2, 3.8 Hz, 2H), 7.48 (s, 1H), 7.29−7.05 (m, 2H), 6.78−6.59 (m, 1H), 4.59 (tt, J = 7.1, 3.2 Hz, 1H), 3.59−3.43 (m, 1H), 3.11 (p, J = 6.1, 5.2 Hz, 2H), 2.90 (dq, J = 13.5, 7.0 Hz, 1H), 2.20−1.53 (m, 14H), 1.12 (d, J = 6.6 Hz, 3H) ppm. ^{13}C NMR (126 MHz, DMSO) δ 175.0, 161.4, 159.4, 159.0, 158.7, 158.4, 158.1, 156.8, 156.4, 148.0, 141.9, 140.6, 130.2, 129.6, 127.6, 120.8, 120.6, 119.1, 117.4, 115.1, 112.2, 110.2, 108.0, 107.8, 107.4, 68.9, 40.5, 38.0, 35.6, 28.5, 27.626 27.3, 27.2, 26.3, 16.2 ppm. $[M + H]^+$ calcd. for $C_{29}H_{35}FN_3O_2$ 476.2713; found, 476.2724.

3-(2-(2-((2-(2,6-Dioxopiperidin-3-yl)-1,3-dioxoisoindolin-4-yl)amino)ethoxy)ethoxy)propanoic Acid (35). To a solution of *tert*-butyl 3-(2-(2-aminoethoxy)ethoxy)propanoate (150 mg, 643 μmol, 1.0 equiv) in DMF (3 mL) was added DIPEA (83.1 mg, 112 μL, 643 μmol, 1.0 equiv) followed by the addition of **33** (213 mg, 772 μmol, 1.2 equiv). The mixture was stirred at 75 °C for 12 h. After cooling to 23 °C, the mixture was diluted with DI water (10 mL) and extracted with EtOAc (3 × 10 mL). The combined organic layers were washed with brine (2 × 20 mL), dried via filtration through an isolute phase separator, and concentrated under reduced pressure. The crude product was purified by column chromatography (SiO_2, CH_2Cl_2/acetone, 100:0 to 70:30) to provide *tert*-butyl 3-(2-(2-((2-(2,6-dioxopiperidin-3-yl)-1,3-dioxoisoindolin-4-yl)amino)ethoxy)ethoxy)-propanoate (80 mg, 25%). ^{1}H NMR (400 MHz, $CDCl_3$): δ 8.15 (br s, 1H), 7.50 (dd, J = 8.4, 7.2 Hz, 1H), 7.11 (d, J = 7.1 Hz, 1H), 6.93 (d, J = 8.5 Hz, 1H), 6.50 (br s, 1H), 4.92 (dd, J = 12.1, 5.3 Hz, 1H), 4.13 (q, J = 7.1 Hz, 1H), 3.75−3.70 (m, 4H), 3.68−3.62 (m, 4H), 3.47 (t, J = 5.4 Hz, 2H), 2.89−2.67 (m, 3H), 2.52 (t, J = 6.6 Hz, 2H), 2.16−2.09 (m, 1H), 1.45 (s, 9H) ppm. Spectral data matched previously reported characterization data.[57] To *tert*-butyl 3-(2-(2-((2-(2,6-dioxopiperidin-3-yl)-1,3-dioxoisoindolin-4-yl)amino)ethoxy)ethoxy)propanoate (80 mg, 0.16 mmol, 1.0 equiv) was added a 1:1 solution of TFA/CH_2Cl_2 (1 mL) at 0 °C. The reaction was allowed to stir at 23 °C for 1 h. The resulting mixture was concentrated under nitrogen atmosphere and the crude reside was triturated with cold Et_2O (3 × 5 mL). The resulting solid was dried under vacuum to provide pure **35** (80 mg, 90%) as a green solid. ^{1}H NMR (400 MHz, $CDCl_3$): δ 8.77 (s, 1H), 7.53−7.44 (m, 1H), 7.09 (d, J = 7.0 Hz, 1H), 6.91 (d, J = 8.5 Hz, 1H), 4.98−4.89 (m, 1H), 3.77 (t, J = 6.3 Hz, 2H), 3.74−3.71 (m, 2H), 3.66 (s, 4H), 3.46 (br t, J = 5.2 Hz, 2H), 2.91−2.70 (m, 3H), 2.64 (t, J = 6.3 Hz, 2H) 2.16−2.08 (m, 1H) ppm. Spectral data matched previously reported characterization data.[57]

3-(2-(2-((2-(2,6-Dioxopiperidin-3-yl)-1,3-dioxoisoindolin-5-yl)amino)ethoxy)ethoxy)propanoic Acid (36). To a solution of *tert*-butyl 3-(2-(2-aminoethoxy)ethoxy)propanoate (200 mg, 857 μmol, 1.0 equiv) in DMF (2 mL) was added DIPEA (111 mg, 149 μL, 857 μmol, 1.0 equiv) followed by **34** (284 mg, 1.03 mmol, 1.2 equiv). The resulting mixture was allowed to stir at 75 °C for 24 h. After cooling to 23 °C, the mixture was diluted with DI water (5 mL) and extracted with EtOAc (3 × 10 mL). The combined organic layers were washed with brine (2 × 15 mL), dried via filtration through an isolute phase separator and concentrated under reduced pressure. The crude

https://doi.org/10.1021/acs.jmedchem.5c00026
J. Med. Chem. XXXX, XXX, XXX−XXX

product was purified by column chromatography (SiO_2, CH_2Cl_2/acetone, 100:0 to 70:30) to provide *tert*-butyl 3-(2-(2-((2-(2,6-dioxopiperidin-3-yl)-1,3-dioxoisoindolin-5-yl)amino)ethoxy)ethoxy)-propanoate (50 mg, 13%) as a yellow solid. Spectral data matched previously reported characterization data.[58] To *tert*-butyl 3-(2-(2-((2-(2,6-dioxopiperidin-3-yl)-1,3-dioxoisoindolin-5-yl)amino)ethoxy)-ethoxy)propanoate (45 mg, 92 μmol, 1.0 equiv) was added a 1:1 solution of TFA/CH_2Cl_2 (1 mL) at 0 °C. The reaction was allowed to stir at 23 °C for 1 h. The resulting mixture was concentrated under nitrogen atmosphere and the crude reside was triturated with Et_2O (3 × 5 mL). The resulting solid was dried under vacuum to provide **36** (40 mg, 80%) as a green solid, which was taken forward without further purification. Spectral data matched previously reported characterization data.[58]

(2*R*)-*N*-(4-((1-(3-(2-(2-((2-(2,6-Dioxopiperidin-3-yl)-1,3-dioxoisoindolin-5-yl)amino)ethoxy)ethoxy)propanoyl)piperidin-4-yl)oxy)phenyl)-2-((1*S*,4*S*)-4-(6-fluoroquinolin-4-yl)cyclohexyl)-propenamide (7). To a solution of **36** (80 mg, 0.15 mmol, 1.0 equiv) in DMF (2 mL) was added HATU (67 mg, 0.18 mmol, 1.2 equiv) and DIPEA (57 mg, 76 μL, 0.44 mmol, 3.0 equiv) at 0 °C. The resulting mixture was allowed to stir at 23 °C for 30 min at which time (R)-2-((1*S*,4*S*)-4-(6-fluoroquinolin-4-yl)cyclohexyl)-N-(4-(piperidin-4-yloxy)phenyl)propanamide (75 mg, 0.15 mmol, 1.0 equiv) was added and the reaction was allowed to continue at 23 °C overnight. The crude product was directly purified by reverse phase HPLC eluting from 10% to 90% MeCN in water (0.1% TFA) to provide pure **7** (39 mg, 26%) as an orange solid. ^{1}H NMR (500 MHz, CD_3CN) δ 8.98 (d, *J* = 6.0 Hz, 2H), 8.41−8.37 (m, 2H), 8.19 (dd, *J* = 10.1, 2.7 Hz, 1H), 7.99 (d, *J* = 5.8 Hz, 1H), 7.91 (ddd, *J* = 9.4, 7.9, 2.7 Hz, 1H), 7.52−7.42 (m, 4H), 6.96 (dd, *J* = 8.0, 1.8 Hz, 1H), 6.84 (ddd, *J* = 17.4, 6.7, 2.6 Hz, 3H), 4.90 (ddd, *J* = 12.3, 5.4, 1.7 Hz, 1H), 4.48 (tt, *J* = 7.5, 3.6 Hz, 1H), 3.74−3.55 (m, 10H), 3.35 (dq, *J* = 20.9, 6.2 Hz, 4H), 2.78−2.56 (m, 6H), 2.08−1.97 (m, 3H), 1.91−1.51 (m, 12H), 1.20 (d, *J* = 6.7 Hz, 3H) ppm. ^{13}C NMR (126 MHz, CD_3CN) δ 175.2, 172.6, 170.3, 169.8, 168.4, 168.0, 163.0, 161.0, 160.8, 160.5, 155.0, 154.0, 145.7, 138.7, 135.1, 132.9, 129.2, 129.1, 127.6, 125.5, 123.4, 123.1, 122.0, 119.7, 117.0, 116.4, 115.8, 109.2, 109.0, 106.3, 73.1, 70.6, 70.5, 69.3, 67.6, 49.5, 43.4, 43.0, 41.5, 39.8, 38.9, 36.5, 33.6, 31.6, 31.5, 30.8, 29.0, 28.3, 27.9, 26.9, 22.9, 16.2. $[M + H]^+$ calcd. for $C_{49}H_{56}FN_6O_9$ 891.4093; found, 891.4098.

(2*R*)-*N*-(4-Chloro-3-((1-(3-(2-(2-((2-(2,6-dioxopiperidin-3-yl)-1,3-dioxoisoindolin-4-yl)amino)ethoxy)ethoxy)propanoyl)-piperidin-4-yl)oxy)phenyl)-2-((1*S*,4*S*)-4-(6-fluoroquinolin-4-yl)cyclohexyl)propenamide (8). To a solution of **35** (80 mg, 0.15 mmol, 1.0 equiv) in DMF (2 mL) was added HATU (67 mg, 0.18 mmol, 1.2 equiv) and DIPEA (57 mg, 76 μL, 0.44 mmol, 3.0 equiv) at 0 °C. The resulting mixture was allowed to stir at 23 °C for 30 min. **31** (80 mg, 0.15 mmol, 1.0 equiv) was then added and the resulting mixture was allowed to stir at 23 °C for 6 h. The resulting mixture was quenched with DI water (1 mL) and the resulting mixture was directly purified by reverse phase HPLC eluting from 10% to 90% MeCN in water (0.1% TFA) to provide pure **8** (31 mg, 22%) was collected as a yellow solid. ^{1}H NMR (500 MHz, CD_3CN) δ 9.08 (s, 1H), 8.99 (h, *J* = 4.0 Hz, 1H), 8.58 (s, 1H), 8.41 (dd, *J* = 9.3, 5.2 Hz, 1H), 8.08 (dd, *J* = 10.4, 2.8 Hz, 1H), 7.90−7.83 (m, 1H), 7.80 (ddd, *J* = 9.3, 7.9, 2.7 Hz, 1H), 7.58 (ddt, *J* = 7.4, 5.2, 2.7 Hz, 1H), 7.53−7.45 (m, 1H), 7.27 (dd, *J* = 8.6, 1.0 Hz, 1H), 7.10 (tt, *J* = 8.8, 2.1 Hz, 1H), 7.06−6.96 (m, 2H), 4.92 (dd, *J* = 12.5, 5.4 Hz, 1H), 4.57 (dt, *J* = 7.0, 3.5 Hz, 1H), 3.74−3.34 (m, 15H), 2.80−2.62 (m, 4H), 2.55 (tt, *J* = 6.3, 3.1 Hz, 2H), 2.13−1.97 (m, 3H), 1.93−1.60 (m, 12H), 1.20 (d, *J* = 6.8 Hz, 3H) ppm. ^{13}C NMR (126 MHz, CD_3CN) δ 176.3, 173.0, 170.6, 170.4, 170.2, 168.6, 163.4, 162.8, 161.5, 161.2, 160.9, 153.5, 147.8, 146.0, 139.9, 139.1, 137.0, 133.4, 131.0, 129.6, 129.5, 128.0, 127.9, 123.8, 123.5, 120.2, 116.2, 113.8, 111.7, 110.8, 109.6, 109.4, 108.5, 108.4, 79.2, 78.9, 78.7, 74.5, 71.0, 70.0, 68.2, 68.2, 49.8, 43.1, 42.9, 42.2, 40.2, 38.9, 36.8, 34.0, 32.0, 31.6, 31.0, 29.4, 28.8, 28.2, 27.3, 23.3, 16.6 ppm. $[M + H]^+$ calcd. for $C_{49}H_{55}ClFN_6O_9$ 925.3703; found, 925.3694.

(2*R*)-*N*-(4-Chloro-3-((1-(3-(2-(2-((2-(2,6-dioxopiperidin-3-yl)-1,3-dioxoisoindolin-5-yl)amino)ethoxy)ethoxy)propanoyl)-piperidin-4-yl)oxy)phenyl)-2-((1*S*,4*S*)-4-(6-fluoroquinolin-4-yl)cyclohexyl)propenamide (9). To a solution of **36** (40 mg, 73 μmol, 1.0 equiv) in DMF (2 mL) was added DIPEA (28 mg, 38 μL, 0.22 mmol, 3.0 equiv) and HATU (33 mg, 88 μmol, 1.2 equiv) at 0 °C. The resulting mixture was stirred at 23 °C for 15 min at which time **31** (40 mg, 73 μmol, 1.0 equiv) was added and the reaction mixture was allowed to stir at 23 °C overnight. The crude product was directly purified by reverse phase HPLC eluting from 10% to 90% MeCN in water (0.1% FA) to provide pure **9** (24 mg, 34%) as a yellow solid. ^{1}H NMR (500 MHz, CD_3CN) δ 9.03 (t, *J* = 11.4 Hz, 1H), 8.83 (t, *J* = 4.9 Hz, 1H), 8.51 (d, *J* = 5.5 Hz, 1H), 8.14 (dd, *J* = 9.3, 5.6 Hz, 1H), 7.90 (dd, *J* = 10.8, 2.8 Hz, 1H), 7.64−7.54 (m, 3H), 7.54−7.49 (m, 1H), 7.31−7.25 (m, 1H), 7.10 (td, *J* = 8.8, 2.3 Hz, 1H), 7.01 (dd, *J* = 4.5, 2.2 Hz, 1H), 6.86 (ddd, *J* = 7.4, 4.9, 2.1 Hz, 1H), 4.94−4.88 (m, 1H), 4.61−4.55 (m, 1H), 3.79−3.31 (m, 15H), 2.78−2.62 (m, 4H), 2.59−2.53 (m, 2H), 2.09−1.97 (m, 3H), 1.93−1.60 (m, 12H), 1.19 (d, *J* = 6.7 Hz, 3H) ppm. ^{13}C NMR (126 MHz, CD_3CN) δ 176.0, 172.6, 170.3, 169.8, 168.5, 168.0, 162.2, 160.2, 155.0, 153.1, 149.3, 144.3, 139.5, 135.1, 132.0, 131.9, 130.6, 128.4, 128.3, 125.5, 120.4, 120.2, 119.2, 116.4, 113.4, 108.1, 108.0, 108.0, 107.9, 106.3, 74.1, 70.6, 70.5, 69.3, 67.6, 49.5, 43.4, 42.6, 41.9, 38.9, 38.5, 36.6, 33.6, 31.6, 31.2, 30.6, 29.2, 28.5, 27.9, 27.9, 27.0, 22.9, 16.1 ppm. $[M + H]^+$ calcd. for $C_{49}H_{56}ClFN_6O_9$ 926.3781; found, 926.3715.

2-(2,6-Dioxopiperidin-3-yl)-4-(piperazin-1-yl)isoindoline-1,3-dione (37). To a solution of **33** (200 mg, 724 μmol, 1.0 equiv) and *tert*-butyl piperazine-1-carboxylate (216 mg, 1.16 mmol, 1.6 equiv) in DMSO (2 mL) was added DIPEA (281 mg, 378 μL, 2.17 mmol, 3.0 equiv). The resulting mixture was stirred at 100 °C for 12 h. After cooling to 23 °C the reaction was quenched with DI water and the resulting suspended solid was filtered and washed with cold DI water to afford the intermediate product as a yellow solid. To the intermediate product was added a solution of CH_2Cl_2:TFA (1:1, 3 mL) at 0 °C and the resulting reaction mixture was allowed to stir for 1h at 23 °C. The mixture was concentrated under nitrogen atmosphere and the crude residue was triturated with cold Et_2O (2 × 10 mL) to yield pure **37** (325 mg, 98%) as a yellow solid. Spectral data matches previously reported characterization data.[59]

2-(2,6-Dioxopiperidin-3-yl)-5-(piperazin-1-yl)isoindoline-1,3-dione (38). To a solution of **34** (500 mg, 1.81 mmol, 1.0 equiv) and *tert*-butyl piperazine-1-carboxylate (539 mg, 2.90 mmol, 1.6 equiv) in DMSO (5 mL) was added DIPEA (702 mg, 946 μL, 5.43 mmol, 3.0 equiv). The resulting mixture was warmed with stirring to 100 °C and allowed to stir for 12 h. After cooling to 23 °C the reaction was quenched with DI water and the resulting suspended solid was filtered and washed with cold DI water to afford the intermediate product as a yellow solid. To the intermediate product was added a solution of CH_2Cl_2:TFA (1:1, 4 mL) at 0 °C and the resulting reaction mixture was allowed to stir for 1h at 23 °C. The mixture was concentrated under nitrogen atmosphere and the crude residue was triturated with cold Et_2O (2 × 10 mL) to yield pure **38** (700 mg, 85%) as a yellow solid. Spectral data matches previously reported characterization data.[59]

3-(2-(4-(2-(2,6-Dioxopiperidin-3-yl)-1,3-dioxoisoindolin-4-yl)piperazin-1-yl)ethoxy)propanoic Acid (39). To a solution of **37** (70 mg, 0.20 mmol, 1.0 equiv) and *tert*-butyl 3-(2-iodoethoxy)-propanoate (98 mg, 1.6 Eq, 0.33 mmol) in DMF (3 mL) was added DIPEA (79 mg, 0.11 mL, 0.61 mmol, 3.0 equiv). The resulting mixture was allowed to stir at 75 °C for 24 h. The reaction was quenched with DI water (5 mL) and the resulting mixture was extracted with CH_2Cl_2 (3 × 5 mL). The organic layers were combined, washed with water (2 × 10 mL), brine (1 × 15 mL), dried via filtration through an isolute phase separator and concentrated *in vacuo*. The crude product was purified by column chromatography (SiO_2, CH_2Cl_2/MeOH, 100:0 to 80:20). The fractions with product were concentrated to yield pure *tert*-butyl 3-(2-(4-(2-(2,6-dioxopiperidin-3-yl)-1,3-dioxoisoindolin-4-yl)piperazin-1-yl)ethoxy)propanoate (100 mg, 95%) as a yellow solid. ^{1}H NMR (500 MHz, DMSO) δ 11.11 (s, 1H), 7.69 (dd, *J* = 8.4, 7.2 Hz, 1H), 7.34 (dd, *J* = 15.5, 7.8 Hz, 2H), 5.09 (dd, *J* = 12.8, 5.5 Hz, 1H), 3.58 (t, *J* = 6.1 Hz, 2H), 3.52 (t, *J* = 5.7 Hz, 2H), 3.27 (t, *J* = 4.9 Hz, 3H), 2.87 (ddd, *J* = 16.9, 13.9, 5.5 Hz, 1H), 2.63−2.55 (m, 5H), 2.54−2.50 (m, 4H), 2.42 (t, *J* = 6.1 Hz, 2H), 2.02 (dtd, *J* = 12.8, 5.1, 2.1 Hz, 1H), 1.39 (s, 9H). ^{13}C NMR (126 MHz, DMSO) δ 172.9, 170.6, 170.1, 167.1, 166.3, 149.8, 136.0, 133.7, 123.8, 116.5, 114.9, 79.8, 68.5, 66.2, 57.2, 53.1, 50.5, 48.8, 35.9, 31.0, 27.8, 22.1 ppm. $[M + H]^+$ calcd. for $C_{26}H_{35}N_4O_7$

https://doi.org/10.1021/acs.jmedchem.5c00026
J. Med. Chem. XXXX, XXX, XXX−XXX

515.2506; found, 515.2508. To *tert*-butyl 3-(2-(4-(2-(2,6-dioxopiperidin-3-yl)-1,3-dioxoisoindolin-4-yl)piperazin-1-yl)ethoxy)propanoate (100 mg, 194 μmol, 1.0 equiv) was added a 1:1 solution of TFA:CH_2Cl_2 (1 mL) at 0 °C. The resulting mixture was allowed to stir at 23 °C for 1h. The mixture was concentrated under nitrogen atmosphere and the crude residue was triturated with cold Et_2O (2 × 5 mL). The resulting solid was dried under vacuum to yield **39** (97 mg, 87%) as a yellow solid which was taken forward without additional purification.

3-(2-(4-(2-(2,6-Dioxopiperidin-3-yl)-1,3-dioxoisoindolin-5-yl)piperazin-1-yl)ethoxy)propanoic Acid (40). To a solution of **38** (118 mg, 345 μmol, 1.0 equiv) and *tert*-butyl 3-(2-iodoethoxy)-propanoate (166 mg, 551 μmol, 1.6 equiv) in DMF (3 mL) was added DIPEA (134 mg, 180 μL, 1.03 mmol, 3.0 equiv). The resulting mixture was stirred at 75 °C for 24 h. The mixture was allowed to cool to 23 °C, quenched with cold DI water (5 mL) and extracted with CH_2Cl_2 (3 × 10 mL). The organic layers were combined, washed with water (2 × 20 mL), brine (1 × 30 mL), dried via filtration through an isolute phase separator, and concentrated *in vacuo*. To the crude residue was added cold Et_2O and the resulting mixture was sonicated. Yellow solid precipitated out and was collected through vacuum filtration. The solid was rinsed with cold Et_2O to provide pure *tert*-butyl 3-(2-(4-(2-(2,6-dioxopiperidin-3-yl)-1,3-dioxoisoindolin-5-yl)piperazin-1-yl)ethoxy)-propanoate (150 mg, 85%) as a yellow solid. To *tert*-butyl 3-(2-(4-(2-(2,6-dioxopiperidin-3-yl)-1,3-dioxoisoindolin-5-yl)piperazin-1-yl)-ethoxy)propanoate (280 mg, 544 μmol, 1.0 equiv) was added a 1:1 solution of TFA:CH_2Cl_2 (2 mL) at 0 °C. The resulting mixture was allowed to stir at 23 °C for 1 h. The mixture was concentrated under nitrogen atmosphere and the crude residue was triturated with cold Et_2O (2 × 5 mL). The resulting solid was dried under vacuum to yield **40** (246 mg, 98%) as a yellow solid which was taken forward without additional purification. ^{1}H NMR (500 MHz, DMSO-d_6) δ 12.20 (s, 1H), 10.98 (s, 1H), 7.66 (d, *J* = 8.4 Hz, 1H), 7.37 (s, 1H), 7.24 (dd, *J* = 8.6, 2.3 Hz, 1H), 4.99 (dd, *J* = 12.8, 5.4 Hz, 1H), 4.07 (t, *J* = 4.2 Hz, 2H), 3.65 (t, *J* = 5.0 Hz, 2H), 3.62−3.39 (m, 5H), 2.78 (ddd, *J* = 16.6, 13.6, 5.3 Hz, 1H), 2.52−2.30 (m, 10H), 1.96−1.88 (m, 1H) ppm. ^{13}C NMR (126 MHz, DMSO) δ 172.8, 172.7, 170.0, 167.4, 166.9, 154.1, 133.8, 125.0, 119.9, 118.8, 108.9, 66.2, 64.0, 54.7, 50.7, 48.9, 44.2, 34.4, 34.3, 31.0, 28.5, 22.1 ppm. $[M + H]^+$ calcd. for $C_{22}H_{27}N_4O_7$ 459.1880; found, 459.1888.

2-(2,6-Dioxopiperidin-3-yl)-4-(4-(piperidin-4-ylmethyl)-piperazin-1-yl)isoindoline-1,3-dione, Trifluoroacetic Acid (41). To a solution of **37** (200 mg, 439 μmol, 1.0 equiv) and *tert*-butyl 4-(bromomethyl)piperidine-1-carboxylate (147 mg, 527 μmol, 1.2 equiv) in DMF (3 mL) was added DIPEA (170 mg, 230 μL, 1.32 mmol, 3.0 equiv). The resulting mixture was stirred at 75 °C overnight. The reaction mixture was cooled to 23 °C, quenched with cold DI water (5 mL) and extracted with CH_2Cl_2 (3 × 10 mL). The organic layers were combined, washed with DI water (2 × 20 mL), brine (1 × 30 mL), dried via filtration through an isolute phase separator, and concentrated *in vacuo*. The crude product was purified was purified by column chromatography (SiO_2, CH_2Cl_2/Acetone, 100:0 to 50:50). The desired fractions were combined and concentrated to yield pure *tert*-butyl 4-((4-(2-(2,6-dioxopiperidin-3-yl)-1,3-dioxoisoindolin-4-yl)piperazin-1-yl)methyl)piperidine-1-carboxylate (245 mg, 78%) as a bright yellow solid. Spectral data matches previously reported characterization data.[59] To *tert*-butyl 4-((4-(2-(2,6-dioxopiperidin-3-yl)-1,3-dioxoisoindolin-4-yl)piperazin-1-yl)methyl)piperidine-1-carboxylate (245 mg, 454 μmol, 1.0 equiv) was added a 1:1 mixture of TFA:CH_2Cl_2 (2 mL) at 0 °C. The resulting mixture was stirred at 23 °C for 2.5 h. The reaction mixture was concentrated under nitrogen atmosphere and the crude product was triturated with diethyl ether (2 × 10 mL) to yield **41** (235 mg, 93%) as a yellow solid which was taken forward without additional purification.

2-(2,6-Dioxopiperidin-3-yl)-5-(4-(piperidin-4-ylmethyl)-piperazin-1-yl)isoindoline-1,3-dione (42). To a solution of **38** (200 mg, 584 μmol, 1.0 equiv) and *tert*-butyl 4-(bromomethyl)-piperidine-1-carboxylate (195 mg, 701 μmol 1.2 equiv) in DMF (2.5 mL) was added DIPEA (227 mg, 305 μL, 1.75 mmol, 3.0 equiv). The resulting mixture was stirred at 75 °C for 12 h. The reaction was allowed to cool to 23 °C and then quenched with DI water and extracted with CH_2Cl_2 (3 × 5 mL). The organic layers were combined and washed with water (2 × 10 mL) and brine (1 × 20 mL). The organic phase was dried using a phase separator and the solvent was removed under vacuum. The crude residue was purified by column chromatography (SiO_2, CH_2Cl_2/acetone, 100:0 to 0:100) to afford *tert*-butyl 4-((4-(2-(2,6-dioxopiperidin-3-yl)-1,3-dioxoisoindolin-5-yl)piperazin-1-yl)-methyl)piperidine-1-carboxylate (300 mg, 556 μmol, 95.2%) as a yellow solid. To *tert*-butyl 4-((4-(2-(2,6-dioxopiperidin-3-yl)-1,3-dioxoisoindolin-5-yl)piperazin-1-yl)methyl)piperidine-1-carboxylate (300 mg, 556 μmol, 1.0 equiv,) was added a TFA:CH_2Cl_2 (1:1, 2.0 mL) at 0 °C. The reaction was stirred at 23 °C for 1 h. The mixture was concentrated to dryness under nitrogen atmosphere. The resulting residue was triturated with Et_2O (2 × 5 mL) to yield **42** (300 mg, 97%) as a yellow solid. ^{1}H NMR (500 MHz, DMSO) δ 11.12 (s, 1H), 7.76 (d, *J* = 8.4 Hz, 1H), 7.49 (s, 1H), 7.36 (d, *J* = 8.5 Hz, 1H), 5.10 (dd, *J* = 12.8, 5.4 Hz, 1H), 4.23 (s, 1H), 3.63 (s, 2H), 3.47−3.26 (m, 7H), 3.14 (d, *J* = 22.1 Hz, 3H), 2.88 (ddt, *J* = 20.6, 9.1, 4.3 Hz, 3H), 2.65−2.51 (m, 2H), 2.23−1.82 (m, 4H), 1.33 (p, *J* = 9.5 Hz, 2H) ppm. Spectral data matches previously reported characterization data.[60]

2-(2,6-Dioxopiperidin-3-yl)-5-(4-(piperidin-4-yl)piperazin-1-yl)isoindoline-1,3-dione (43). To a solution of **38** (150 mg, 329 μmol, 1.0 equiv) and *tert*-butyl 4-oxopiperidine-1-carboxylate (78.8 mg, 395 μmol, 1.2 equiv) in DMF (2 mL) was added sodium triacetoxyhydroborate (209 mg, 988 μmol, 3.0 equiv). The reaction mixture was allowed to stir at 23 °C. After 2 h the reaction was quenched with DI water and extracted with EtOAc (3 × 5 mL). The organic layers were combined and washed with brine (1 × 15 mL). The organic layer was dried by filtering through phase separator and concentrated to a yellow oil to provide pure *tert*-butyl 4-(4-(2-(2,6-dioxopiperidin-3-yl)-1,3-dioxoisoindolin-5-yl)piperazin-1-yl)-piperidine-1-carboxylate (160 mg, 92%). ^{1}H NMR (500 MHz, $CDCl_3$) δ 8.10 (s, 1H), 7.69 (d, *J* = 8.5 Hz, 1H), 7.28 (d, *J* = 2.3 Hz, 1H), 7.06 (dd, *J* = 8.6, 2.3 Hz, 1H), 4.94 (dd, *J* = 12.3, 5.4 Hz, 1H), 4.17 (s, 2H), 3.43 (s, 4H), 2.93−2.62 (m, 9H), 2.45 (s, 1H), 2.21−2.06 (m, 2H), 1.82 (s, 2H), 1.62 (s, 2H), 1.46 (s, 9H) ppm. Spectral data matches previously reported characterization data.[61] To *tert*-butyl 4-(4-(2-(2,6-dioxopiperidin-3-yl)-1,3-dioxoisoindolin-5-yl)piperazin-1-yl)-piperidine-1-carboxylate (250 mg, 476 μmol, 1.0 equiv) was added CH_2Cl_2:TFA (1:1, 3.0 mL) at 0 °C. The resulting mixture was allowed to stir at 23 °C. After 1 h the reaction was concentrated to dryness under nitrogen atmosphere. The crude residue was triturated with Et_2O (2 × 10 mL) and then concentrated to yield **43** (245 mg, 96%) as a dark yellow solid. The product was taken forward without further purification.

2-(4-((4-(2-(2,6-Dioxopiperidin-3-yl)-1,3-dioxoisoindolin-4-yl)piperazin-1-yl)methyl)piperidin-1-yl)acetic Acid (44). To a solution of **41** (150 mg, 271 μmol, 1.0 equiv) and *tert*-butyl 2-bromoacetate (58.2 mg, 38.6 μL, 299 μmol, 1.1 equiv) in DMF (2 mL) was added DIPEA (42.1 mg, 56.7 μL, 326 μmol, 1.2 equiv). The resulting mixture was stirred at 23 °C for 1 h. The mixture was quenched with DI water (2 mL) and extracted with CH_2Cl_2 (3 × 5 mL). The organic layers were combined, washed with water (2 × 10 mL), brine (1 × 15 mL), filtered through isolute phase separator and concentrated to dryness. To the resulting crude residue was added cold Et_2O. After sonicating for 10 min, a bright yellow solid precipitated out. The Et_2O was removed with trituration and the resulting solid was concentrated *in vacuo* to provide pure *tert*-butyl 2-(4-((4-(2-(2,6-dioxopiperidin-3-yl)-1,3-dioxoisoindolin-4-yl)piperazin-1-yl)methyl)-piperidin-1-yl)acetate (80 mg, 53%) as a yellow solid. ^{1}H NMR (500 MHz, $CDCl_3$) δ 8.18 (s, 1H), 7.59 (dd, *J* = 8.4, 7.2 Hz, 1H), 7.41 (d, *J* = 7.1 Hz, 1H), 7.21−7.14 (m, 1H), 4.95 (dd, *J* = 12.3, 5.4 Hz, 1H), 3.37 (d, *J* = 25.9 Hz, 4H), 3.15 (s, 2H), 2.99 (d, *J* = 11.0 Hz, 2H), 2.95−2.53 (m, 6H), 2.47−2.16 (m, 4H), 2.15−2.07 (m, 1H), 1.79 (d, *J* = 13.0 Hz, 2H), 1.46 (s, 12H), 1.25 (d, *J* = 2.6 Hz, 1H) ppm. ^{13}C NMR (126 MHz, $CDCl_3$) δ 171.1, 168.3, 167.4, 166.8, 135.9, 134.2, 127.9, 123.6, 116.1, 114.0, 81.3, 64.5, 60.2, 53.8, 53.6, 53.3, 49.2, 32.6, 31.5, 30.8, 29.4, 28.3, 22.8. $[M + H]^+$ calcd. for $C_{29}H_{40}N_5O_6$ 554.2979; found, 554.2990. To *tert*-butyl 2-(4-((4-(2-(2,6-dioxopiperidin-3-yl)-1,3-dioxoisoindolin-4-yl)piperazin-1-yl)methyl)piperidin-1-yl)acetate (50 mg, 90 μmol, 1.0 equiv) was added a 1:1 mixture of CH_2Cl_2:TFA (1.5 mL) at 0 °C. The

https://doi.org/10.1021/acs.jmedchem.5c00026
J. Med. Chem. XXXX, XXX, XXX−XXX

resulting reaction was allowed to stir at 23 °C for 4 h at which time the mixture was concentrated under nitrogen atmosphere. The crude residue was taken up in Et_2O and triturated (3 × 5 mL). The resulting solid was dried under vacuum to provide **44** (55 mg, 99%) as a yellow solid which was taken forward without additional purification.

2-(4-((4-(2-(2,6-Dioxopiperidin-3-yl)-1,3-dioxoisoindolin-5-yl)piperazin-1-yl)methyl)piperidin-1-yl)acetic Acid (45). To a solution of **42** (300 mg, 543 μmol, 1.0 equiv) and *tert*-butyl 2-bromoacetate (127 mg, 84.2 μL, 652 μmol, 1.2 equiv) in DMF (3.0 mL) was added DIPEA (84.2 mg, 113 μL, 652 μmol, 1.2 equiv). The resulting mixture was stirred at 23 °C for 3 h. The reaction mixture was diluted with DI water (5 mL) and extracted with CH_2Cl_2 (3 × 10 mL). The organic layers were combined, washed with brine (1 × 20 mL), filtered through a phase separator, and concentrated to dryness. The crude mixture was purified by column chromatography (SiO_2, CH_2Cl_2/acetone, 100:0 to 0:100) to afford *tert*-butyl 2-(4-((4-(2-(2,6-dioxopiperidin-3-yl)-1,3-dioxoisoindolin-5-yl)piperazin-1-yl)methyl)-piperidin-1-yl)acetate (250 mg, 83%) as a yellow solid. LCMS (*m*/*z*): 555.3 $[M+2]^+$. ^{1}H NMR (500 MHz, $CDCl_3$) δ 8.07 (s, 1H), 7.68 (d, *J* = 8.5 Hz, 1H), 7.27 (d, *J* = 2.3 Hz, 1H), 7.04 (dd, *J* = 8.6, 2.4 Hz, 1H), 4.93 (dd, *J* = 12.3, 5.4 Hz, 1H), 3.41 (t, *J* = 5.1 Hz, 4H), 3.15 (s, 2H), 2.98 (d, *J* = 11.0 Hz, 2H), 2.93−2.67 (m, 4H), 2.55 (t, *J* = 5.1 Hz, 4H), 2.24 (d, *J* = 7.1 Hz, 3H), 2.21−2.07 (m, 2H), 1.76 (d, *J* = 13.0 Hz, 2H), 1.48 (s, 9H), 1.36 (q, *J* = 8.3 Hz, 2H). ppm. ^{13}C NMR (126 MHz, $CDCl_3$) δ 171.1, 168.4, 168.1, 167.4, 155.7, 134.4, 125.5, 119.5, 117.9, 108.7, 81.2, 64.6, 60.3, 53.4, 53.2, 49.3, 47.6, 33.0, 31.6, 30.8, 28.3, 22.9 ppm. $[M + H]^+$ calcd. for $C_{29}H_{40}N_5O_6$ 554.2979; found, 554.2990. To *tert*-butyl 2-(4-((4-(2-(2,6-dioxopiperidin-3-yl)-1,3-dioxoisoindolin-5-yl)-piperazin-1-yl)methyl)piperidin-1-yl)acetate (300 mg, 542 μmol, 1.0 equiv) was added a solution of TFA:CH_2Cl_2 (1:1, 2.0 mL) at 0 °C. The resulting mixture was stirred at 23 °C for 2 h. The reaction mixture was concentrated to dryness under nitrogen atmosphere to provide crude product, The crude oil was triturated with Et_2O (2 × 10 mL) to yield **45** (293 mg, 88%) as a yellow solid. The product was taken forward without further purification.

2-(4-(4-(2-(2,6-Dioxopiperidin-3-yl)-1,3-dioxoisoindolin-5-yl)piperazin-1-yl)piperidin-1-yl)acetic Acid (46). To a solution of **43** (200 mg, 371 μmol, 1.0 equiv) in DMF (2.5 mL) was added DIPEA (144 mg, 194 μL, 1.11 mmol, 3.0 equiv) followed by *tert*-butyl 2-bromoacetate (86.9 mg, 57.6 μL, 446 μmol, 1.2 equiv). The resulting mixture was stirred for 2 h at 23 °C. The resulting mixture was diluted with water (5 mL) and extracted with CH_2Cl_2 (3 × 5 mL). The organic layers were combined and washed with brine (1 × 15 mL), dried via filtration through a phase separator, and the filtrate was concentrated to a yellow oil. Cold Et_2O was added to initiate precipitation of product and the solid was filtered and washed with cold Et_2O to yield *tert*-butyl 2-(4-(4-(2-(2,6-dioxopiperidin-3-yl)-1,3-dioxoisoindolin-5-yl)-piperazin-1-yl)piperidin-1-yl)acetate (190 mg, 95%) as a yellow solid. LCMS (*m*/*z*): 540.3 $[M+1]^+$. ^{1}H NMR (500 MHz, $CDCl_3$) δ 8.30 (s, 1H), 7.69 (d, *J* = 8.5 Hz, 1H), 7.28 (d, *J* = 2.3 Hz, 1H), 7.05 (dd, *J* = 8.6, 2.4 Hz, 1H), 4.93 (dd, *J* = 12.3, 5.4 Hz, 1H), 3.46 (s, 4H), 3.13 (s, 2H), 3.05 (d, *J* = 10.9 Hz, 2H), 2.94−2.67 (m, 7H), 2.22 (t, *J* = 11.4 Hz, 2H), 2.15−2.03 (m, 1H), 1.73 (d, *J* = 12.3 Hz, 5H), 1.46 (s, 9H) ppm. ^{13}C NMR (126 MHz, $CDCl_3$) δ 171.2, 169.8, 168.4, 168.0, 167.4, 155.5, 134.4, 125.5, 118.1, 108.8, 81.3, 61.8, 59.9, 53.9, 52.9, 49.3, 48.5, 47.7, 31.6, 29.4, 28.3, 22.9 ppm. To *tert*-butyl 2-(4-(4-(2-(2,6-dioxopiperidin-3-yl)-1,3-dioxoisoindolin-5-yl)piperazin-1-yl)piperidin-1-yl)-acetate (100 mg, 185 μmol, 1.0 equiv) was added CH_2Cl_2:TFA (1:1, 2.0 mL) at 0 °C. The resulting mixture was stirred at 23 °C for 2 h. The reaction mixture was concentrated to dryness under nitrogen atmosphere and the crude residue was triturated with Et_2O (2 × 5 mL) to yield pure **46** (100 mg, 90%) as a yellow solid. The product was taken forward without further purification.

(2*R*)-*N*-(4-((1-(2-(4-((4-(2-(2,6-Dioxopiperidin-3-yl)-1,3-dioxoisoindolin-4-yl)piperazin-1-yl)methyl)piperidin-1-yl)acetyl)-piperidin-4-yl)oxy)phenyl)-2-((1*S*,4*S*)-4-(6-fluoroquinolin-4-yl)cyclohexyl)propenamide (10). To a solution of **44** (25 mg, 41 μmol, 1.0 equiv) in DMF (0.5 mL) was added HATU (19 mg, 49 μmol, 1.2 equiv) and DIPEA (16 mg, 0.12 mmol, 3.0 equiv) at 0 °C under nitrogen atmosphere. The resulting mixture was stirred at 23 °C for 15 min at which time (R)-2-((1*S*,4*S*)-4-(6-fluoroquinolin-4-yl)-cyclohexyl)-N-(4-(piperidin-4-yloxy)phenyl)propanamide (21 mg, 41 μmol, 1.0 equiv) was added and the reaction was allowed to stir at 23 °C overnight. The reaction mixture was concentrated under nitrogen atmosphere and the crude product was directly purified by reverse phase HPLC eluting from 5% to 75% MeCN in water (0.1% TFA) to provide pure **10** (9 mg, 20%) was collected as a yellow solid. ^{1}H NMR (500 MHz, CD_3CN) δ 8.98 (d, *J* = 4.1 Hz, 2H), 8.42 (s, 1H), 8.35 (dd, *J* = 9.3, 5.4 Hz, 1H), 8.03 (dd, *J* = 10.6, 2.7 Hz, 1H), 7.80 (d, *J* = 5.2 Hz, 1H), 7.78−7.67 (m, 2H), 7.53−7.47 (m, 2H), 7.44 (dd, *J* = 7.3, 0.7 Hz, 1H), 7.34−7.28 (m, 1H), 6.98−6.86 (m, 2H), 4.98 (dd, *J* = 12.8, 5.3 Hz, 1H), 4.55 (s, 1H), 3.99 (d, *J* = 8.9 Hz, 2H), 3.86−2.98 (m, 23H), 2.85−2.57 (m, 4H), 2.18−1.97 (m, 5H), 1.92−1.56 (m, 11H), 1.19 (d, *J* = 6.7 Hz, 3H) ppm. ^{13}C NMR (126 MHz, CD_3CN) δ 175.3, 172.5, 170.0, 167.7, 167.4, 162.8, 162.3, 160.8, 153.8, 149.1, 146.8, 140.6, 136.6, 134.5, 133.2, 129.0, 128.9, 124.3, 122.4, 122.2, 122.0, 119.6, 118.8, 117.1, 116.9, 108.8, 108.6, 72.3, 61.1, 57.5, 54.9, 54.0, 52.8, 49.7, 48.1, 41.9, 41.5, 39.6, 39.4, 36.5, 31.6, 30.8, 30.3, 29.1, 29.0, 28.3, 28.0, 27.5, 27.0, 26.5, 22.7, 16.2 ppm. $[M + H]^+$ calcd. for $C_{54}H_{64}FN_8O_7$ 955.4882; found, 955.4885.

(2*R*)-*N*-(4-((1-(2-(4-((4-(2-(2,6-Dioxopiperidin-3-yl)-1,3-dioxoisoindolin-5-yl)piperazin-1-yl)methyl)piperidin-1-yl)acetyl)-piperidin-4-yl)oxy)phenyl)-2-((1*S*,4*S*)-4-(6-fluoroquinolin-4-yl)cyclohexyl)propanamide (11). To a solution of **45** (50 mg, 82 μmol, 1.0 equiv) in DMF (1 mL) was added HATU (37 mg, 98 μmol, 1.2 equiv) and DIPEA (32 mg, 43 μL, 0.25 mmol, 3.0 equiv) at 0 °C under nitrogen atmosphere. The resulting mixture was stirred for 15 min at 23 °C at which time (R)-2-((1*S*,4*S*)-4-(6-fluoroquinolin-4-yl)cyclohexyl)-N-(4-(piperidin-4-yloxy)phenyl)propanamide (42 mg, 82 μmol, 1.0 equiv) was added. The reaction was stirred at 23 °C overnight at which time it was dried with nitrogen atmosphere. The crude product was directly purified by reverse phase HPLC eluting from 5% to 50% MeCN in water (0.1% FA) to provide pure **11** (10 mg, 13%) as a yellow solid. ^{1}H NMR (500 MHz, DMSO) δ 11.06 (s, 1H), 10.13 (s, 1H), 8.92 (d, *J* = 4.7 Hz, 1H), 8.12 (dd, *J* = 9.2, 5.8 Hz, 1H), 8.04 (dd, *J* = 10.9, 2.8 Hz, 1H), 7.77−7.65 (m, 2H), 7.65−7.56 (m, 2H), 7.34 (d, *J* = 8.7 Hz, 1H), 7.15 (dd, *J* = 18.4, 8.7 Hz, 2H), 7.06 (dd, *J* = 7.1, 2.5 Hz, 1H), 6.63 (s, 1H), 5.10−5.00 (m, 1H), 4.61 (s, 1H), 3.73 (dt, *J* = 50.7, 5.0 Hz, 8H), 3.57−3.39 (m, 7H), 3.35−3.23 (m, 3H), 3.12−2.80 (m, 5H), 2.64−2.51 (m, 2H), 2.05−1.56 (m, 19H), 1.13 (d, *J* = 6.6 Hz, 3H) ppm. ^{13}C NMR (126 MHz, DMSO) δ 174.4, 172.8, 170.9, 167.4, 166.9, 162.5, 161.0, 159.1, 158.4, 158.2, 157.9, 157.6 154.1, 152.5, 149.3, 144.4, 133.8, 132.8, 132.1, 127.3, 125.0, 120.9, 119.9 119.6, 119.4, 118.8, 117.6, 116.3, 115.3, 112.9, 109.0, 107.4, 71.5, 56.1, 52.6, 50.8, 48.9, 44.1, 41.5, 37.6, 35.6, 31.0, 30.5, 30.1, 28.5, 27.7, 27.4, 26.7, 26.4, 22.1, 16.2 ppm. $[M + H]^+$ calcd. for $C_{54}H_{64}FN_8O_7$ 955.4882; found, 955.4890.

(2*R*)-*N*-(4-Chloro-3-((1-(2-(4-((4-(2-(2,6-dioxopiperidin-3-yl)-1,3-dioxoisoindolin-4-yl)piperazin-1-yl)methyl)piperidin-1-yl)acetyl)piperidin-4-yl)oxy)phenyl)-2-((1*S*,4*S*)-4-(6-fluoroquinolin-4-yl)cyclohexyl)propenamide (12). To a solution of **44** (55 mg, 90 μmol, 1.0 equiv) in DMF (2 mL) was added HATU (41 mg, 0.11 mmol, 1.2 equiv) and DIPEA (35 mg, 47 μL, 0.27 mmol, 3.0 equiv) at 0 °C under nitrogen atmosphere. The resulting mixture was allowed to stir at 23 °C under nitrogen atmosphere for 15 min. **31** (39 mg, 72 μmol, 0.8 equiv) was then added and the reaction was allowed to stir at 23 °C for 48 h. The crude product was directly purified by reverse phase HPLC eluting from 5% to 70% MeCN in water (0.1% TFA) to provide pure **12** (27 mg, TFA salt, 30%) was collected as a yellow solid. ^{1}H NMR (500 MHz, CD_3CN) δ 9.10 (s, 1H), 9.06−8.93 (m, 2H), 8.43 (dd, *J* = 9.3, 5.2 Hz, 1H), 8.10 (dd, *J* = 10.3, 2.7 Hz, 1H), 7.95 (d, *J* = 5.4 Hz, 1H), 7.87−7.77 (m, 1H), 7.74−7.61 (m, 2H), 7.43 (d, *J* = 7.2 Hz, 1H), 7.28 (dd, *J* = 13.1, 8.5 Hz, 2H), 7.15 (dd, *J* = 8.6, 2.2 Hz, 1H), 4.99 (dd, *J* = 12.8, 5.4 Hz, 1H), 4.65 (s, 1H), 4.02 (d, *J* = 4.6 Hz, 2H), 3.89−3.00 (m, 18H), 2.88−2.57 (m, 4H), 2.26 (s, 1H), 2.18−1.68 (m, 19H), 1.18 (d, *J* = 6.6 Hz, 3H) ppm. ^{13}C NMR (126 MHz, CD_3CN) δ 176.5, 173.0, 170.5, 168.2, 167.9, 163.5, 161.5, 153.4, 149.4, 145.6, 140.1, 138.5, 137.0, 134.9, 131.0, 129.6, 127.4, 124.7, 124.1, 123.8, 120.4, 119.2, 117.3, 114.0, 109.6, 108.6, 73.6, 61.6, 58.0, 54.4, 53.2, 50.1, 48.5, 42.0, 40.3, 39.5, 36.8, 32.0, 30.9, 30.4, 29.5, 28.6, 28.3, 27.9, 27.3, 23.1,

https://doi.org/10.1021/acs.jmedchem.5c00026
J. Med. Chem. XXXX, XXX, XXX−XXX

16.6 ppm. $[M + H]^+$ calcd. for $C_{54}H_{63}ClFN_8O_7$ 989.4492; found, 989.4486.

(2*R*)-*N*-(4-Chloro-3-((1-(2-(4-((4-(2-(2,6-dioxopiperidin-3-yl)-1,3-dioxoisoindolin-5-yl)piperazin-1-yl)methyl)piperidin-1-yl)acetyl)piperidin-4-yl)oxy)phenyl)-2-((1*S*,4*S*)-4-(6-fluoroquinolin-4-yl)cyclohexyl)propenamide (13). To a solution of **45** (60 mg, 98 μmol, 1.0 equiv) and **31** (54 mg, 98 μmol, 1.0 equiv) in DMF (1 mL) was added DIPEA (42 mg, 56 μL, 0.32 mmol, 3.3 equiv) and HATU (56 mg,, 0.15 mmol, 1.5 equiv) at 0 °C under nitrogen atmosphere. The reaction mixture was allowed to stir at 0 °C for 30 min and allowed to warm to 23 °C. After 1h the reaction was complete, and the resulting mixture was concentrated under nitrogen atmosphere and the crude product was directly purified by reverse phase HPLC eluting from 10% to 90% MeCN in water (0.1% TFA) to provide pure **13** (63 mg, 53%) as a light green solid. ^{1}H NMR (500 MHz, DMSO) δ 11.13 (s, 1H), 10.22 (s, 1H), 8.92 (d, *J* = 4.6 Hz, 1H), 8.13 (dd, *J* = 9.2, 5.8 Hz, 1H), 8.05 (dd, *J* = 10.9, 2.8 Hz, 1H), 7.83−7.67 (m, 3H), 7.63 (d, *J* = 4.7 Hz, 1H), 7.56−7.47 (m, 1H), 7.37 (dd, *J* = 11.2, 8.7 Hz, 2H), 7.14 (ddd, *J* = 8.8, 5.1, 2.2 Hz, 1H), 5.10 (dd, *J* = 12.8, 5.5 Hz, 1H), 4.67 (s, 1H), 4.29 (dd, *J* = 43.3, 8.9 Hz, 4H), 3.76−2.83 (m, 20H), 2.66−2.55 (m, 1H), 2.07−1.53 (m, 19H), 1.13 (d, *J* = 6.6 Hz, 3H) ppm. ^{13}C NMR (126 MHz, DMSO) δ 175.3, 172.9, 170.1, 167.5, 167.0, 162.6, 161.2, 159.2, 158.7, 158.4, 158.1, 157.8, 154.2, 152.1, 149.1, 143.8, 139.4, 133.9, 130.1, 127.4, 125.1, 119.9, 119.8, 118.9, 118.8, 117.6, 116.5, 115.2, 112.9, 109.1, 107.7, 107.5, 107.2, 72.8, 59.9, 56.1, 52.7, 50.8, 48.9, 44.1, 41.2, 38.3, 37.7, 35.6, 31.0, 30.4, 29.8, 28.6, 28.1, 27.6, 27.5, 26.7, 26.3, 22.2, 16.2 ppm. $[M + H]^+$ calcd. for $C_{54}H_{63}ClFN_8O_7$ 989.4492; found, 989.4493.

(2*R*)-*N*-(4-((1-(3-(2-(4-(2-(2,6-Dioxopiperidin-3-yl)-1,3-dioxoisoindolin-4-yl)piperazin-1-yl)ethoxy)propanoyl)piperidin-4-yl)oxy)phenyl)-2-((1*S*,4*S*)-4-(6-fluoroquinolin-4-yl)cyclohexyl)-propenamide (14). To a solution of **39** (40 mg, 70 μmol, 1.0 equiv) in DMF (2 mL) was added HATU (32 mg, 84 μmol, 1.2 equiv) and DIPEA (27 mg, 37 μL, 0.21 mmol, 3.0 equiv) at 0 °C under nitrogen atmosphere. The mixture was stirred for 30 min and then (R)-2-((1*S*,4*S*)-4-(6-fluoroquinolin-4-yl)cyclohexyl)-N-(4-(piperidin-4-yloxy)phenyl)propanamide (36 mg, 70 μmol, 1.0 equiv) was added. The mixture was allowed to warm to 23 °C and allowed to stir overnight. The reaction mixture was concentrated under nitrogen atmosphere and the crude product was directly purified by reverse phase HPLC eluting from 10% to 90% MeCN in water (0.1% FA) to provide pure **14** (28 mg, 42%) as a yellow solid. ^{1}H NMR (500 MHz, CD3CN) δ 8.83 (s, 1H), 8.66 (d, *J* = 4.6 Hz, 1H), 8.18 (s, 1H), 7.95−7.91 (m, 1H), 7.69 (dd, *J* = 11.0, 2.8 Hz, 1H), 7.49 (dd, *J* = 8.4, 7.2 Hz, 1H), 7.38 (ddd, *J* = 9.3, 8.2, 2.8 Hz, 1H), 7.34 (d, *J* = 4.6 Hz, 1H), 7.33−7.29 (m, 2H), 7.19 (d, *J* = 7.2 Hz, 1H), 7.11 (d, *J* = 8.4 Hz, 1H), 6.76−6.68 (m, 2H), 4.81 (dd, *J* = 12.5, 5.4 Hz, 1H), 4.34 (dq, *J* = 7.6, 3.8 Hz, 1H), 3.71 (ddd, *J* = 12.2, 6.8, 3.8 Hz, 1H), 3.50 (dt, *J* = 24.5, 5.8 Hz, 5H), 3.21 (dt, *J* = 14.4, 5.1 Hz, 6H), 2.70 (t, *J* = 4.9 Hz, 3H), 2.67−2.39 (m, 9H), 1.92 (dtd, *J* = 12.8, 5.1, 2.5 Hz, 1H), 1.84 (dt, *J* = 14.7, 3.3 Hz, 2H), 1.75−1.47 (m, 9H), 1.42 (dp, *J* = 12.7, 3.9 Hz, 1H), 1.02 (d, *J* = 6.7 Hz, 3H) ppm. ^{13}C NMR (126 MHz, CD_3CN) δ 175.4, 172.5, 170.2, 170.0, 167.9, 167.3, 163.0, 161.9, 160.0, 153.9, 153.3, 150.4, 150.3, 146.2, 136.3, 134.6, 133.4, 133.3, 133.0, 128.2, 128.1, 124.2, 121.9, 119.4, 119.2, 119.0, 117.0, 115.9, 107.7, 107.5, 72.9, 67.1, 66.6, 57.0, 53.3, 50.5, 49.7, 42.9, 41.5, 39.0, 38.7, 36.7, 33.3, 31.6, 31.4, 30.8, 29.3, 28.5, 28.1, 27.2, 22.8, 16.2 ppm. $[M + H]^+$ calcd. for $C_{51}H_{59}FN_7O_8$ 916.4409; found, 917.4488.

(2*R*)-*N*-(4-((1-(3-(2-(4-(2-(2,6-Dioxopiperidin-3-yl)-1,3-dioxoisoindolin-5-yl)piperazin-1-yl)ethoxy)propanoyl)piperidin-4-yl)oxy)phenyl)-2-((1*S*,4*S*)-4-(6-fluoroquinolin-4-yl)cyclohexyl)-propenamide (15). To a solution of **40** (100 mg, 175 μmol, 1.0 equiv) in DMF (3 mL) was added HATU (79.7 mg, 210 μmol, 1.2 equiv) and DIPEA (67.7 mg, 91.3 μL, 524 μmol, 3.0 equiv) at 0 °C under nitrogen atmosphere. The resulting mixture was allowed to stir at 23 °C for 30 min at which time (R)-2-((1*S*,4*S*)-4-(6-fluoroquinolin-4-yl)-cyclohexyl)-N-(4-(piperidin-4-yloxy)phenyl)propanamide (89.4 mg, 175 μmol, 1.0 equiv) was added and the resulting mixture was stirred overnight. The reaction mixture was concentrated under nitrogen atmosphere and the crude product was directly purified by reverse phase HPLC eluting from 10% to 90% MeCN in water (0.1% FA) to provide pure **15** (63 mg, 37%) as a yellow solid. ^{1}H NMR (500 MHz, CD_3CN) δ 9.01 (d, *J* = 15.2 Hz, 1H), 8.82 (d, *J* = 4.5 Hz, 1H), 8.35 (s, 1H), 8.17−8.00 (m, 2H), 7.85 (dd, *J* = 11.0, 2.8 Hz, 1H), 7.67 (d, *J* = 8.5 Hz, 1H), 7.54 (ddd, *J* = 9.2, 8.1, 2.8 Hz, 1H), 7.51−7.44 (m, 3H), 7.32 (d, *J* = 2.3 Hz, 1H), 7.18 (dd, *J* = 8.6, 2.4 Hz, 1H), 6.97−6.77 (m, 2H), 4.94 (ddd, *J* = 12.4, 5.3, 1.5 Hz, 1H), 4.50 (tt, *J* = 7.4, 3.6 Hz, 1H), 3.85 (ddd, *J* = 12.3, 7.2, 3.9 Hz, 1H), 3.68 (dt, *J* = 11.3, 5.7 Hz, 5H), 3.53 (t, *J* = 5.1 Hz, 4H), 3.36 (ddd, *J* = 13.7, 8.4, 3.6 Hz, 4H), 2.88 (dt, *J* = 11.1, 5.3 Hz, 6H), 2.83−2.58 (m, 7H), 2.12−1.98 (m, 2H), 1.92−1.49 (m, 9H), 1.17 (d, *J* = 6.7 Hz, 3H) ppm. ^{13}C NMR (126 MHz, CD_3CN) δ 175.4, 172.6, 172.6, 170.4, 170.2, 170.1, 168.3, 167.7, 162.8, 161.9, 160.0, 155.7, 153.9, 153.4, 153.3, 150.4, 150.4, 146.1, 134.8, 133.3, 133.1, 128.2, 128.1, 125.4, 121.9, 120.4, 119.5, 119.2, 119.1, 118.9, 117.0, 109.0, 107.7, 107.5, 72.9, 66.2, 66.1, 56.5, 52.6, 49.6, 46.8, 42.9, 41.5, 39.1, 38.7, 36.7, 33.2, 31.6, 31.4, 30.7, 29.3, 28.5, 28.1, 27.2, 22.8, 16.2 ppm. $[M + H]^+$ calcd. for $C_{51}H_{59}FN_7O_8$ 916.4409; found, 916.4414.

(2*R*)-*N*-(4-Chloro-3-((1-(3-(2-(4-(2-(2,6-dioxopiperidin-3-yl)-1,3-dioxoisoindolin-4-yl)piperazin-1-yl)ethoxy)propanoyl)-piperidin-4-yl)oxy)phenyl)-2-((1*S*,4*S*)-4-(6-fluoroquinolin-4-yl)cyclohexyl)propenamide (16). To a solution of **39** (40 mg, 70 μmol, 1.0 equiv) in DMF (2 mL) was added HATU (32 mg, 84 μmol, 1.2 equiv) and DIPEA (27 mg, 37 μL, 0.21 mmol, 3.0 equiv) at 0 °C under nitrogen atmosphere. The resulting mixture was allowed to stir for 30 min at 23 °C. **31** (38 mg, 70 μmol, 1.0 equiv) was added and the reaction was stirred at 23 °C overnight. The reaction mixture was concentrated under nitrogen atmosphere and the crude product was directly purified by reverse phase HPLC eluting from 10% to 90% MeCN in water (0.1% FA) to provide pure **16** (15 mg, 22%) as a yellow solid. ^{1}H NMR (500 MHz, CD_3CN) δ 9.02 (s, 1H), 8.82 (d, *J* = 4.5 Hz, 1H), 8.53 (s, 1H), 8.09 (dd, *J* = 9.2, 5.8 Hz, 1H), 7.84 (dd, *J* = 11.0, 2.8 Hz, 1H), 7.61 (ddt, *J* = 13.8, 8.0, 2.4 Hz, 2H), 7.57−7.47 (m, 2H), 7.32 (dd, *J* = 7.2, 3.8 Hz, 1H), 7.26 (t, *J* = 8.1 Hz, 2H), 7.10 (tt, *J* = 7.1, 2.2 Hz, 1H), 4.96 (dd, *J* = 12.5, 5.4 Hz, 1H), 4.66−4.56 (m, 1H), 3.78−3.63 (m, 4H), 3.62−3.21 (m, 9H), 2.81−2.51 (m, 11H), 2.11−1.95 (m, 5H), 1.91−1.64 (m, 10H), 1.18 (d, *J* = 6.7 Hz, 3H) ppm. ^{13}C NMR (126 MHz, CD_3CN) δ 176.0, 172.6, 170.1, 169.9, 167.9, 167.3, 161.9, 160.0, 153.2, 153.1, 150.7, 150.4, 146.2, 139.6, 136.2, 134.7, 133.4, 133.303 130.6, 128.2, 128.1, 124.2, 119.5, 119.2, 119.0, 115.5, 113.3, 108.0, 107.7, 107.5, 74.1, 68.7, 67.5, 57.9, 53.7, 51.2, 49.7, 42.7, 41.8, 38.7, 38.5, 36.6, 33.6, 31.6, 31.3, 30.6, 29.3, 28.5, 28.0, 27.1, 22.7, 16.2 ppm. $[M + H]^+$ calcd. for $C_{51}H_{58}ClFN_7O_8$ 950.4019; found, 950.4019.

(2*R*)-*N*-(4-Chloro-3-((1-(3-(2-(4-(2-(2,6-dioxopiperidin-3-yl)-1,3-dioxoisoindolin-5-yl)piperazin-1-yl)ethoxy)propanoyl)-piperidin-4-yl)oxy)phenyl)-2-((1*S*,4*S*)-4-(6-fluoroquinolin-4-yl)cyclohexyl)propenamide (17). To a solution of **40** (100 mg, 175 μmol, 1.0 equiv) in DMF (3 mL) was added HATU (79.7 mg, 210 μmol, 1.2 equiv) and DIPEA (67.7 mg, 91.3 μL, 524 μmol, 3.0 equiv) at 0 °C under nitrogen atmosphere. The resulting mixture was allowed to stir at 23 °C for 30 min. After 30 min **31** (95.5 mg, 175 μmol, 1.0 equiv) was added and the reaction was stirred at 23 °C overnight. The reaction mixture was concentrated under nitrogen atmosphere and the crude product was directly purified by reverse phase HPLC eluting from 10% to 90% MeCN in water (0.1% FA) to provide pure **17** (57 mg, 33%) as a yellow solid. ^{1}H NMR (500 MHz, CD_3CN) δ 9.04−8.91 (m, 1H), 8.81 (d, *J* = 4.5 Hz, 1H), 8.52 (s, 1H), 8.12−8.04 (m, 2H), 7.84 (dd, *J* = 11.0, 2.9 Hz, 1H), 7.68−7.58 (m, 2H), 7.58−7.47 (m, 2H), 7.31−7.22 (m, 2H), 7.16 (dd, *J* = 8.6, 2.4 Hz, 1H), 7.08 (dt, *J* = 8.7, 2.2 Hz, 1H), 4.93 (dd, *J* = 12.4, 5.4 Hz, 1H), 4.61 (dt, *J* = 7.1, 3.5 Hz, 1H), 3.70 (q, *J* = 6.8 Hz, 4H), 3.63 (td, *J* = 5.6, 1.6 Hz, 2H), 3.58−3.30 (m, 7H), 2.83−2.64 (m, 13H), 2.11−1.98 (m, 3H), 1.89−1.68 (m, 9H), 1.18 (d, *J* = 6.7 Hz, 3H) ppm. ^{13}C NMR (126 MHz, DMSO) δ 175.1, 172.8, 170.1, 168.8, 167.5, 167.0, 163.0, 160.9, 159.0, 152.4, 152.2, 149.7, 145.2, 139.3, 133.8, 132.7, 129.9, 127.2, 124.9, 119.2, 119.0, 118.6, 116.5, 112.7, 107.3, 107.1, 73.3, 66.7, 48.8, 41.8, 37.8, 37.4, 35.6, 32.7, 31.0, 30.7, 30.0, 28.5, 27.6, 27.5, 26.3, 22.2, 16.1. $[M + H]^+$ calcd. for $C_{51}H_{58}ClFN_7O_8$ 950.4019; found, 950.4017.

(2*R*)-*N*-(4-((1-(2-(4-(4-(2-(2,6-Dioxopiperidin-3-yl)-1,3-dioxoisoindolin-5-yl)piperazin-1-yl)piperidin-1-yl)acetyl)-piperidin-4-yl)oxy)phenyl)-2-((1*S*,4*S*)-4-(6-fluoroquinolin-4-yl)cyclohexyl)propenamide (18). To a solution of **46** (44 mg, 74

https://doi.org/10.1021/acs.jmedchem.5c00026
J. Med. Chem. XXXX, XXX, XXX−XXX

μmol, 1.0 equiv) in DMF (2 mL) was added HATU (34 mg, 88 μmol, 1.2 equiv) and DIPEA (29 mg, 38 μL, 0.22 mmol, 3.0 equiv) at 0 °C under nitrogen atmosphere. The resulting mixture was allowed to stir at 23 °C under nitrogen atmosphere for 15 min. (R)-2-((1*S*,4*S*)-4-(6-fluoroquinolin-4-yl)cyclohexyl)-N-(4-(piperidin-4-yloxy)phenyl)-propanamide (30 mg, 59 μmol, 0.8 equiv) was then added and the reaction was stirred at 23 °C for 4 h. The resulting mixture was concentrated under nitrogen atmosphere and the crude product was directly purified by reverse phase HPLC eluting from 5% to 70% MeCN in water (0.1% TFA) to provide pure **18** (14 mg, 18%) was collected as a yellow solid. ^{1}H NMR (500 MHz, CD_3CN) δ 9.00 (d, *J* = 6.2 Hz, 2H), 8.47 (s, 1H), 8.40 (dd, *J* = 9.3, 5.3 Hz, 1H), 8.07 (dd, *J* = 10.5, 2.7 Hz, 1H), 7.86 (d, *J* = 5.3 Hz, 1H), 7.84−7.75 (m, 1H), 7.71 (d, *J* = 8.4 Hz, 1H), 7.53−7.46 (m, 2H), 7.37 (d, *J* = 2.4 Hz, 1H), 7.23 (dd, *J* = 8.5, 2.4 Hz, 1H), 6.96−6.84 (m, 2H), 4.95 (dd, *J* = 12.5, 5.4 Hz, 1H), 4.55 (tt, *J* = 7.2, 3.5 Hz, 1H), 4.07 (s, 2H), 3.85−3.13 (m, 17H), 2.85−2.61 (m, 5H), 2.40−2.28 (m, 4H), 2.15−1.97 (m, 4H), 1.91−1.62 (m, 10H), 1.19 (d, *J* = 6.6 Hz, 3H) ppm. ^{13}C NMR (126 MHz, CD_3CN) δ 175.8, 173.0, 170.5, 168.5, 168.1, 163.4, 161.4, 155.2, 154.2, 146.4, 139.6, 135.2, 133.6, 129.5, 128.3, 125.9, 123.4, 122.4, 121.9, 120.2, 119.9, 117.5, 110.0, 109.4, 72.7, 68.3, 60.2, 50.1, 49.2, 45.7, 42.3, 41.9, 40.2, 39.8, 36.9, 32.0, 31.2, 30.8, 29.5, 28.7, 28.4, 27.4, 26.2, 23.2, 16.6 ppm. $[M + H]^+$ calcd. for $C_{53}H_{62}FN_8O_7$ 941.4725; found, 941.4723.

(2*R*)-*N*-(4-Chloro-3-((1-(2-(4-(4-(2-(2,6-dioxopiperidin-3-yl)-1,3-dioxoisoindolin-5-yl)piperazin-1-yl)piperidin-1-yl)acetyl)-piperidin-4-yl)oxy)phenyl)-2-((1*S*,4*S*)-4-(6-fluoroquinolin-4-yl)cyclohexyl)propenamide (19). To a solution of the **43** (150 mg, 251 μmol, 1.0 equiv) in DMF (2.5 mL) was added DIPEA (162 mg, 219 μL, 1.26 mmol, 5.0 equiv) and **31** (137 mg, 251 μmol, 1.0 equiv). The reaction mixture was cooled to 0 °C and 2,4,6-tripropyl-1,3,5,2,4,6-trioxatriphosphinane 2,4,6-trioxide (480 mg, 449 μL, 50% Wt in EtOAc, 754 μmol, 3.0 equiv) was added slowly. The reaction mixture was allowed to warm to 23 °C and stirred for 1 h. The reaction was quenched with cold DI water (2 mL), extracted with EtOAc (3 × 5 mL), and dried via filtration through a phase separator. The filtrate was concentrated under reduced pressure the crude product was directly purified by reverse phase HPLC eluting from 10% to 90% MeCN in water (0.1% TFA) to provide pure **19** (150 mg, 49%) as a yellow solid. ^{1}H NMR (500 MHz, DMSO) δ 11.13 (s, 1H), 10.22 (d, *J* = 2.0 Hz, 1H), 8.92 (d, *J* = 4.7 Hz, 1H), 8.13 (dd, *J* = 9.3, 5.7 Hz, 1H), 8.05 (dd, *J* = 10.9, 2.8 Hz, 1H), 7.84−7.70 (m, 3H), 7.64 (d, *J* = 4.8 Hz, 1H), 7.51 (d, *J* = 2.3 Hz, 1H), 7.37 (dd, *J* = 11.9, 8.7 Hz, 2H), 7.15 (ddd, *J* = 8.0, 5.4, 2.1 Hz, 1H), 5.10 (dd, *J* = 12.8, 5.4 Hz, 1H), 4.68 (s, 1H), 4.35 (s, 4H), 3.75−3.10 (m, 15H), 3.02 (s, 2H), 2.97−2.82 (m, 2H), 2.70−2.53 (m, 1H), 2.32 (d, *J* = 12.5 Hz, 2H), 2.08−1.56 (m, 16H), 1.14 (s, 3H) ppm. ^{13}C NMR (126 MHz, DMSO) δ 175.3, 172.9, 170.1, 167.5, 167.0, 162.6, 161.2, 159.2, 158.7, 158.4, 158.1, 157.9, 154.2, 152.1, 149.1, 143.9, 139.4, 133.8, 131.8, 130.1, 127.4, 125.1, 120.0, 119.7, 118.9, 118.8, 117.6, 116.5, 115.2, 112.9, 109.0, 107.7, 107.5, 107.2, 72.7, 59.2, 55.9, 51.6, 48.9, 48.0, 44.5, 41.2, 38.4, 37.7, 35.6, 31.0, 30.3, 29.8, 28.6, 27.6, 27.5, 26.3, 23.7, 22.2, 16.2 ppm. $[M + H]^+$ calcd. for $C_{53}H_{61}ClFN_8O_7$ 975.4336; found, 975.4339.

(2*R*)-*N*-(3-((1-(2-(4-((4-(2-(2,6-Dioxopiperidin-3-yl)-1,3-dioxoisoindolin-5-yl)piperazin-1-yl)methyl)piperidin-1-yl)acetyl)-piperidin-4-yl)oxy)phenyl)-2-((1*S*,4*S*)-4-(6-fluoroquinolin-4-yl)cyclohexyl)propenamide (20). To a solution of **45** (50 mg, 82 μmol, 1.0 equiv) in DMF (1 mL) was added DIPEA (32 mg, 43 μL, 0.25 mmol, 3.0 equiv) and HATU (31 mg, 82 μmol, 1.0 equiv) at 0 °C under nitrogen atmosphere. The resulting reaction mixture was stirred at 23 °C for 30 min. **32** (42 mg, 82 μmol, 1.0 equiv) was then added and the reaction was stirred at 23 °C for 1 h. The resulting mixture was concentrated under nitrogen atmosphere and the crude product was directly purified by reverse phase HPLC eluting from 10% to 90% MeCN in water (0.1% TFA) to provide pure **20** (32 mg, 2 x TFA salt, 33%) as a yellow solid. ^{1}H NMR (500 MHz, DMSO) δ 11.13 (s, 1H), 10.03 (s, 1H), 8.90 (d, *J* = 4.5 Hz, 1H), 8.11 (dd, *J* = 9.2, 5.8 Hz, 1H), 8.02 (dd, *J* = 11.0, 2.8 Hz, 1H), 7.78 (d, *J* = 8.4 Hz, 1H), 7.70 (td, *J* = 8.6, 2.8 Hz, 1H), 7.60 (d, *J* = 4.7 Hz, 1H), 7.55−7.42 (m, 2H), 7.38 (d, *J* = 8.7 Hz, 1H), 7.20 (td, *J* = 8.1, 2.5 Hz, 1H), 7.07 (d, *J* = 7.9 Hz, 1H), 6.69 (dd, *J* = 8.2, 2.5 Hz, 1H), 5.10 (dd, *J* = 12.8, 5.5 Hz, 1H), 4.62 (s, 1H), 4.34−4.21 (m, 3H), 3.90−2.79 (m, 22H), 2.69−2.51 (m, 2H), 2.17−1.44 (m, 17H), 1.12 (d, *J* = 6.6 Hz, 3H) ppm. ^{13}C NMR (126 MHz, DMSO) δ 175.1, 172.9, 170.1, 167.5, 167.0, 162.6, 161.1, 159.1, 158.4, 158.2, 157.9, 157.7, 157.1, 149.5, 144.7, 140.6, 133.9, 132.3, 129.7, 127.4, 127.3, 125.1, 119.6, 119.3, 118.8, 118.0, 115.6, 111.9, 110.2, 109.1, 107.5, 107.3, 71.1, 56.1, 52.7, 50.8, 48.9, 44.1, 41.5, 37.6, 35.6, 31.0, 30.6, 30.1, 28.6, 27.7, 27.4, 26.7, 26.4, 22.2, 16.2 ppm. $[M + H]^+$ calcd. for $C_{54}H_{64}FN_8O_7$ 955.4882; found, 955.4873.

(2*R*)-*N*-(3-((1-(2-(4-(4-(2-(2,6-Dioxopiperidin-3-yl)-1,3-dioxoisoindolin-5-yl)piperazin-1-yl)piperidin-1-yl)acetyl)-piperidin-4-yl)oxy)phenyl)-2-((1*S*,4*S*)-4-(6-fluoroquinolin-4-yl)cyclohexyl)propenamide (21). To a solution of **46** (125 mg, 210 μmol, 1.0 equiv) in DMF (3 mL) was added DIPEA (81.2 mg, 109 μL, 629 μmol, 3.0 equiv) and HATU (79.7 mg, 210 μmol, 1.0 equiv) at 0 °C under nitrogen atmosphere. The resulting reaction mixture was stirred at 23 °C for 30 min at which time **32** (85.8 mg, 168 μmol, 0.8 equiv) was added. The reaction mixture was stirred at 23 °C for 1 h and then concentrated to dryness under nitrogen atmosphere. The crude product was directly purified by reverse phase HPLC eluting from 10% to 90% MeCN in water (0.1% TFA) to provide pure **21** (87 mg, 36%) as a yellow solid. ^{1}H NMR (500 MHz, DMSO) δ 11.13 (s, 1H), 10.01 (s, 1H), 8.89 (d, *J* = 4.6 Hz, 1H), 8.10 (dd, *J* = 9.2, 5.8 Hz, 1H), 8.01 (dd, *J* = 10.9, 2.8 Hz, 1H), 7.78 (d, *J* = 8.3 Hz, 1H), 7.69 (td, *J* = 8.7, 2.8 Hz, 1H), 7.59 (d, *J* = 4.6 Hz, 1H), 7.56−7.31 (m, 3H), 7.20 (t, *J* = 8.1 Hz, 1H), 7.06 (d, *J* = 8.0 Hz, 1H), 6.69 (dd, *J* = 8.4, 2.4 Hz, 1H), 5.10 (dd, *J* = 12.8, 5.5 Hz, 1H), 4.62 (s, 1H), 4.33 (s, 2H), 3.94−2.82 (m, 25H), 2.67−2.54 (m, 2H), 2.42−2.19 (m, 2H), 2.17−1.51 (m, 13H), 1.12 (d, *J* = 6.5 Hz, 3H) ppm. ^{13}C NMR (126 MHz, DMSO) δ 175.0, 172.8, 170.0, 167.4, 166.9, 162.5, 161.1, 159.2, 158.6, 158.3, 158.1, 157.8, 157.1, 154.2, 153.9, 149.2, 144.1, 140.6, 133.8, 131.9, 129.6, 127.4, 127.3, 125.0, 120.0, 119.8, 119.6, 118.8, 117.6, 115.3, 112.0, 110.3, 109.0, 107.6, 107.4, 71.2, 59.2, 55.9, 51.6, 48.9, 48.0, 44.6, 41.5, 40.2, 38.7, 37.7, 35.6, 31.0, 30.5, 30.0, 28.5, 27.6, 27.4, 26.4, 23.7, 22.2, 16.2 ppm. $[M + H]^+$ calcd. for $C_{53}H_{62}FN_8O_7$ 941.4725; found, 941.4713.

3-(4-(2-(2,6-Dioxopiperidin-3-yl)-1,3-dioxoisoindolin-5-yl)-piperazin-1-yl)propanoic acid (47). To a solution of **38** (100 mg, 292 μmol, 1.0 equiv) in DMF (1.5 mL) was added DIPEA (113 mg, 876 μmol, 3.0 equiv) and *tert*-butyl 3-bromopropanoate (73.3 mg, 58.6 μL, 351 μmol, 1.2 equiv). The resulting reaction mixture was allowed to stir at 23 °C for 12 h. The reaction mixture was quenched with DI water (3 mL) and extracted with CH_2Cl_2 (3 × 5 mL). The organic layers were combined, washed with brine (1 x), filtered through a phase separator and concentrated *in vacuo* to provide an oil residue. The resulting residue was triturated with Et_2O (2 × 5 mL) and concentrated *in vacuo* to provide pure intermediate as a yellow solid. The intermediate was then taken up in a 1:1 mixture of TFA:CH_2Cl_2 (1 mL) at 0 °C and stirred at 23 °C for 24 h. The resulting reaction mixture was concentrated under nitrogen atmosphere. The resulting residue was triturated with Et_2O (2 × 10 mL) and the resulting yellow solid was dried *in vacuo* to provide **47** (70 mg, 45%) as a yellow solid. Spectral data matches previously reported characterization data.[62]

2-(4-(2-(2,6-Dioxopiperidin-3-yl)-1,3-dioxoisoindolin-5-yl)-piperazin-1-yl)acetic Acid (48). To a solution of **38** (100 mg, 292 μmol, 1.0 equiv) in DMF (1.5 mL) was added DIPEA (113 mg, 876 μmol, 3.0 equiv) and *tert*-butyl 2-bromoacetate (68.4 mg, 351 μmol, 1.2 equiv). The resulting reaction mixture was stirred at 23 °C for 2 h at which time the reaction mixture was quenched with DI water and extracted with CH_2Cl_2 (3 × 5 mL). The organic layers were combined, washed with brine (1 × 15 mL), filtered through a phase separator and concentrated *in vacuo* to provide an oil residue. The resulting residue was triturated with Et_2O (2 × 5 mL) and concentrated *in vacuo* to provide pure intermediate as a yellow solid. The intermediate was then taken up in a 1:1 mixture of TFA:CH_2Cl_2 (1 mL) at 0 °C and stirred at 23 °C for 24 h. The resulting reaction mixture was concentrated under nitrogen atmosphere. The resulting residue was triturated with Et_2O (2 × 10 mL) and the resulting yellow solid was dried *in vacuo* to provide **48** (100 mg, 67%) as a yellow solid. Spectral data matches previously reported characterization data.[62]

https://doi.org/10.1021/acs.jmedchem.5c00026
J. Med. Chem. XXXX, XXX, XXX−XXX

(2*R*)-*N*-(3-((1-(2-(4-(2-(2,6-Dioxopiperidin-3-yl)-1,3-dioxoisoindolin-5-yl)piperazin-1-yl)acetyl)piperidin-4-yl)oxy)phenyl)-2-((1*S*,4*S*)-4-(6-fluoroquinolin-4-yl)cyclohexyl)propenamide (22). To a solution of **47** (20 mg, 39 μmol, 1.0 equiv) in DMF (1 mL) was added DIPEA (15 mg, 20 μL, 0.12 mmol, 3.0 equiv) and HATU (18 mg, 147 μmol, 1.2 equiv) at 0 °C under nitrogen atmosphere3. The resulting mixture was stirred at 23 °C for 15 min at which time **32** (16 mg, 31 μmol, 0.8 equiv) was added and the resulting mixture was stirred at 23 °C. After 30 min the reaction was complete, and the resulting mixture was concentrated under nitrogen atmosphere. The crude product was directly purified by reverse phase HPLC eluting from 10% to 90% MeCN in water (0.1% TFA) to provide pure **22** (10 mg, 26%) as a yellow solid. ^{1}H NMR (500 MHz, DMSO) δ 11.09 (s, 1H), 9.97 (s, 1H), 8.89 (d, J = 4.6 Hz, 1H), 8.11 (dd, J = 9.2, 5.8 Hz, 1H), 8.03−7.97 (m, 1H), 7.78 (d, J = 8.5 Hz, 1H), 7.73−7.66 (m, 1H), 7.59 (d, J = 4.7 Hz, 1H), 7.48 (s, 2H), 7.38−7.31 (m, 1H), 7.22−7.18 (m, 1H), 7.08 (d, J = 7.8 Hz, 1H), 6.72−6.66 (m, 1H), 5.10 (dd, J = 12.8, 5.5 Hz, 1H), 4.61 (s, 1H), 4.43−3.17 (m, 7H, hidden under water peak), 2.88 (q, J = 11.7 Hz, 3H), 2.65−2.53 (m, 3H), 2.36 (s, 1H), 2.06−1.55 (m, 19H), 1.13 (d, J = 6.6 Hz, 3H) ppm. $[M + H]^+$ calcd. for $C_{48}H_{53}FN_7O_7$ 858.3991; found, 858.3986.

(2*R*)-*N*-(3-((1-(3-(4-(2-(2,6-Dioxopiperidin-3-yl)-1,3-dioxoisoindolin-5-yl)piperazin-1-yl)propanoyl)piperidin-4-yl)oxy)phenyl)-2-((1*S*,4*S*)-4-(6-fluoroquinolin-4-yl)cyclohexyl)propenamide (23). To a solution of **48** (20 mg, 48 μmol, 1.0 equiv) in DMF (1 mL) was added DIPEA (19 mg, 25 μL, 0.14 mmol, 3.0 equiv) and HATU (15 mg, 39 μmol, 0.8 equiv) at 0 °C under nitrogen atmosphere. The resulting reaction mixture was allowed to stir at 23 °C for 15 min at which time **32** (20 mg, 39 μmol, 0.8 equiv) was added at 0 °C. The resulting mixture was stirred at 23 °C for 30 min. The mixture was quenched with DI water (1 mL) and concentrated under nitrogen atmosphere. The resulting crude product was directly purified by reverse phase HPLC eluting from 10% to 90% MeCN in water (0.1% TFA) to provide pure **23** (10 mg, 21%) as a yellow solid. ^{1}H NMR (500 MHz, DMSO) δ 11.09 (s, 1H), 9.96 (s, 1H), 8.89 (d, J = 4.6 Hz, 1H), 8.10 (dd, J = 9.2, 5.8 Hz, 1H), 8.00 (dd, J = 10.9, 3.1 Hz, 1H), 7.77 (d, J = 8.5 Hz, 1H), 7.69 (td, J = 8.6, 2.8 Hz, 1H), 7.59 (d, J = 4.7 Hz, 1H), 7.52−7.46 (m, 2H), 7.37 (dd, J = 8.6, 2.3 Hz, 1H), 7.22−7.17 (m, 1H), 7.07 (d, J = 8.7 Hz, 1H), 6.68 (dt, J = 7.8, 3.8 Hz, 1H), 5.09 (dd, J = 12.8, 5.4 Hz, 1H), 4.58 (s, 1H), 4.23 (d, J = 13.8 Hz, 1H), 3.83 (s, 1H), 3.76−3.14 (m, 7H, hidden under water peak), 2.94−2.81 (m, 4H), 2.63−2.53 (m, 2H), 2.15−1.44 (m, 19H), 1.13 (d, J = 6.6 Hz, 3H) ppm. $[M + H]^+$ calcd. for $C_{49}H_{55}FN_7O_7$ 872.4147; found, 872.4148.

5-Fluoro-2-(1-methyl-2,6-dioxopiperidin-3-yl)isoindoline-1,3-dione (49). To a solution of **34** (1.5 g, 5.4 mmol, 1.0 equiv) in DMF (12 mL) at 12 was added iodomethane (2.3 g, 1.0 mL, 16 mmol, 3.0 equiv) followed by K_2CO_3 (1.1 g, 8.1 mmol, 1.5 equiv). The resulting mixture was allowed to stir at 23 °C for 12 h. The reaction mixture was poured into cold DI water and the resulting solid precipitate was collected via vacuum filtration with copious cold DI water washes to provide pure **49** (1.3 g, 82%) as a light purple/gray solid. Spectral data matches previously reported characterization data.[63]

2-(1-Methyl-2,6-dioxopiperidin-3-yl)-5-(piperazin-1-yl)-isoindoline-1,3-dione (50). To a solution of **49** (700 mg, 2.41 mmol, 1.0 equiv) and DIPEA (719 mg, 3.86 mmol, 1.6 equiv) in DMSO (7 mL) was added DIPEA (935 mg, 1.26 mL, 7.24 mmol, 3.0 equiv). The resulting mixture was stirred at 100 °C for 2.5 h. The reaction mixture was allowed to cool to 23 °C and then quenched with DI water. The resulting solid precipitate was collected via vacuum filtration with copious water rinses to provide pure *tert*-butyl 4-(2-(1-methyl-2,6-dioxopiperidin-3-yl)-1,3-dioxoisoindolin-5-yl)piperazine-1-carboxylate (1.0 g, 90%) as a yellow solid. To *tert*-butyl 4-(2-(1-methyl-2,6-dioxopiperidin-3-yl)-1,3-dioxoisoindolin-5-yl)piperazine-1-carboxylate (1.0 g, 2.0 mmol, 1.0 equiv) was added a solution of TFA:CH_2Cl_2 (5 mL, 1:1) at 0 °C. The reaction mixture was allowed to stir at 23 °C for 2 h. The resulting mixture was concentrated under nitrogen atmosphere to provide a crude residue. The crude residue was triturated with Et_2O (3 × 10 mL) and the resulting solid was dried under reduced pressure to provide **50** (900 mg, 90%) as a yellow solid. Spectral data matches previously reported characterization data.[64]

2-(1-Methyl-2,6-dioxopiperidin-3-yl)-5-(4-(piperidin-4-yl)-piperazin-1-yl)isoindoline-1,3-dione (51). To a solution of **50** (250 mg, 701 μmol, 1.0 equiv) and *tert*-butyl 4-oxopiperidine-1-carboxylate (168 mg, 842 μmol, 1.2 equiv) in DMF (4 mL) was added sodium triacetoxyhydroborate (446 mg, 2.10 mmol, 3.0 equiv). The resulting mixture was stirred at 23 °C for 1.5 h. The reaction was quenched with DI water (10 mL) and then extracted with CH_2Cl_2 (3 × 10 mL). The organic layers were combined, washed with water (2 × 15 mL), brine (1 × 20 mL), filtered through phase separator, and concentrated *in vacuo* to provide crude product. The crude residue was triturated with Et_2O (3 × 5 mL) and concentrated *in vacuo* to provide pure intermediate as a yellow solid. The intermediate was then taken up in a 1:1 mixture of TFA:CH_2Cl_2 (1 mL) at 0 °C and stirred at 23 °C overnight. The resulting reaction mixture was concentrated under nitrogen atmosphere. The resulting residue was triturated with Et_2O (2 × 10 mL) and the resulting yellow oil (could not get solid) was dried *in vacuo* to provide **51** (300 mg, 77%) as a yellow oil.

2-(4-(4-(2-(1-Methyl-2,6-dioxopiperidin-3-yl)-1,3-dioxoisoindolin-5-yl)piperazin-1-yl)piperidin-1-yl)acetic Acid (52). To a solution of **51** (250 mg, 569 μmol, 1.0 equiv) in DMF (3 mL) was added *tert*-butyl 2-bromoacetate (133 mg, 88.2 μL, 683 μmol, 1.2 equiv) and DIPEA (221 mg, 297 μL, 1.71 mmol, 3.0 equiv). The resulting mixture was stirred at 23 °C overnight. The reaction mixture was quenched with DI water and extracted with CH_2Cl_2 (3 × 5 mL). The organic layers were combined, washed with brine (1 × 15 mL), filtered through a phase separator and concentrated *in vacuo* to provide an oil residue. The resulting residue was triturated with Et_2O (2 × 5 mL) and concentrated *in vacuo* to provide intermediate as a yellow solid. The intermediate product was dissolved in a 1:1 mixture of CH_2Cl_2:TFA (2 mL) at 0 °C and stirred at 23 °C for 4 h. The resulting mixture was concentrated under nitrogen atmosphere. The crude residue was triturated in Et_2O (3 × 5 mL) and the solid product was further dried under vacuum to provide **52** (250 mg, 72%) as a yellow solid (over two steps). ^{1}H NMR (500 MHz, DMSO-d_6) δ 7.76 (d, J = 8.4 Hz, 1H), 7.47 (d, J = 2.4 Hz, 1H), 7.36 (dd, J = 8.6, 2.3 Hz, 1H), 5.16 (dd, J = 13.1, 5.3 Hz, 1H), 3.99 (s, 1H), 3.65−3.40 (m, 12H covered by the water peak), 3.01 (s, 3H), 2.95 (ddd, J = 17.3, 13.8, 5.4 Hz, 3H), 2.76 (ddd, J = 17.2, 4.6, 2.5 Hz, 1H), 2.57 (td, J = 13.3, 4.6 Hz, 1H), 2.22 (d, J = 13.1 Hz, 2H), 2.04 (dtd, J = 11.2, 5.5, 2.5 Hz, 1H), 1.93 (q, J = 13.1 Hz, 2H) ppm. ^{13}C NMR (126 MHz, DMSO) δ 171.8, 169.8, 167.4, 166.9, 154.3, 133.8, 125.0, 119.7, 118.6, 108.8, 50.9, 49.4, 47.9, 44.9, 31.1, 26.6, 21.3 ppm. $[M + H]^+$ calcd. for $C_{25}H_{32}N_5O_6$ 498.2353; found, 498.2355.

(2*R*)-2-((1*S*,4*S*)-4-(6-Fluoroquinolin-4-yl)cyclohexyl)-*N*-(3-((1-(2-(4-(4-(2-(1-methyl-2,6-dioxopiperidin-3-yl)-1,3-dioxoisoindolin-5-yl)piperazin-1-yl)piperidin-1-yl)acetyl)piperidin-4-yl)oxy)phenyl)propenamide (24). To a solution of **52** (150 mg, 246 μmol, 1.0 equiv) and DIPEA (95.3 mg, 128 μL, 737 μmol, 3.0 equiv) in DMF (5 mL) was added HATU (74.7 mg, 197 μmol, 0.8 equiv) at 0 °C under nitrogen atmosphere. The resulting mixture was allowed to stir at 23 °C for 30 min. To the resulting mixture was added **32** (101 mg, 197 μmol, 0.8 equiv) at 0 °C. The reaction mixture was allowed to stir at 23 °C for 30 min at which time the reaction mixture was quenched with DI water (1.5 mL) and concentrated under nitrogen atmosphere. The crude product was directly purified by reverse phase HPLC eluting from 10% to 90% MeCN in water (0.1% TFA) to provide pure **24** (139 mg, 48%) as a yellow solid. ^{1}H NMR (500 MHz, DMSO) δ 9.98 (s, 1H), 8.89 (d, J = 4.6 Hz, 1H), 8.11 (dd, J = 9.2, 5.8 Hz, 1H), 8.00 (dd, J = 11.0, 2.9 Hz, 1H), 7.78 (d, J = 8.4 Hz, 1H), 7.69 (td, J = 8.7, 2.8 Hz, 1H), 7.59 (d, J = 4.6 Hz, 1H), 7.50 (t, J = 2.9 Hz, 2H), 7.37 (d, J = 8.3 Hz, 1H), 7.20 (t, J = 8.1 Hz, 1H), 7.06 (d, J = 8.1 Hz, 1H), 6.69 (dd, J = 8.3, 2.5 Hz, 1H), 5.17 (dd, J = 13.1, 5.4 Hz, 1H), 4.62 (s, 2H), 4.32 (s, 4H), 3.88−3.15 (m, 8H covered by the water peak), 3.01 (s, 7H), 2.87 (dd, J = 11.0, 6.6 Hz, 1H), 2.81−2.74 (m, 1H), 2.64−2.53 (m, 2H), 2.38−2.23 (m, 2H), 2.10−1.53 (m, 19H), 1.13 (d, J = 6.6 Hz, 3H) ppm. ^{13}C NMR (126 MHz, DMSO) δ 175.0, 171.8, 169.8, 167.4, 166.9, 161.1, 159.1, 158.5, 158.3, 158.0, 157.7, 157.1, 154.2, 149.3, 144.3, 140.6, 133.8, 132.1, 129.6, 127.3, 125.0, 120.0, 119.9, 119.6, 119.4, 118.8, 117.8, 115.3, 111.9, 110.3, 108.9, 107.5, 107.3, 71.2, 59.2, 55.9, 51.6, 49.5, 48.0, 44.6, 41.5, 37.6, 35.6, 31.2, 30.5, 30.0, 28.5, 27.6,

https://doi.org/10.1021/acs.jmedchem.5c00026
J. Med. Chem. XXXX, XXX, XXX−XXX

27.5, 26.6, 26.4, 23.7, 21.4, 16.2 ppm. $[M + H]^+$ calcd. for $C_{54}H_{64}FN_8O_7$ 955.4882; found, 955.4887.

Cell Lines, Cell Culture Methods, and PROTAC Treatment. The human U87 GBM cell line and human GBM43 patient-derived xenograft (PDX) line from human adults were obtained from American Type Culture Collection (ATCC). GBM6 and GBM38 were obtained from the Mayo Clinic brain tumor PDX national resource that were developed and maintained by the Sarkaria lab at Mayo Clinic. The human pediatric glioma cell line, KNS42 GBM, was obtained from Dr. Rintaro Hashizume. The human prostate cancer cell line, PC-3, and the human pancreatic cancer cell line, SW-1990, were provided by Drs. Steve Kregel and Ali Vaziri-Gohar, respectively. The human triple negative breast cancer cell line, MDA-MB-231, and the human ovarian cancer cell line, SKOV-3, were provided by Drs. Marcelo Bonini and Dr. Daniela Matei at Northwestern University, respectively. U87, GBM6, GBM38, and KNS-42 cells were cultured in complete DMEM/F12, GBM43, SW-1990, and MDA-MB-231 were cultured in DMEM, and SKOV-3 and PC-3 were cultured in RPMI. All lines were supplemented with 10% fetal bovine serum (FBS) (Gibco) and 100 U/mL penicillin and 100 μg/mL streptomycin (Thermo Fisher Scientific) at 37 °C in a humidified chamber containing 5% CO_2 as described.[39]

U87-HiBit-IDO1 Degradation Assay. U87 cells were CRISPR/Cas9 genome edited to introduce the HiBiT tag fused to the N-terminus of IDO1. The IDO1-HiBiT protein level was quantified using a Nano-Glo HiBiT lytic detection system following the manufacturer's instructions (Promega). U87 CRISPR-edited IDO1-HiBit cells were seeded in 384-well plates at 20 μL and 2,000 cells per well (Day 0). Twenty to twenty-four hours after plating, cells were treated with 20 μL of human IFN-γ (PeproTech) at a final concentration of 12.5 ng/mL (Day 1). 40 nL of compounds or DMSO control were dispensed to corresponding test wells using an Echo 555 (Labcyte) 24 h after IFN-γ treatment (Day 2). Another 24 h later (Day 3), cells were taken out to equilibrate at room temperature for 30 min. Twenty μL of the culture media was removed from the 40 μL total media in each well, and an equal volume of room temperature Nano-Glo HiBiT lytic mix (Promega) were added to each well. Luminescence signal was measured using Synergy Neo2 (BioTeck) plate reader and analyzed with GraphPad Prism version 10.

Screening Compounds by Western Blotting. Protein samples were prepared by lysing the cells in RIPA buffer (Sigma-Aldrich, Cat# R0278) supplemented with protease and phosphatase inhibitors on ice for 30 min. Cell lysates were clarified by centrifugation at 16,000 x *g* for 15 min at 4 °C. Equal amounts of proteins as quantified by bicinchoninic acid assay (Pierce) were separated on an SDS-polyacrylamide gel electrophoresis and proteins were electrophoretically transferred onto a polyvinylidene fluoride (PVDF) membrane using a Trans-Blot Turbo Transfer System (Bio-Rad, Hercules, CA, USA). The blotted membranes were blocked for 1 h at room temperature in blocking buffer containing 5% (w/v) nonfat dry milk in Tris-buffered saline and 0.1% Tween 20 (TBS-T) followed by incubating the membranes overnight at 4 °C with primary antibodies against a target protein diluted at a standardized concentration in blocking buffer. The blots were washed three times with TBS-T and incubated for 1 h at room temperature with horseradish peroxidase-conjugated secondary antibody generated against the host antigen in which the primary antibody was generated. The protein bands were detected using an enhanced chemiluminescence reagent (SuperSignal West Femto Maximum Sensitivity substrate) and blots were visualized with Bio-Rad ImageLab software on a Bio-Rad ChemiDoc MP imaging system. All blots were stripped and reprobed with glyceraldehyde phosphate dehydrogenase (GAPDH) to ensure the proteins were loaded equally across all the samples in a particular blot. Western blotting analysis for proteins of interest used antibodies at optimized concentrations.

Biolayer Interferometry (BLI) Assays. A FortéBio Octet K2 BLI instrument (Sartorius) available in the Keck Biophysics Facility at Northwestern University was used for monitoring the interactions of the compounds with the IDO and CRBN proteins. 6xHis tagged recombinant IDO1 protein (Active Motif, Carlsbad, CA, cat# 81031) was reconstituted in PBS at 80 mg/mL, activated by pretreatment with apo-myoglobin as described,[32] then captured on prehydrated Ni-NTA biosensors (Sartorius, FortéBio, cat# 18-5103). The sensors loaded with IDO1 were then equilibrated in the reaction buffer (PBS plus 0.5% DMSO, pH 7.4) for 200 s at 30 °C. For studies of the binary complexes between the NU227326, NU227327, and IDO1, compounds were diluted in reaction buffer to obtain stock concentrations of 60 μM. For each complex, after baseline equilibration in reaction buffer, the kinetics of association were monitored by moving individual sensors into wells containing 200 μL of analyte solutions at the concentrations shown. After the association step, the sensors were moved to reaction buffer to monitor dissociation. During the entire kinetic assay, the 96-well sample plate was kept at 30 °C with shaking at 1000 rpm. Biosensors without ligand were titrated with analyte and used as a parallel reference control. Ligand-loaded biosensors without analyte were used as baseline. Double-referenced data were fitted globally with a steady state 1:1 model using the Data Analysis HT 11.0.0.50 (FortéBio) software suite.

For examining the interaction of CRBN with NU227326, NU227327, and NU227248, BLI experiments and data analysis were performed as described above, except sensors with immobilized CRBN were used. To prepare these sensors, CRBN protein (Sino Biological, Wayne, PA) was reconstituted in Acetate Buffer, pH 6, and amine-coupled to AR2G sensors (Sartorius, FortéBio, cat# 18-5092) following the manufacturer recommendations.

For experiments examining the formation of ternary complex, IDO1 was immobilized on NiNTA sensors as described above from 30 μg/mL solutions. Compounds NU227326 and NU227327 at concentrations of 1.5 μM were preincubated in sperate reactions with 20 molar excess of CRBN.[65,66] After 15 min of equilibration at 30 °C, a dilution series was prepared. These dilutions were allowed to equilibrate for an additional 20 min at 30 °C before binding reactions were monitored with BLI. Separately, experiments with identical sequences and preparation were performed using compounds NU227326 and NU227327 without CRBN and with CRBN but without NU227326 and NU227327. For the ternary and binary complexes shown, each data set was fitted globally with a 1:1 kinetic model, using the Data Analysis HT 11.0.0.50 (FortéBio) software.

Kynurenine Assay. Kynurenine levels in cell culture supernatants were measured using a modified Erhlich method.[67] Briefly, cell culture supernatants were incubated with a 10% final concentration of trichloroacetic acid in Eppendorf tubes for 20 min at 60 °C to release kynurenine from cells and to precipitate proteins. After 20 min, samples were centrifuged for 20 min at 2500 × *g* and supernatants were mixed with 20 mg/mL 4-dimethylamino benzaldehyde in acetic acid (Sigma-Aldrich) at a 1:1 ratio and absorbance was measured at 490 nm using a plate reader.

RNA Isolation and Gene Expression Analysis Using Real-Time PCR. Total RNA was extracted with lysis reagent (Ambion - Invitrogen) according to the manufacturer's instructions. First-strand cDNA synthesis was performed with 1 μg of purified RNA using a iScript cDNA systhesi kit (Bio-Rad). Then, gene expression was performed using SYBR Green chemistry (ThermoFisher) on the ABI7300 Real-Time PCR system using QuantStudio 6 and 7 Flex software (Applied Biosystems) and analyzed by ΔΔCt method. The levels of GAPDH were used to normalize mRNA levels of target genes. The sequences of the primers used in this study were previously reported.[39]

Statistical Analysis. Comparisons between two experimental groups were performed with GraphPad Prism using Student unpaired *t* test, and among more than two experimental groups were analyzed using one-way ANOVA with Tukey post hoc analysis for multiple comparisons. The data are expressed as means ± SEM from three technical replicates and three independent experiments. A value of $P < 0.05$ was considered to be significant between the two groups.

Pharmacokinetics. All of the procedures involving animals (pharmacokinetics studies and MTD toxicity studies) were conducted in accordance with the Institutional Animal Care and Use Committee (IACUC) of HD Biosciences Co., Ltd., WuXi Apptec Co., Ltd.

Compounds **NU227326** (**21**) and **NU227327** (**20**) were formulated for IP administration in mouse *in vivo* PK studies as 5.0 mg/mL

https://doi.org/10.1021/acs.jmedchem.5c00026
J. Med. Chem. XXXX, XXX, XXX−XXX

solutions. Solutions were made by dissolving compound in DMSO (5%), then adding Solutol HS-15 (10%), followed by normal saline (85%) to give a yellow, clear, solution. Sample was given by IP administration at a volume of 10 mL/kg.

Female 9−10-week-old C57BL/6J mice weighing 18−23 g and three mice per time point were used. An UPLC (Waters) chromatographic system equipped with an API 6500+ mass spectrometer (Applied Biosystems, Concord, Ontario, Canada) was used for bioanalytical analyses. Chromatographic separation was achieved on a Waters Acquity UPLC BEH C18 1.7 μm, 2.1*50 mm column maintained at RT. The flow rate was maintained at 0.7 mL/min and a mobile phase gradient of H_2O:acetonitrile (0.1% formic acid) was used. Analyst 1.7 software packages (Applied Biosystems) were used to control the LC-MS/MS system, as well as for data acquisition and processing. All data were acquired using Analyst 1.7 software (Applied Biosystems). Plasma concentration versus time data was analyzed by noncompartmental approaches using PKSolver 2.0. Data were plotted using GraphPad Prism 10.

At each time point, around 100 μL of blood was collected and quickly put on ice. Around 50 μL plasma sample was collected from blood after 4 °C, 4000 rpm centrifugation, and stored at −80 °C until LC/MS analysis. All plasma and brain samples were stored at −80 °C before PK analysis. An aliquot of 20 μL plasma was spiked into a 96-well plate, and 120 μL of acetonitrile containing internal standard were added for protein precipitation. The mixture was vortexed, centrifuged at 4000 rpm for 10 min. 100 μL of supernatant was transferred into a clean 96-well plate, and 300 μL of water were added, the mixture was vortexed and 5.0 μL of the final solution was injected for LC-MS/MS analysis. For concentrated samples, 2 μL of plasma was diluted 10x then analyzed as above. Brain samples were homogenized with ice-cold phosphate buffer saline (pH 7.4) at a ratio of 2 (buffer): 1 (tissue) (v/w). An aliquot of 50 μL homogenate was spiked into a 1.5 mL tube, and 300 μL of acetonitrile containing internal standard was added for protein precipitation. The mixture was vortexed, centrifuged at 14000 rpm for 10 min. 100 μL of supernatant was transferred into a clean 96-well plate, and 300 μL of water were added, the mixture was vortexed and 5.0 μL of the final solution was injected for LC-MS/MS analysis.

Proteomics. Sample Preparation LFQ Quantitative Mass Spectrometry. Cells were lysed by addition of lysis buffer (8 M Urea, 50 mM NaCl, 50 mM 4-(2-hydroxyethyl)-1-piperazineethanesulfonic acid (EPPS) pH 8.5, Protease and Phosphatase inhibitors) and homogenization by bead beating (BioSpec) for three repeats of 30 at 2400 strokes/min. Bradford assay was used to determine the final protein concentration in the clarified cell lysate. Fifty micrograms of protein for each sample was reduced, alkylated and precipitated using methanol/chloroform as previously described[46] and the resulting washed precipitated protein was allowed to air-dry. Precipitated protein was resuspended in 4 M urea, 50 mM HEPES pH 7.4, followed by dilution to 1 M urea with the addition of 200 mM EPPS, pH 8. Proteins were digested with the addition of LysC (1:50; enzyme:protein) and trypsin (1:50; enzyme:protein) for 12 h at 37 °C. Sample digests were acidified with formic acid to a pH of 2−3 before desalting using C18 solid phase extraction plates (SOLA, Thermo Fisher Scientific). Desalted peptides were dried in a vacuum-centrifuged and reconstituted in 0.1% formic acid for liquid chromatography−mass spectrometry analysis.

Data were collected using a TimsTOF HT (Bruker Daltonics, Bremen, Germany) coupled to a nanoElute LC pump (Bruker Daltonics, Bremen, Germany) via a CaptiveSpray nanoelectrospray source. Peptides were separated on a reversed-phase C_{18} column (25 cm x 75 μm ID, 1.6 μM, IonOpticks, Australia) containing an integrated captive spray emitter. Peptides were separated using a 50 min gradient of 2−30% buffer B (acetonitrile in 0.1% formic acid) with a flow rate of 250 nL/min and column temperature maintained at 50 °C.

The TIMS elution voltages were calibrated linearly with three points (Agilent ESI-L Tuning Mix Ions; 622, 922, 1,222 m/z) to determine the reduced ion mobility coefficients ($1/K_0$). To perform diaPASEF, we used py_diAID,[68] a python package, to assess the precursor distribution in the m/z-ion mobility plane to generate a diaPASEF acquisition scheme with variable window isolation widths that are aligned to the precursor density in m/z. Data was acquired using 20 cycles with three mobility window scans each (creating 60 windows) covering the diagonal scan line for doubly and triply charged precursors, with singly charged precursors able to be excluded by their position in the m/z-ion mobility plane. These precursor isolation windows were defined between 350−1250 m/z and 1/k0 of 0.6−1.45 V·s/cm^2.

LC-MS Data Analysis. The diaPASEF raw file processing and controlling peptide and protein level false discovery rates, assembling proteins from peptides, and protein quantification from peptides were performed using library free analysis in DIA-NN 1.8.[69] Library free mode performs an in silico digestion of a given protein sequence database alongside deep learning-based predictions to extract the DIA precursor data into a collection of MS2 spectra. The search results are then used to generate a spectral library which is then employed for the targeted analysis of the DIA data searched against a Swissprot human database (January 2021). Database search criteria largely followed the default settings for directDIA including: tryptic with two missed cleavages, carbamidomethylation of cysteine, and oxidation of methionine and precursor Q-value (FDR) cutoff of 0.01. Precursor quantification strategy was set to Robust LC (high accuracy) with RT-dependent cross run normalization. Proteins with low sum of abundance (<2,000 x no. of treatments) were excluded from further analysis and resulting data was filtered to only include proteins that had a minimum of 3 counts in at least 4 replicates of each independent comparison of treatment sample to the DMSO control. Protein with missing values were imputed by random selection from a Gaussian distribution either with a mean of the nonmissing values for that treatment group or with a mean equal to the median of the background (in cases when all values for a treatment group are missing) using in-house scripts in the R framework (R Development Core Team, 2014). Significant changes comparing the relative protein abundance of these treatment to DMSO control comparisons were assessed by moderated t test as implemented in the limma package within the R framework.[70]

■ ASSOCIATED CONTENT

Supporting Information

The Supporting Information is available free of charge at https://pubs.acs.org/doi/10.1021/acs.jmedchem.5c00026.

Kynurenine inhibition data for compound **21** (**NU227326**), global quantitative proteomics data for **NU227326** and **NU227327**, BLI data for inactive control compound **24** (**NU227428**), pharmacokinetics data for **20** (**NU227327**), ^{1}H NMR, ^{13}C NMR, and HPLC of key final compounds, raw Western blot images (PDF)

SMILES strings table of the compounds described here and their IDO1 DC_{50} (CSV)

■ AUTHOR INFORMATION

Corresponding Authors

Derek A. Wainwright − *Department of Cancer Biology, Loyola University Chicago Stritch School of Medicine, Maywood, Illinois 60153, United States; Cardinal Bernardin Cancer Center, Maywood, Illinois 60153, United States; Department of Neurological Surgery, Loyola University Medical Center, Maywood, Illinois 60153, United States;* orcid.org/0000-0001-7232-4264; Phone: (708) 327-3130; Email: dwainwr@luc.edu

Gary E. Schiltz − *Department of Chemistry, Northwestern University, Evanston, Illinois 60208, United States; Robert H. Lurie Comprehensive Cancer Center, Chicago, Illinois 60611, United States; Department of Pharmacology, Northwestern University, Feinberg School of Medicine, Chicago, Illinois 60611, United States;* orcid.org/0000-0003-4180-5051; Phone: (847) 467-2287; Email: gary-schiltz@northwestern.edu

https://doi.org/10.1021/acs.jmedchem.5c00026
J. Med. Chem. XXXX, XXX, XXX−XXX

Authors

Paige J. Monsen − *Department of Chemistry, Northwestern University, Evanston, Illinois 60208, United States;* Present Address: Foghorn Therapeutics, 500 Technology Square, Suite 700, Cambridge, MA 02139

Prashant V. Bommi − *Department of Cancer Biology, Loyola University Chicago Stritch School of Medicine, Maywood, Illinois 60153, United States;* orcid.org/0000-0002-9457-1730

Arabela A. Grigorescu − *Department of Molecular Biosciences, Northwestern University Weinberg College of Arts and Sciences, Evanston, Illinois 60208, United States*

Kristen L. Lauing − *Department of Cancer Biology, Loyola University Chicago Stritch School of Medicine, Maywood, Illinois 60153, United States*

Yingyu Mao − *High-Throughput Analysis Laboratory, Chemistry of Life Processes Institute, Northwestern University, Evanston, Illinois 60208, United States*

Payton Berardi − *Department of Cancer Biology, Loyola University Chicago Stritch School of Medicine, Maywood, Illinois 60153, United States*

Lijie Zhai − *Department of Cancer Biology, Loyola University Chicago Stritch School of Medicine, Maywood, Illinois 60153, United States*

Oluwatomilayo Ojo − *Department of Cancer Biology, Loyola University Chicago Stritch School of Medicine, Maywood, Illinois 60153, United States*

Manon Penco-Campillo − *Department of Cancer Biology, Loyola University Chicago Stritch School of Medicine, Maywood, Illinois 60153, United States;* orcid.org/0000-0002-9438-6041

Taylor Koch − *Department of Cancer Biology, Loyola University Chicago Stritch School of Medicine, Maywood, Illinois 60153, United States*

Michael Egozi − *Department of Cancer Biology, Loyola University Chicago Stritch School of Medicine, Maywood, Illinois 60153, United States*

Sonam Jha − *Department of Chemistry, Northwestern University, Evanston, Illinois 60208, United States*

Sara F. Dunne − *High-Throughput Analysis Laboratory, Chemistry of Life Processes Institute, Northwestern University, Evanston, Illinois 60208, United States*

Hong Jiang − *HD Biosciences (China) Co., Ltd., A WuXi AppTec Company, Shanghai 201201, China*

Guiqin Song − *HD Biosciences (China) Co., Ltd., A WuXi AppTec Company, Shanghai 201201, China*

Fang Zhang − *HD Biosciences (China) Co., Ltd., A WuXi AppTec Company, Shanghai 201201, China*

Steven Kregel − *Department of Cancer Biology, Loyola University Chicago Stritch School of Medicine, Maywood, Illinois 60153, United States; Cardinal Bernardin Cancer Center, Maywood, Illinois 60153, United States*

Ali Vaziri-Gohar − *Department of Cancer Biology, Loyola University Chicago Stritch School of Medicine, Maywood, Illinois 60153, United States; Cardinal Bernardin Cancer Center, Maywood, Illinois 60153, United States; Department of Surgery, Loyola University Chicago Stritch School of Medicine, Maywood, Illinois 60153, United States*

Sean W. Fanning − *Department of Cancer Biology, Loyola University Chicago Stritch School of Medicine, Maywood, Illinois 60153, United States;* orcid.org/0000-0002-9428-0060

Pilar Sanchez-Gomez − *Neuro-Oncology Unit, Unidad Funcional de Investigación en Enfermedades Crónicas (UFIEC), Instituto de Salud Carlos III (ISCIII), Madrid 28029, Spain*

Jacob M. Allen − *Department of Health and Kinesiology, University of Illinois at Urbana−Champaign, Urbana, Illinois 61801, United States*

Bakhtiar Yamini − *Department of Neurological Surgery, University of Chicago Medicine, Chicago, Illinois 60637, United States*

Rimas V. Lukas − *Department of Neurology, Northwestern University Feinberg School of Medicine, Chicago, Illinois 60611, United States*

Complete contact information is available at: https://pubs.acs.org/10.1021/acs.jmedchem.5c00026

Author Contributions

†Paige J. Monsen and Prashant V. Bommi contributed equally to this work. The manuscript was written through contributions of all authors. All authors read and intellectually contributed to the manuscript.

Notes

The authors declare the following competing financial interest(s): The IDO-PROTACs described herein are the subject of a U.S. patent application filed by Northwestern University and lists G.E.S., D.A.W., and P.J.M. as inventors. Dr. Lukas has received honoraria for serving on a Scientific Advisory Board for Merck, and honoraria for serving on the Speakers Bureau for Novocure. He has received research support for drug only use from BMS.

■ ACKNOWLEDGMENTS

This work was supported in part by National Institutes of Health (NIH) Grants R01NS097851 (D.A.W. and G.E.S.), K02AG068617 (D.A.W.), R01NS129835 (D.A.W.), American Cancer Scholar Research Scholar Award RSG-21-058-01-CCE (D.A.W.), and the GBM Foundation (D.A.W.). This work was supported by the Northwestern University High Throughput Analysis Core, which received funding from the Lurie Cancer Center (NCI Grant CA060553) and the Acoustic liquid handler SIG (NIH S10OD023681). This work made use of the IMSERC NMR facility at Northwestern University, which has received support from the Soft and Hybrid Nanotechnology Experimental (SHyNE) Resource (NSF ECCS-2025633), the State of Illinois, the International Institute for Nanotechnology (IIN), and Northwestern University. Some of the work was completed in the Keck Biophysics Facility, a shared resource of the Robert H. Lurie Comprehensive Cancer Center of Northwestern University supported in part by the NCI Cancer Center Support Grant P30CA060553. We thank Katherine A. Donovan, Eric S. Fischer, and the Fischer Lab Degradation Proteomics Initiative for collection of the global proteomics data supported by NIH CA214608 and CA218278. Global proteomics data will be publicly available at the Fischer Lab's Proteomics database: https://proteomics.fischerlab.org.

■ ABBREVIATIONS USED

AR2G, amine reactive second generation; BLI, biolayer Interferometry; CRBN, cereblon; CH_2Cl_2, dichloromethane; DIPEA, diisopropylethylamine; DMF, *N*,*N*-dimethylformamide; DMSO, dimethyl sulfoxide; EDCI, 1-ethyl-3-(3-dimethylaminopropyl)carbodiimide; GAPDH, glyceraldehyde

phosphate dehydrogenase; GBM, glioblastoma; HATU, hexafluorophosphate azabenzotriazole tetramethyl uronium; ICB, immune checkpoint blockade; IDO1, indoleamine 2,3-dioxygenase 1; IFNγ, interferon gamma; ITC, isothermal titration calorimetry; KYN, kynurenine; MeOH, methanol; PROTAC, proteolysis targeting chimera; SAR, structure−activity relationship; STAB, sodium triacetoxyborohydride; *t*-BuOK, potassium *tert*-butoxide; THF, tetrahydrofuran; Treg, regulatory T-cell; Trp, tryptophan; T3P, propanephosphonic acid anhydride; VHL, Von Hippel−Lindau

REFERENCES

(1) Adamson, C.; Kanu, O. O.; Mehta, A. I.; Di, C.; Lin, N.; Mattox, A. K.; Bigner, D. D. Glioblastoma multiforme: a review of where we have been and where we are going. *Expert Opin. Investig. Drugs* **2009**, *18* (8), 1061−1083.

(2) Lukas, R. V.; Wainwright, D. A.; Ladomersky, E.; Sachdev, S.; Sonabend, A. M.; Stupp, R. Newly Diagnosed Glioblastoma: A Review on Clinical Management. *Oncology (Williston Park)* **2019**, *33* (3), 91−100.

(3) Ostrom, Q. T.; Price, M.; Neff, C.; Cioffi, G.; Waite, K. A.; Kruchko, C.; Barnholtz-Sloan, J. S. CBTRUS Statistical Report: Primary Brain and Other Central Nervous System Tumors Diagnosed in the United States in 2016-2020. *Neuro-Oncology* **2023**, *25* (Suppl. 4), iv1−iv99.

(4) Cao, T. Q.; Wainwright, D. A.; Lee-Chang, C.; Miska, J.; Sonabend, A. M.; Heimberger, A. B.; Lukas, R. V. Next Steps for Immunotherapy in Glioblastoma. *Cancers (Basel)* **2022**, *14* (16), 4023.

(5) Eggermont, A. M.; Chiarion-Sileni, V.; Grob, J.-J.; Dummer, R.; Wolchok, J. D.; Schmidt, H.; Hamid, O.; Robert, C.; Ascierto, P. A.; Richards, J. M.; et al. Prolonged survival in stage III melanoma with ipilimumab adjuvant therapy. *N. Engl. J. Med.* **2016**, *375* (19), 1845−1855.

(6) Reck, M.; Rodríguez-Abreu, D.; Robinson, A. G.; Hui, R.; Csőszi, T.; Fülöp, A.; Gottfried, M.; Peled, N.; Tafreshi, A.; Cuffe, S.; et al. Pembrolizumab versus chemotherapy for PD-L1-positive non-small-cell lung cancer. *N. Engl. J. Med.* **2016**, *375*, 1823−1833.

(7) Weber, J.; Mandala, M.; Del Vecchio, M.; Gogas, H. J.; Arance, A. M.; Cowey, C. L.; Dalle, S.; Schenker, M.; Chiarion-Sileni, V.; Marquez-Rodas, I.; et al. Adjuvant nivolumab versus ipilimumab in resected stage III or IV melanoma. *N. Engl. J. Med.* **2017**, *377* (19), 1824−1835.

(8) Reardon, D. A.; Brandes, A. A.; Omuro, A.; Mulholland, P.; Lim, M.; Wick, A.; Baehring, J.; Ahluwalia, M. S.; Roth, P.; Bähr, O.; Phuphanich, S.; Sepulveda, J. M.; De Souza, P.; Sahebjam, S.; Carleton, M.; Tatsuoka, K.; Taitt, C.; Zwirtes, R.; Sampson, J.; Weller, M. Effect of Nivolumab vs Bevacizumab in Patients With Recurrent Glioblastoma: The CheckMate 143 Phase 3 Randomized Clinical Trial. *JAMA Oncology* **2020**, *6* (7), 1003−1010. Accessed Jan 17, 2023.

(9) Chan, H. Y.; Choi, J.; Jackson, C.; Lim, M. Combination immunotherapy strategies for glioblastoma. *J. Neuro-Oncol.* **2021**, *151* (3), 375−391.

(10) Weller, M.; Lim, M.; Idbaih, A.; Steinbach, J.; Finocchiaro, G.; Raval, R.; Ashby, L.; Ansstas, G.; Baehring, J.; Taylor, J.; Honnorat, J.; Petrecca, K.; de Vos, F.; Wick, A.; Sumrall, A.; Roberts, M.; Slepetis, R.; Warad, D.; Lee, M.; Reardon, D.; Omuro, A. CTIM-25. A RANDOMIZED PHASE 3 STUDY OF NIVOLUMAB OR PLACEBO COMBINED WITH RADIOTHERAPY PLUS TEMOZOLOMIDE IN PATIENTS WITH NEWLY DIAGNOSED GLIOBLASTOMA WITH METHYLATED MGMT PROMOTER: CHECKMATE 548. *Neuro-Oncology* **2021**, *23* (Supplement_6), vi55−vi56. Accessed Jan 17, 2023.

(11) Pearson, J. R. D.; Cuzzubbo, S.; McArthur, S.; Durrant, L. G.; Adhikaree, J.; Tinsley, C. J.; Pockley, A. G.; McArdle, S. E. B. Immune Escape in Glioblastoma Multiforme and the Adaptation of Immunotherapies for Treatment. *Front. Immunol.* **2020**, *11*, 582106. Review.

(12) Zhai, L.; Ladomersky, E.; Lenzen, A.; Nguyen, B.; Patel, R.; Lauing, K. L.; Wu, M.; Wainwright, D. A. IDO1 in cancer: a Gemini of immune checkpoints. *Cell. Mol. Immunol.* **2018**, *15* (5), 447−457.

(13) Zhai, L.; Spranger, S.; Binder, D. C.; Gritsina, G.; Lauing, K. L.; Giles, F. J.; Wainwright, D. A. Molecular Pathways: Targeting IDO1 and Other Tryptophan Dioxygenases for Cancer Immunotherapy. *Clin. Cancer Res.* **2015**, *21*, 5427.

(14) Munn, D. H.; Mellor, A. L. Indoleamine 2,3 dioxygenase and metabolic control of immune responses. *Trends Immunol.* **2013**, *34* (3), 137−143.

(15) Zhai, L.; Bell, A.; Ladomersky, E.; Lauing, K. L.; Bollu, L.; Sosman, J. A.; Zhang, B.; Wu, J. D.; Miller, S. D.; Meeks, J. J.; Lukas, R. V.; Wyatt, E.; Doglio, L.; Schiltz, G. E.; McCusker, R. H.; Wainwright, D. A. Immunosuppressive IDO in Cancer: Mechanisms of Action, Animal Models, and Targeting Strategies. *Front. Immunol.* **2020**, *11*, 1185. Review.

(16) Wainwright, D. A.; Chang, A. L.; Dey, M.; Balyasnikova, I. V.; Kim, C.; Tobias, A. L.; Cheng, Y.; Kim, J.; Zhang, L.; Qiao, J.; Han, Y.; Lesniak, M. S. Durable therapeutic efficacy utilizing combinatorial blockade against IDO, CTLA-4 and PD-L1 in mice with brain tumors. *Clin. Cancer Res.* **2014**, *20*, 5290.

(17) Zhai, L.; Ladomersky, E.; Lauing, K. L.; Wu, M.; Genet, M.; Gritsina, G.; Győrffy, B.; Brastianos, P. K.; Binder, D. C.; Sosman, J. A.; et al. Infiltrating T cells increase IDO1 expression in glioblastoma and contribute to decreased patient survival. *Clin. Cancer Res.* **2017**, *23* (21), 6650−6660.

(18) Wainwright, D. A.; Balyasnikova, I. V.; Chang, A. L.; Ahmed, A. U.; Moon, K.-S.; Auffinger, B.; Tobias, A. L.; Han, Y.; Lesniak, M. S. IDO Expression in Brain Tumors Increases the Recruitment of Regulatory T Cells and Negatively Impacts SurvivalIDO Regulates Treg Infiltration in Brain Tumors. *Clin. Cancer Res.* **2012**, *18* (22), 6110−6121.

(19) Rosenberg, A. J.; Wainwright, D. A.; Rademaker, A.; Galvez, C.; Genet, M.; Zhai, L.; Lauing, K. L.; Mulcahy, M. F.; Hayes, J. P.; Odell, D. D.; et al. Indoleamine 2,3-dioxygenase 1 and overall survival of patients diagnosed with esophageal cancer. *Oncotarget* **2018**, *9* (34), 23482.

(20) Wang, W.; Huang, L.; Jin, J.-Y.; Pi, W.; Ellsworth, S. G.; Jolly, S.; Mellor, A. L.; Machtay, M.; Kong, F.-M. S. A Validation Study on IDO Immune Biomarkers for Survival Prediction in Non-Small Cell Lung Cancer: Radiation Dose Fractionation Effect in Early-Stage DiseaseRadiotherapy Dose Fractionation Affects IDO Immune Status. *Clin. Cancer Res.* **2020**, *26* (1), 282−289.

(21) Inaba, T.; Ino, K.; Kajiyama, H.; Yamamoto, E.; Shibata, K.; Nawa, A.; Nagasaka, T.; Akimoto, H.; Takikawa, O.; Kikkawa, F. Role of the immunosuppressive enzyme indoleamine 2, 3-dioxygenase in the progression of ovarian carcinoma. *Gynecol. Oncol.* **2009**, *115* (2), 185−192.

(22) Mangaonkar, A.; Mondal, A. K.; Fulzule, S.; Pundkar, C.; Park, E. J.; Jillella, A.; Kota, V.; Xu, H.; Savage, N. M.; Shi, H.; et al. A novel immunohistochemical score to predict early mortality in acute myeloid leukemia patients based on indoleamine 2,3 dioxygenase expression. *Sci. Rep.* **2017**, *7* (1), 1−7.

(23) Pallotta, M. T.; Orabona, C.; Volpi, C.; Vacca, C.; Belladonna, M. L.; Bianchi, R.; Servillo, G.; Brunacci, C.; Calvitti, M.; Bicciato, S.; Mazza, E. M.; Boon, L.; Grassi, F.; Fioretti, M. C.; Fallarino, F.; Puccetti, P.; Grohmann, U. Indoleamine 2,3-dioxygenase is a signaling protein in long-term tolerance by dendritic cells. *Nat. Immunol.* **2011**, *12* (9), 870−878.

(24) Ladomersky, E.; Zhai, L.; Lauing, K. L.; Bell, A.; Xu, J.; Kocherginsky, M.; Zhang, B.; Wu, J. D.; Podojil, J. R.; Platanias, L. C.; Mochizuki, A. Y.; Prins, R. M.; Kumthekar, P.; Raizer, J. J.; Dixit, K.; Lukas, R. V.; Horbinski, C.; Wei, M.; Zhou, C.; Pawelec, G.; Campisi, J.; Grohmann, U.; Prendergast, G. C.; Munn, D. H.; Wainwright, D. A. Advanced Age Increases Immunosuppression in the Brain and Decreases Immunotherapeutic Efficacy in Subjects with Glioblastoma. *Clin. Cancer Res.* **2020**, *26* (19), 5232−5245.

(25) Zhai, L.; Bell, A.; Ladomersky, E.; Lauing, K. L.; Bollu, L.; Nguyen, B.; Genet, M.; Kim, M.; Chen, P.; Mi, X.; Wu, J. D.; Schipma,

https://doi.org/10.1021/acs.jmedchem.5c00026
J. Med. Chem. XXXX, XXX, XXX−XXX

M. J.; Wray, B.; Griffiths, J.; Unwin, R. D.; Clark, S. J.; Acharya, R.; Bao, R.; Horbinski, C.; Lukas, R. V.; Schiltz, G. E.; Wainwright, D. A. Tumor Cell IDO Enhances Immune Suppression and Decreases Survival Independent of Tryptophan Metabolism in Glioblastoma. *Clin. Cancer Res.* **2021**, *27* (23), 6514−6528. Accessed Jan 17, 2023.

(26) Long, G. V.; Dummer, R.; Hamid, O.; Gajewski, T.; Caglevic, C.; Dalle, S.; et al. Epacadostat plus pembrolizumab versus pembrolizumab alone in patients with unresectable or metastatic melanoma: Results of the phase 3 ECHO-301/KEYNOTE-252 study. *J. Clin. Oncol.* **2018**, *36* (15_suppl), 108.

(27) Long, G. V.; Dummer, R.; Hamid, O.; Gajewski, T. F.; Caglevic, C.; Dalle, S.; Arance, A.; Carlino, M. S.; Grob, J.-J.; Kim, T. M.; et al. Epacadostat plus pembrolizumab versus placebo plus pembrolizumab in patients with unresectable or metastatic melanoma (ECHO-301/KEYNOTE-252): a phase 3, randomised, double-blind study. *Lancet Oncol.* **2019**, *20* (8), 1083−1097.

(28) Mautino, M. R.; Jaipuri, F. A.; Waldo, J.; Kumar, S.; Adams, J.; Van Allen, C.; Marcinowicz-Flick, A.; Munn, D.; Vahanian, N.; Link, C. J. NLG919, a novel indoleamine-2, 3-dioxygenase (IDO)-pathway inhibitor drug candidate for cancer therapy. *Canc. Res.* **2013**, *73* (8_Supplement), 491−491.

(29) Kumar, S.; Waldo, J. P.; Jaipuri, F. A.; Marcinowicz, A.; Van Allen, C.; Adams, J.; Kesharwani, T.; Zhang, X.; Metz, R.; Oh, A. J.; et al. Discovery of Clinical Candidate (1 R, 4 r)-4-((R)-2-((S)-6-Fluoro-5 H-imidazo [5, 1-a] isoindol-5-yl)-1-hydroxyethyl) cyclohexan-1-ol (Navoximod), a Potent and Selective Inhibitor of Indoleamine 2, 3-Dioxygenase 1. *J. Med. Chem.* **2019**, *62* (14), 6705−6733.

(30) Tumang, J.; Gomes, B.; Wythes, M.; Crosignani, S.; Bingham, P.; Bottemanne, P.; Cannelle, H.; Cauwenberghs, S.; Chaplin, J.; Dalvie, D.; et al. PF-06840003: a highly selective IDO-1 inhibitor that shows good in vivo efficacy in combination with immune checkpoint inhibitors. *Cancer Res.* **2016**, *76* (14_Supplement), 4863−4863.

(31) Luke, J. J.; Tabernero, J.; Joshua, A.; Desai, J.; Varga, A. I.; Moreno, V.; Gomez-Roca, C. A.; Markman, B.; De Braud, F. G.; Patel, S. P.; et al. BMS-986205, an indoleamine 2, 3-dioxygenase 1 inhibitor (IDO1i), in combination with nivolumab (nivo): Updated safety across all tumor cohorts and efficacy in advanced bladder cancer (advBC). *J. Clin. Oncol.* **2019**, *37*, 358.

(32) Nelp, M. T.; Kates, P. A.; Hunt, J. T.; Newitt, J. A.; Balog, A.; Maley, D.; Zhu, X.; Abell, L.; Allentoff, A.; Borzilleri, R.; et al. Immune-modulating enzyme indoleamine 2, 3-dioxygenase is effectively inhibited by targeting its apo-form. *Proc. Natl. Acad. Sci. U.S.A.* **2018**, *115* (13), 3249−3254.

(33) Chen, S.; Tan, J.; Zhang, A. The ups, downs and new trends of IDO1 inhibitors. *Bioorganic Chemistry* **2021**, *110*, 104815.

(34) Ladomersky, E.; Zhai, L.; Lenzen, A.; Lauing, K. L.; Qian, J.; Scholtens, D. M.; Gritsina, G.; Sun, X.; Liu, Y.; Yu, F.; Gong, W.; Liu, Y.; Jiang, B.; Tang, T.; Patel, R.; Platanias, L. C.; James, C. D.; Stupp, R.; Lukas, R. V.; Binder, D. C.; Wainwright, D. A. IDO1 Inhibition Synergizes with Radiation and PD-1 Blockade to Durably Increase Survival Against Advanced Glioblastoma. *Clin. Cancer Res.* **2018**, *24* (11), 2559−2573.

(35) Békés, M.; Langley, D. R.; Crews, C. M. PROTAC targeted protein degraders: the past is prologue. *Nat. Rev. Drug Discovery* **2022**, *21*, 181.

(36) Samarasinghe, K. T. G.; Crews, C. M. Targeted protein degradation: A promise for undruggable proteins. *Cell Chem. Biol.* **2021**, *28* (7), 934−951.

(37) Sakamoto, K. M.; Kim, K. B.; Kumagai, A.; Mercurio, F.; Crews, C. M.; Deshaies, R. J. Protacs: Chimeric molecules that target proteins to the Skp1-Cullin-F box complex for ubiquitination and degradation. *Proc. Natl. Acad.* **2001**, *98* (15), 8554−8559.

(38) Hu, M.; Zhou, W.; Wang, Y.; Yao, D.; Ye, T.; Yao, Y.; Chen, B.; Liu, G.; Yang, X.; Wang, W.; Xie, Y. Discovery of the first potent proteolysis targeting chimera (PROTAC) degrader of indoleamine 2,3-dioxygenase 1. *Acta Pharm. Sin. B* **2020**, *10* (10), 1943−1953.

(39) Bollu, L. R.; Bommi, P. V.; Monsen, P. J.; Zhai, L.; Lauing, K. L.; Bell, A.; Kim, M.; Ladomersky, E.; Yang, X.; Platanias, L. C.; Matei, D. E.; Bonini, M. G.; Munshi, H. G.; Hashizume, R.; Wu, J. D.; Zhang, B.; James, C. D.; Chen, P.; Kocherginsky, M.; Horbinski, C.; Cameron, M. D.; Grigorescu, A. A.; Yamini, B.; Lukas, R. V.; Schiltz, G. E.; Wainwright, D. A. Identification and Characterization of a Novel Indoleamine 2,3-Dioxygenase 1 Protein Degrader for Glioblastoma. *J. Med. Chem.* **2022**, *65* (23), 15642−15662.

(40) Troup, R. I.; Fallan, C.; Baud, M. G. J. Current strategies for the design of PROTAC linkers: a critical review. *Explor. target. anti-tumor ther.* **2020**, *1* (5), 273−312.

(41) Klein, V. G.; Townsend, C. E.; Testa, A.; Zengerle, M.; Maniaci, C.; Hughes, S. J.; Chan, K.-H.; Ciulli, A.; Lokey, R. S. Understanding and Improving the Membrane Permeability of VH032-Based PROTACs. *ACS Med. Chem. Lett.* **2020**, *11* (9), 1732−1738.

(42) Hornberger, K. R.; Araujo, E. M. V. Physicochemical Property Determinants of Oral Absorption for PROTAC Protein Degraders. *J. Med. Chem.* **2023**, *66* (12), 8281−8287.

(43) Bemis, T. A.; La Clair, J. J.; Burkart, M. D. Unraveling the Role of Linker Design in Proteolysis Targeting Chimeras. *J. Med. Chem.* **2021**, *64* (12), 8042−8052.

(44) Schwinn, M. K.; Machleidt, T.; Zimmerman, K.; Eggers, C. T.; Dixon, A. S.; Hurst, R.; Hall, M. P.; Encell, L. P.; Binkowski, B. F.; Wood, K. V. CRISPR-Mediated Tagging of Endogenous Proteins with a Luminescent Peptide. *ACS Chem. Biol.* **2018**, *13* (2), 467−474.

(45) Soucy, T. A.; Smith, P. G.; Rolfe, M. Targeting NEDD8-activated cullin-RING ligases for the treatment of cancer. *Clin. Cancer Res.* **2009**, *15* (12), 3912−3916.

(46) Donovan, K. A.; An, J.; Nowak, R. P.; Yuan, J. C.; Fink, E. C.; Berry, B. C.; Ebert, B. L.; Fischer, E. S. Thalidomide promotes degradation of SALL4, a transcription factor implicated in Duane Radial Ray syndrome. *eLife* **2018**, *7*, e38430.

(47) Donovan, K. A.; Ferguson, F. M.; Bushman, J. W.; Eleuteri, N. A.; Bhunia, D.; Ryu, S.; Tan, L.; Shi, K.; Yue, H.; Liu, X.; Dobrovolsky, D.; Jiang, B.; Wang, J.; Hao, M.; You, I.; Teng, M.; Liang, Y.; Hatcher, J.; Li, Z.; Manz, T. D.; Groendyke, B.; Hu, W.; Nam, Y.; Sengupta, S.; Cho, H.; Shin, I.; Agius, M. P.; Ghobrial, I. M.; Ma, M. W.; Che, J.; Buhrlage, S. J.; Sim, T.; Gray, N. S.; Fischer, E. S. Mapping the Degradable Kinome Provides a Resource for Expedited Degrader Development. *Cell* **2020**, *183* (6), 1714−1731.

(48) Concepcion, J.; Witte, K.; Wartchow, C.; Choo, S.; Yao, D.; Persson, H.; Wei, J.; Li, P.; Heidecker, B.; Ma, W.; Varma, R.; Zhao, L. S.; Perillat, D.; Carricato, G.; Recknor, M.; Du, K.; Ho, H.; Ellis, T.; Gamez, J.; Howes, M.; Phi-Wilson, J.; Lockard, S.; Zuk, R.; Tan, H. Label-free detection of biomolecular interactions using BioLayer interferometry for kinetic characterization. *Comb. Chem. High Throughput Screen.* **2009**, *12* (8), 791−800.

(49) Fraunhoffer, K. J.; DelMonte, A. J.; Beutner, G. L.; Bultman, M. S.; Camacho, K.; Cohen, B.; Dixon, D. D.; Fan, Y.; Fanfair, D.; Freitag, A. J.; Glace, A. W.; Gonzalez-Bobes, F.; Gujjar, M.; Haley, M. W.; Hickey, M. R.; Ho, J.; Iyer, V.; Maity, P.; Patel, S.; Rosso, V. W.; Schmidt, M. A.; Stevens, J. M.; Tan, Y.; Wilbert, C.; Young, I. S.; Yu, M. Rapid Development of a Commercial Process for Linrodostat, an Indoleamine 2,3-Dioxygenase (IDO) Inhibitor. *Org. Process Res. Dev.* **2019**, *23* (11), 2482−2498.

(50) Uyttenhove, C.; Pilotte, L.; Theate, I.; Stroobant, V.; Colau, D.; Parmentier, N.; Boon, T.; Van den Eynde, B. J. Evidence for a tumoral immune resistance mechanism based on tryptophan degradation by indoleamine 2,3-dioxygenase. *Nat. Med.* **2003**, *9* (10), 1269−1274. Research Support, Non-U.S. Gov't.

(51) Zhai, L.; Lauing, K. L.; Chang, A. L.; Dey, M.; Qian, J.; Cheng, Y.; Lesniak, M. S.; Wainwright, D. A. The role of IDO in brain tumor immunotherapy. *J. Neurooncol.* **2015**, *123* (3), 395−403.

(52) Wainwright, D. A.; Dey, M.; Chang, A.; Lesniak, M. S. Targeting Tregs in Malignant Brain Cancer: Overcoming IDO. *Front. Immunol.* **2013**, *4*, 116.

(53) Zhai, L.; Ladomersky, E.; Dostal, C. R.; Lauing, K. L.; Swoap, K.; Billingham, L. K.; Gritsina, G.; Wu, M.; McCusker, R. H.; Binder, D. C.; Wainwright, D. A. Non-tumor cell IDO1 predominantly contributes to enzyme activity and response to CTLA-4/PD-L1 inhibition in mouse glioblastoma. *Brain Behav. Immun.* **2017**, *62*, 24−29.

https://doi.org/10.1021/acs.jmedchem.5c00026
J. Med. Chem. XXXX, XXX, XXX−XXX

(54) Wang, Q.; Liu, F.; Wang, B.; Zou, F.; Qi, Z.; Chen, C.; Yu, K.; Hu, C.; Qi, S.; Wang, W.; Hu, Z.; Liu, J.; Wang, W.; Wang, L.; Liang, Q.; Zhang, S.; Ren, T.; Liu, Q.; Liu, J. Discovery of 4-Methyl-N-(4-((4-methylpiperazin-1-yl)methyl)-3-(trifluoromethyl)phenyl)-3-((1-nicotinoylpiperidin-4-yl)oxy)benzamide (CHMFL-ABL/KIT-155) as a Novel Highly Potent Type II ABL/KIT Dual Kinase Inhibitor with a Distinct Hinge Binding. *J. Med. Chem.* **2017**, *60* (1), 273−289.
(55) Noguchi, T.; Tanaka, N.; Nishimata, T.; Goto, R.; Hayakawa, M.; Sugidachi, A.; Ogawa, T.; Asai, F.; Ozeki, T.; Fujimoto, K. Indoline derivatives II: synthesis and factor Xa (FXa) inhibitory activities. *Chem. Pharm. Bull. (Tokyo)* **2007**, *55* (3), 393−402.
(56) Wang, Q.; Liu, F.; Wang, B.; Zou, F.; Chen, C.; Liu, X.; Wang, A.; Qi, S.; Wang, W.; Qi, Z.; Zhao, Z.; Hu, Z.; Wang, W.; Wang, L.; Zhang, S.; Wang, Y.; Liu, J.; Liu, Q. Discovery of N-(3-((1-Isonicotinoylpiperidin-4-yl)oxy)-4-methylphenyl)-3-(trifluoromethyl)benzamide (CHMFL-KIT-110) as a Selective, Potent, and Orally Available Type II c-KIT Kinase Inhibitor for Gastrointestinal Stromal Tumors (GISTs). *J. Med. Chem.* **2016**, *59* (8), 3964−3979.
(57) Li, Z.; Pinch, B. J.; Olson, C. M.; Donovan, K. A.; Nowak, R. P.; Mills, C. E.; Scott, D. A.; Doctor, Z. M.; Eleuteri, N. A.; Chung, M.; Sorger, P. K.; Fischer, E. S.; Gray, N. S. Development and Characterization of a Wee1 Kinase Degrader. *Cell Chem. Biol.* **2020**, *27* (1), 57−65.
(58) Plewe, M. B.; Wang, J.; Han, X.; Chen, L. Compounds and methods of treating cancers. US20230093099A1, 2023.
(59) Zhang, J.; Che, J.; Luo, X.; Wu, M.; Kan, W.; Jin, Y.; Wang, H.; Pang, A.; Li, C.; Huang, W.; Zeng, S.; Zhuang, W.; Wu, Y.; Xu, Y.; Zhou, Y.; Li, J.; Dong, X. Structural Feature Analyzation Strategies toward Discovery of Orally Bioavailable PROTACs of Bruton's Tyrosine Kinase for the Treatment of Lymphoma. *J. Med. Chem.* **2022**, *65* (13), 9096−9125.
(60) Netherton, M.; Schiller, S. E. R.; Deng, J.; Anthony, N. J.; Brucelle, F.; Ruppel, S. K.; Voigt, J. H. Heteroaromatic compounds for the treatment of BAF complex-related diseases and their preparation. WO2021155321, 2021.
(61) Choi, H.; Wang, G.; Peng, X.; Kang, B.; Kim, H.; Jung, H.. Compounds and methods for the targeted degradation of estrogen receptors. WO2022217010, 2022.
(62) Palmer, W. S. W.; Jeffrey; Zipfel, S.; Ozboya, K.; Weiss, D.. Preparation of bifunctional degraders of interleukin-1 receptor-associated kinases and therapeutic use thereof. WO2021168197, 2021.
(63) Han, X.; Zhao, L.; Xiang, W.; Qin, C.; Miao, B.; McEachern, D.; Wang, Y.; Metwally, H.; Wang, L.; Matvekas, A.; Wen, B.; Sun, D.; Wang, S. Strategies toward Discovery of Potent and Orally Bioavailable Proteolysis Targeting Chimera Degraders of Androgen Receptor for the Treatment of Prostate Cancer. *J. Med. Chem.* **2021**, *64* (17), 12831−12854.
(64) Castro, A. C. B.; Michael. Preparation of heterocyclic compounds as TEAD degraders and uses thereof. WO2022120355, 2022.
(65) Hughes, S. J.; Ciulli, A. Molecular recognition of ternary complexes: a new dimension in the structure-guided design of chemical degraders. *Essays Biochem.* **2017**, *61* (5), 505−516.
(66) Roy, M. J.; Winkler, S.; Hughes, S. J.; Whitworth, C.; Galant, M.; Farnaby, W.; Rumpel, K.; Ciulli, A. SPR-Measured Dissociation Kinetics of PROTAC Ternary Complexes Influence Target Degradation Rate. *ACS Chem. Biol.* **2019**, *14* (3), 361−368.
(67) Zhai, L.; Ladomersky, E.; Bell, A.; Dussold, C.; Cardoza, K.; Qian, J.; Lauing, K. L.; Wainwright, D. A. Quantification of IDO1 enzyme activity in normal and malignant tissues. *Methods Enzymol.* **2019**, *629*, 235−256.
(68) Skowronek, P.; Thielert, M.; Voytik, E.; Tanzer, M. C.; Hansen, F. M.; Willems, S.; Karayel, O.; Brunner, A.-D.; Meier, F.; Mann, M. Rapid and in-depth coverage of the (phospho-) proteome with deep libraries and optimal window design for dia-PASEF. *bioRxiv* **2022**.
(69) Demichev, V.; Messner, C. B.; Vernardis, S. I.; Lilley, K. S.; Ralser, M. DIA-NN: neural networks and interference correction enable deep proteome coverage in high throughput. *Nat. methods* **2020**, *17* (1), 41−44.
(70) Ritchie, M. E.; Phipson, B.; Wu, D.; Hu, Y.; Law, C. W.; Shi, W.; Smyth, G. K. limma powers differential expression analyses for RNA-sequencing and microarray studies. *Nucleic Acids Res.* **2015**, *43* (7), No. e47.

https://doi.org/10.1021/acs.jmedchem.5c00026
J. Med. Chem. XXXX, XXX, XXX−XXX